EVALUATION OF STRUCTURAL DAMAGE IDENTIFICATION METHODS BASED ON DYNAMIC CHARACTERISTICS

By

Juan Carlos Herrera Sánchez

A thesis submitted in partial fulfillment of the requirements for the degree of

DOCTOR OF PHILOSOPHY

in

CIVIL ENGINEERING

UNIVERSITY OF PUERTO RICO
MAYAGÜEZ CAMPUS
2005

Approved by :

_____   _____
Luis A. Godoy, Ph.D   Date
Member, Graduate Committee

_____   _____
Ricardo López, Ph.D.   Date
Member, Graduate Committee

_____   _____
Mario Rivera Borrero, Ph.D.   Date
Member, Graduate Committee

_____   _____
Luis E. Suárez , Ph.D.   Date
President, Graduate Committee

_____   _____
José Arroyo Caraballo, Ph. D.   Date
Representative of Graduate Studies

_____   _____
Prof. Ismael Pagán Trinidad.   Date
Chairperson of the Department

_____   _____
José A. Mari Mutt, Ph. D.   Date
Director of Graduate Studies

ABSTRACT

In this thesis, structural damage identification methods based on changes in the dynamic characteristics of the structure are examined and new methodologies are also developed. These are based on the modal curvature matrix, the Frequency Response Function (FRF) curvature and the Discrete Wavelet Transform. Damage indices based on the concept of Receptance-Energy are presented to predict the damage location and to estimate the severity of the damage directly from the measured FRF. The methods are evaluated for several damage scenarios in a simply-supported beam and a plane frame. The damage is simulated by reducing the stiffness of assumed elements and by introducing cracked elements at different locations. The results of the analyses indicate that the proposed method based on the Receptance-Energy performs well in detecting, locating and quantifying damage in single and multiple damage scenarios. The numerical examples show that the Wavelets Transform analysis is capable of detecting the discontinuities in the FRF signal to locate damage.

RESUMEN

Esta tesis examina los métodos de identificación de daño estructural que se basan en cambios de las características dinámicas de la estructura. También se formulan nuevos métodos de identificación de daño basados, respectivamente, en la matriz de curvatura modal, la curvatura de la Función Respuesta en Frecuencia y en la aplicación de la Transformada Discreta de "Wavelets" para indicar la localización del daño mediante la detección de discontinuidades en la señal de la respuesta. Los índices del daño basados en el concepto de Energía de Receptancia, se conciben para localizar y estimar la severidad del daño en una estructura directamente de la Función Respuesta en Frecuencia. Para evaluar la efectividad de los métodos propuestos se realizaron simulaciones numéricas mediante modelos de elementos finitos de una viga simplemente apoyada y un pórtico plano. Para cada estructura se investigan varios escenarios de daño, en los cuales el daño estructural se simula mediante la reducción de la rigidez de algunos elementos y la introducción de elementos agrietados. Los resultados indican que el método propuesto basado en la Energía de Receptancia es efectivo para localizar y cuantificar el daño en escenarios de daño múltiple. Asimismo, los ejemplos muestran que el método basado en la Transformada Discreta de "Wavelets" puede localizar efectivamente las zonas con daño y como esta metodología no requiere la respuesta de la estructura sin daño, puede proporcionar una alternativa a los métodos de identificación de daño basados en el análisis modal.

A la memoria de mi padre,

a mi madre,

a Victoria Eugenia, mi continua esperanza.

ACKNOWLEDGMENTS

I would like to express my gratitude to Dr. Luis E. Suarez, for his guidance, advice and his friendship, throughout my doctoral studies.

I would like to acknowledge Dr. Ricardo Lopez for his advice during the time of my graduate studies. Also, I would like to thank Dr. Luis Godoy and Dr. Mario Rivera for their reviews and comments.

I am grateful to the Civil Engineering and Surveying Department of the University of Puerto Rico for giving me the opportunity of pursuing my graduate studies and to its director, Prof. Ismael Pagán for providing economic assistance during my graduate studies.

Finally, I would like to thank my family.

CONTENTS

LIST OF FIGURES

xvii

LIST OF TABLES

CHAPTER I

INTRODUCTION

The condition assessment of existing civil infrastructures such as buildings, highway and railways bridges and structures of airports, ports, and water treatment plants is crucial to prevent potential catastrophic events and for planning the future investments in repair and rehabilitation of this infrastructure. Also, the rapid assessment after strong earthquakes and hurricanes of critical structures like hospitals, fire stations, power stations and major bridges, is imperative for the concerned government agencies. Many infrastructure components are now decaying because of age, deterioration, and lack of maintenance or repair. Additionally, some of the existing structures were not designed for the current provisions specified in modern design codes.

Current nondestructive damage detection (NDD) techniques are either visual or are based on experimental methods such as acoustic or ultrasonic techniques, magnetic field procedures, radiography, etc. In general, many experimental methods require that the damaged region be identified *a priori*, and that the segment of the structure being examined must be easily accessible. Subjected to these constraints, these methods can detect damage on or near the surface of the structure.

The civil engineering community is especially aware of the limitations of the condition assessment based on visual inspections frequently used in the current practice.

Typical routine applications of condition assessment are applied to bridges, dams, and buildings for evaluating seismic vulnerability or post-earthquake damage, and other types of structures after overloadings, accidents, or when new and more severe environmental loads are expected.

One way to overcome the previously mentioned limitations is by using global damage detection methods. Structural damage identification based on changes in dynamic characteristics provides a global way to evaluate the structural condition. These methods are based on the premise that modal parameters (i. e., natural frequencies, mode shapes, modal damping ratios, etc.) are a function of the physical properties of the structure (stiffness, damping, mass and boundary conditions). Therefore, changes in the stiffness or flexibility of the structure will cause changes in the modal properties. The need for new structural damage detection methods that can be applied to complex structures has led to the development of methodologies that examine changes in the vibration characteristics of the structure. In view of the above, it is important to examine some of the global damage detection methodologies for the structural damage identification currently in use.

1.1 PREVIOUS WORKS

During the last three decades a variety of dynamics-based damage identification methods have been proposed. Doebling et al. (1996) provided an extensive review on the subject.

1.1.1 Classification of damage.

The effects of damage on a structure can be classified as linear or nonlinear. A linear damage situation is defined as a case where an initially linear-elastic structure remains linear-elastic after damage. The changes in modal properties are the result of changes in the geometry and/or the material properties of the structure, but the structural response can still be modeled using linear equations of motion.

Nonlinear damage refers to a case when an initially linear elastic structure behaves in a nonlinear manner after the damage has occurred (Doebling et al. 1996). In this work only the problem of linear damage detection is studied.

A different classification scheme for damage-identification methods defines four levels of damage identification, as follows (Rytter 1993):

• Level 1: Only whether damage is present in the structure is determined.

• Level 2: Level 1 plus determination of the geometric location of the damage.

• Level 3: Level 2 plus quantification of the severity of the damage.

• Level 4: Level 3 plus prediction of the remaining service life of the structure.

The modal-based damage identification methods that do not make use of some structural model primarily provide Level 1 and Level 2 damage identification. When modal-based methods are coupled with a structural model, a Level 3 damage detection

can be obtained in some cases. Level 4 prediction is generally associated with the fields

of fracture mechanics, fatigue life analysis and structural design assessment.

1.1.2. Methods based on frequency and mode shape changes.

One of the approaches in detecting damage has been to use changes in the modal

parameters, mainly changes in the modal frequencies. Cawley and Adams (1979)

provided a formulation to detect damage in composite materials from frequency shifts. A

number of mode pairs is considered for each potential damage location, and the pair

giving the lowest error indicates the location of the damage. The formulation does not

account for possible multiple-damage locations.

Yuen (1985) presented a systematic study of the relationship between damage

location, damage size, and the changes in the eigenvalues and eigenvectors of a cantilever

subjected to damage. A finite element model of a cantilever with uniform cross-section

was chosen to provide data for the analysis. In this study it was assumed that damage in

the structure would affect only the stiffness matrix but not the inertia matrix in the

eigenproblem formulation. The changes in the eigenvalues and eigenvectors were shown

to follow a definite trend in relation to the location and extent of damage.

Stubbs and Osegueda (1990a, 1990b) presented a method for damage

identification based on changes in modal characteristics. Expressions relating variations

in stiffnesses of structural members to the variations in modal stiffness were generated

using matrix structural analysis. Damage was defined as a reduction in the stiffness of

one of the elements forming the structure. The stiffness reductions were located by solving a general inverse problem. The authors demonstrated that the damage locations in structural elements and the magnitudes could be predicted. Damage was predicted at single and multiple locations in a simply-supported beam. For the damage cases investigated the formulation predicted the damage 91 percent of the time.

Salawu and Williams (1993) investigated the performance of four damage detection methods. One method is based on changes in the eigenparameters and the others use system identification and model updating procedures. The results showed that the eigenparameter method is the best, although it was incapable of locating the damage in a lightly stressed zone.

Ko et al. (1994) proposed a damage detection method combining Sensitivity Analysis and Modal Assurance Criterion (MAC)/Coordinate Modal Assurance Criterion (COMAC) for a steel frame. Before and after the structure was damaged, six sets of vibration data were measured under two different joint conditions (rigid and pinned) and two different damage locations (beam-column and column-base connections). The sensitivities of the modal vectors obtained analytically to particular damage conditions were computed to determine which DOFs are most significant. Then a MAC analysis is applied between the measured modes from the undamaged frame and damaged frame to find the correlated mode pairs. Using the modes selected with the above analysis, the COMAC is computed and used as an indicator of damage. The results demonstrate that particular mode pairs can indicate damage, but when all available mode pairs are used, the COMAC results cannot indicate the right damage location.

Ren and De Roeck (2002) proposed a damage identification method based on changes in frequencies and mode shapes of vibration for predicting damage location and severity. The method is applied at an element level with a finite-element model. The element damage equations were established through the eigenvalue equations that characterized the dynamic behavior. Several solution techniques are discussed and compared. The method was verified by simulating a number of damage scenarios in beams and it predicted the exact location and severity of damage. It was demonstrated that by multiplying the damaged eigenvalue equations with the undamaged or damaged mode shapes provides more equations and guarantees the damage localization.

1.1.3. Methods based on modal curvature/modal strain energy.

Kim et al. (2003) presented a methodology to locate and estimate the size of damage in structures for which a few natural frequencies or a few mode shapes are available. A frequency-based damage detection (FBDD) method and a mode-shape-based damage detection (MBDD) method are presented. A damage index algorithm to localize and estimate the severity of damage from monitoring changes in modal strain energy is formulated. The FBDD method and the MBDD method were evaluated for several damage scenarios by locating and sizing damage in numerically simulated prestressed concrete beams. The result of the analyses indicates that the methods correctly localize the damage and accurately estimate the sizes of the cracks simulated in the test beam.

Salawu and Williams (1994) evaluated the performance of the curvature mode shape method and the mode shape relative difference method. They found that the

performance using experimental data was poor. The results showed that the procedures were unsatisfactory in predicting the most severe damage case, and were unable to satisfactorily differentiate between damage cases with close degrees of severity.

Dong et al. (1994) carried out a systematic analytical study and experiments to correlate the crack of a beam with changes in its modal parameters. The sensitivity to both crack location and crack size was developed for each modal parameter. They examined a parameter which is based on the change in the strain mode shape and another one that depends on natural frequency. The authors showed that the strain eigenparameter is more sensitive to the size of the crack than the frequency eigenparameter.

Pandey et al. (1991) proposed a parameter called curvature mode shape to identify and locate damage in a structure. By using a cantilever and a simply supported analytical beam models, they showed that the absolute changes in the curvature mode shapes are localized in the region of damage and hence they can be used to detect damage in a structure. The changes in the curvature mode shape increase with the increasing size of damage and this information can be used to obtain the amount of damage in the structure. A finite element analysis was used to obtain the displacement mode shapes of the two models. By using a central difference approximation, curvature mode shapes were calculated from the displacement mode shapes.

1.1.4. Methods based on changes in flexibility.

Pandey et al. (1994) presented a method to detect the presence and location of structural damage based on changes in the measured flexibility of the structure. The authors showed that the flexibility matrix can be accurately estimated from a few of the lower frequency modes of vibration of the structure, which can be easily measured. First, the effect of damage in a structure on its flexibility was studied with simple analytical beam models. By using these analytical models, the effectiveness of using changes in the flexibility matrix in detecting and locating damages is demonstrated. The procedure formulated was tested with experimental data collected on a wide-flange steel beam.

Raghavendrachar and Aktan (1992) presented a multireference impact testing of a bridge in which frequency-response functions (FRF) were measured and a large number of modal parameters were reliably identified. The mode shape coefficients obtained by processing the measured FRF were directly transformed into flexibility of the test bridge. The authors presented analytical studies using a calibrated analytical model to demonstrate that the flexibility coefficients are more sensitive to local damage than either the frequencies or mode shapes.

Mannan and Richardson (1992) proposed a method for determining the mass, stiffness, and damping properties of the structure from the measured Frequency Response Functions (FRFs). They used an approach that involves curve fitting the FRFs directly to estimate the mass, stiffness, and damping matrices. The authors found that the higher frequency modes are most important for detecting faults which cause stiffness changes.

Park et al. (1988) introduced a method to detect stiffness damages based on the error matrix. This matrix is defined as the difference between the stiffness matrices of the damaged and undamaged structures. This method proved to be useful when the stiffness changes were large, but it was not effective for searching out small local defects. The weighted-error-matrix (WEM) method was tested to magnify the effect of small stiffness reduction in the error matrix. Through the WEM the damaged area in the error matrix was magnified by adding the information from the eigenproperties changing patterns through sensitivity analysis. By applying this formulation to beam and plate models, they concluded that the WEM is a better method than the error-matrix method for identifying defects.

Gysin (1986) tested the error matrix method on a 9 degrees of freedom spring-mass-system and on a beam in bending. Three different reduction techniques were used to reduce the stiffness or mass matrix. It was demonstrated that the efficiency of the method depends on the type of matrix reduction used and on the number of modes utilized to form the flexibility matrices.

1.1.5. Methods based on the Frequency Response Function.

Lee and Shin (2002) proposed a structural damage identification method based on the frequency response function for beam structures. The damage within a beam structure was characterized by introducing a damage distribution function. It was shown that damage may induce coupling between vibration modes. They investigated the effects the accuracy of the predicted vibration characteristics of damaged beams of the damage-

induced coupling of vibration modes and the higher vibration modes omitted in the analysis on were numerically investigated. The feasibility of the proposed method was verified through numerically simulated damage identification tests.

Sampaio et al. (1999) reported a frequency response function curvature method that covers three steps of the process of damage detection, namely existence, localization, and extent. The technique is based on the measured data without the need for any modal identification. The method was described theoretically and compared with two methods: the mode shape curvature method and the damage index method. Numerically generated data from a lumped-mass system and experimental data from a real bridge were used to illustrate the application of the proposed procedure.

1.1.6. Methodologies based on the Wavelet Transform.

Ovanesova and Suarez (2004) applied the wavelet transform to detect cracks in single structural frameworks, such as beams and plane frames. They showed that the procedure can detect the localization of the cracks by using a response signal from either static or dynamic loads. The results show that if a suitable wavelet is selected, the method is capable to extract damage information from these response signals.

Hou et al. (2000) used a simple structural model with multiple breakable springs subjected to a harmonic excitation and showed that the wavelets transform can be successfully used to identify both abrupt and cumulative damages.

Wang and Deng (1999) presented a structural damage detection technique based on wavelet analysis of spatially distributed structural response measurements. In the numerical examples, the displacement response was analyzed with the wavelet transform, and the presence of the crack was detected by a sudden change in the spatial variation of the transformed response. This damage detection technique may be used for structural health monitoring in situations where spatially distributed measurements of structural response in regions of critical concern can be obtained with networks of distributed sensors and optical fibers.

Liew and Wang (1998) also reported the application of the wavelet theory for crack identification in structures. The crack identification makes use of the wavelet theory applied to a simply supported beam with a transverse on-edge open crack. A mathematical model of the cracked beam was derived and the wavelet expressions in the space domain were proposed. For comparison purposes, the simply supported cracked beam was analyzed using both the eigentheory and the wavelet-based method.

1.1.7. Modeling of cracked beam elements.

Qian et al. (1990) derived an element stiffness matrix of a beam with a crack by first integrating the stress intensity factors, and then used this to develop a finite element model of a cracked beam. This model was applied to a cantilever beam with an edge-crack, and their eigenfrequencies were determined for different crack lengths and locations. The results were compared with experimental data. In order to consider the effect of crack closure, the modal parameters were identified by means of an

identification technique in the time domain. The authors proposed a direct method for determining the crack position, based on a relationship between the crack and the eigencouple (eigenvalue and eigenvector) of a beam.

Haisty and Springer (1988) derived a general beam element which contains a symmetric discontinuity in the form of a double-sided open crack. The finite element model was developed by determining the force-displacement relationships for two undamaged beams connected by a set of springs. They argued that the element may be used to model damage in complex structures. The method used to determine the stiffness terms necessary to model the damage in an element was explained.

Gounaris and Dimarogonas (1988) developed a finite element for a cracked beam that can be used to model structures for finite element analysis. Strain energy concentration arguments lead to the development of a compliance matrix for the behavior of the beam in the vicinity of the crack. This matrix was used to develop the stiffness matrix for the cracked beam element and the consistent mass matrix. The element developed was used to evaluate the dynamic response of a cracked cantilever beam to a harmonic point force excitation.

1.2 RESEARCH OBJECTIVES

The main objective of this research is to implement, compare and evaluate the global methods currently proposed for damage identification that use changes in the modal properties of the structure (i.e. modal frequencies and mode shapes) and to

provide an assessment of the effectiveness of the methodologies studied by applying them to the same structures. Another important objective is to formulate new structural damage identification methodologies based on the methods examined that can be used for damage assessment of existing structures.

Two plane structures are considered in this work: a simply-supported beam and a plane frame modeled using the Euler-Bernoulli beam theory. Several damage scenarios are investigated. The structural damage is simulated by reducing the stiffness of specific elements and by introducing cracks at different locations using specially formulated finite elements. A comparison of the results obtained with the different damage localization methods analyzed is carried out in order to establish their limitations for use in structural damage detection. This work is limited only to the analytical and numerical simulation aspects of the damage identification problem. It is expected that by screening the most promising methods for damage identification, the number of techniques that must be experimentally verified in a next stage can be reduced substantially.

1.3 SIGNIFICANCE OF THE RESEARCH WORK

The results of this research will provide an evaluation of the effectiveness of the global damage identification methods selected. Moreover, original contributions to the damage identification field will be made. The first damage identification methodology developed in this thesis is based on the modal curvature matrix. The second proposed methodology is based on a new concept, called the Receptance-Energy. Damage indices

are presented to predict the damage location and to estimate the severity of the damage in a structure directly from its Frequency Response Function (FRF). The third method proposed is based on the curvature of the FRF and the fourth damage identification methodology is based on the application of the Discrete Wavelet Transform to indicate the location of damage by detecting the discontinuities in the FRF signal.

1.4 ORGANIZATION OF THE THESIS

Chapter I is a general introduction to the thesis. The justification and problem description is discussed. The chapter continues with a literature review of the previous works on the subject of structural damage identification and crack modeling. The objectives and the significance of the research work presented in the thesis are defined.

Chapter II presents the finite element model used to model the crack-like damage in frame structures. The stiffness matrix of the cracked beam element is formulated for elements with rectangular cross section.

Chapter III contains a brief introduction to the modal analysis theory. The structures considered in the thesis are described and the damage scenarios used to compare the damage identification methods are defined. Next, a direct comparison of the natural frequencies and mode shapes of the selected undamaged and damaged structures is presented.

Chapter IV introduces several structural damage identification methods based on changes in displacement mode shapes. The methodologies studied are coded in

MATLAB and numerical simulations are performed to compare the effectiveness of the procedures to locate damage in different damage scenarios simulated in a simply-supported beam and in a plane frame.

Chapter V presents the application of the damage identification methods that use a flexibility matrix defined in terms of experimentally measured modal properties. Numerical examples are prepared to illustrate the effectiveness of the procedure to locate damage. The same damage scenarios and structures analyzed in the previous chapter are considered.

Chapter VI examines several damage identification methods based on the modal curvature and modal strain energy. The modal curvatures are numerically generated. A structural damage identification method that is based on a new modal matrix referred to as the "curvature-energy matrix" is proposed. The proposed and existing methodologies studied are implemented in MATLAB and numerical simulations are performed to compare the effectiveness of the procedures to locate damage for the same damage scenarios described in Chapter III.

Chapter VII contains the formulation of several damage identification methods based on the FRF-curvature. A new structural damage identification method based on the concept of Receptance-Energy is proposed. The damage location and the severity of the damage are estimated by means of proposed damage indices. At the end of the chapter several examples are presented to verify the effectiveness of the proposed methodology.

Chapter VIII begins with a review of the continuous and discrete wavelet transforms. Next, a damage identification method based on the discrete wavelet transform is formulated. In this methodology the Receptance FRF and the FRF-first derivative are used as the response signal. The applicability of this new procedure is illustrated with numerical examples. It is shown that the proposed method does not require to know the response or the dynamic properties of the undamaged structure.

The last chapter of the thesis, chapter IX, contains conclusions and recommendations for future research.

CHAPTER II

MODELING OF CRACK-LIKE DAMAGE

2.1 INTRODUCTION

In most cases, the damage to a structure is due to the presence of cracks. Vibration monitoring has been a very feasible way to detect damage in the structure. This kind of monitoring work is based on a better understanding of the relationship between crack location, crack size and the corresponding changes in modal parameters, such as natural frequencies and vibration modes. A crack on a beam element introduces considerable local flexibility due to the strain energy concentration in the vicinity of the crack tip. In this chapter the finite element model for the cracked prismatic beam with an on-edge open crack proposed by Qian et al. (1990) is presented. This model was also evaluated by Dong et al. (1994). The numerical results obtained with this model agree well with the experimental results. Herein, this finite element model is adopted to simulate the crack-like damage in the elements.

2.2 THE STIFFNESS MATRIX OF THE CRACKED ELEMENT

According to the principle of Saint-Venant, the stress field is affected only in the region adjacent to the crack. It is very difficult to find an appropriate shape function to approximate the kinetic energy and elastic potential energy approximately, because of the discontinuity of deformation in the cracked element. The calculation of the additional

stress energy of a crack, however, has been studied in fracture mechanics and the flexibility coefficient expressed by a stress intensity factor can be easily derived by applying the Castigliano's theorem in the linear-elastic range.

As an example, a beam can be divided into elements and the behavior of the elements located to the right of the cracked element may be regarded as external forces applied to the cracked element, while the behavior of elements situated to its left as constraints (see Figure 2.1). Thus, the flexibility matrix of a cracked element with constraints may be calculated. From the condition of equilibrium, the stiffness matrix of the cracked element in the free-free state can be easily derived.

Neglecting shear action, the strain energy of an undamaged element is

$$W^{(0)} = \frac{1}{2EI}\left(M^2 L + MPL^2 + P^2 L^3 / 3\right) \tag{2.1}$$

Where E is the elastic modulus, P and M are the shear and bending internal forces at the right node, I the moment of inertia of the undamaged element and L the length of the finite element. For a rectangular beam having width b and thickness h the additional strain energy due to the crack can be written as

$$W^{(1)} = b\int_0^a \left[\frac{\left(K_I^2 + K_{II}^2\right)}{E_p} + \frac{\left(1+v\right)K_{III}^2}{E}\right]da \tag{2.2}$$

where K_I, K_{II}, K_{III} are stress intensity factors for opening type, sliding type and tearing type cracks, respectively. $E_p=E$ for plane stress, $E_p=E/(1-v^2)$ for plane strain, and a is the crack depth. Taking into account only bending, equation (2.2) becomes

$$W^{(1)} = b\int_0^a \left\{ \left[\left(K_{IM} + K_{IP} \right)^2 + K_{IIP}^2 \right] / E_p \right\} da \qquad (2.3)$$

where K_{IM}, K_{IP}, K_{IIP} are stress intensity factors for opening-type and sliding-type cracks due to M and P, respectively

$$K_{IM} = \left(6M / bh^2 \right) \sqrt{\pi a} F_I (s)$$

$$K_{IP} = \left(3PL / bh^2 \right) \sqrt{\pi a} F_I (s) \qquad (2.4)$$

$$K_{IIP} = \left(P / bh \right) \sqrt{\pi a} F_{II} (s)$$

$F_I(s)$ anf $F_{II}(s)$ are function of the ratio s between the crack depth and the height of the element ($s=a/h$), defined as

$$F_I (s) = \sqrt{(2/\pi s) tg(\pi s/2)} \; \frac{0\cdot923 + 0\cdot199\left[1 - \sin(\pi s/2) \right]^4}{\cos(\pi s/2)} \qquad (2.5)$$

$$F_{II} (s) = \left(3s - 2s^2 \right) \frac{1\cdot122 - 0\cdot561s + 0\cdot085s^2 + 0\cdot18s^3}{\sqrt{1-s}} \qquad (2.6)$$

The flexibility coefficient of the uncracked element can be derived as

$$C_{ij}^{(0)} = \frac{\partial^2 W^{(0)}}{\partial P_i \partial P_j}$$

$$P_1 = P, \quad P_2 = M, \quad i, j = 1, 2$$

(2.7)

and the additional flexibility coefficient are

$$C_{ij}^{(1)} = \frac{\partial^2 W^{(1)}}{\partial P_i \partial P_j}$$

$$P_1 = P, \quad P_2 = M, \quad i, j = 1, 2$$

(2.8)

The flexibility matrix of the uncracked element can be expressed as

$$\left[C^{(0)}\right] = \frac{1}{EI}\begin{bmatrix} \dfrac{L^3}{3} & \dfrac{L^2}{2} \\ \dfrac{L^2}{2} & L \end{bmatrix}$$

(2.9)

Similarly the coefficients $C_{ij}^{(1)}$ can be expressed in matrix form as

$$\left[C^{(1)}\right] = \frac{b\pi a^2}{E_p}\begin{bmatrix} 9\beta_1^2 L^2 + \beta_2^2 & 18\beta_1^2 L \\ 18\beta_1^2 L & 36\beta_1^2 \end{bmatrix}$$

(2.10)

where $\beta_1 = F_I(s)/bh^2$ and $\beta_2 = F_{II}(s)/bh$

The total flexibility coefficients for the element with an open crack are

$$C_{ij} = C_{ij}^{(0)} + C_{ij}^{(1)}$$

(2.11)

The total flexibility matrix for the element with an open crack can be expressed as

$$\left[C\right] = \left[C^{(0)}\right] + \left[C^{(1)}\right]$$

(2.12)

From the equilibrium conditions (shown in Figure 2.2), the following relationship holds

$$\{P_i \ M_i \ P_{i+1} \ M_{i+1}\}^T = [T]\{P_{i+1} \ M_{i+1}\}^T$$

(2.13)

where

$$[T] = \begin{bmatrix} -1 & -L & 1 & 0 \\ 0 & -1 & 0 & 1 \end{bmatrix}^T$$

(2.14)

The stiffness matrix of the undamaged element can be written as

$$[K_u] = [T]\left[C^{(0)}\right]^{-1}[T]^T$$

(2.15)

and the stiffness matrix of the cracked element can be written as

$$[K_c] = [T][C]^{-1}[T]^T$$

(2.16)

The derivation of the matrices $\left[C^{(1)}\right]$ and $[K_c]$ is presented in Appendix D. The stiffness matrix of the undamaged element with rectangular cross-section is that given by Bernoulli–Euler theory with Hermite shape functions:

$$
[K_u] = \frac{Ebh^3}{12L^3}
\begin{array}{cccc}
u_i & \theta_i & u_{i+1} & \theta_{i+1}
\end{array}
\begin{bmatrix}
12 & 6L & -12 & 6L \\
 & 4L^2 & -6L & 2L^2 \\
 & & 12 & -6L \\
sym & & & 4L^2
\end{bmatrix}
\begin{array}{c}
u_i \\ \theta_i \\ u_{i+1} \\ \theta_{i+1}
\end{array}
\tag{2.17}
$$

The mass matrix for an element without a crack is

$$
[M_u] = \frac{\bar{m}L}{420}
\begin{bmatrix}
156 & 22L & 54 & -13L \\
 & 4L^2 & 13L & -3L^2 \\
 & & 156 & -22L \\
sym & & & 4L^2
\end{bmatrix}
\tag{2.18}
$$

where $\bar{m}$ is the mass per unit length.
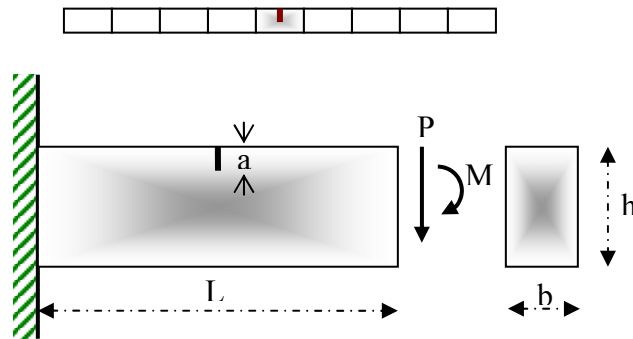
Figure 2.1 Diagram of a generic element.
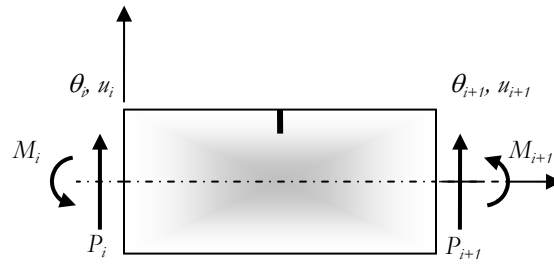
Figure 2.2 Equilibrium conditions of a generic element.

CHAPTER III

FREE VIBRATION ANALYSIS

In this chapter the free vibration analysis of a simply supported and a plane frame is considered for the undamaged and damaged cases. First, a brief introduction to the theory used in modal analysis is discussed. The frequencies and mode shapes generated here are used to compare the damage identification methodologies in the following chapters. Also, the geometric and material properties of the structures analyzed and the damage scenarios used in the numerical simulations, are presented.

3.1 ORTHOGONALITY PROPERTIES OF THE NORMAL MODES

The computation of the mode shapes and natural frequencies of a structural system is carried out by solving a matrix eigenvalue problem, obtained from the formulation of the equation of motion for free undamped vibration. In general the matrix eigenvalue problem is given by:

$$\left[[K] - \omega^2 [M] \right] \{\Psi\} = \{0\}$$

(3.1)

where

$[K]$: stiffness matrix of the system

$[M]$: mass matrix of the system

ω : natural frequency

$\{\Psi\}$: mode shape vector

The non-trivial solution of the eigenproblem must satisfy:

$$\left\|[K] - \omega^2 [M]\right\| = \{0\} \tag{3.2}$$

This algebraic equation, known as the characteristic equation, yields n possible positive real solutions known as the eigenvalues of the equation (3.2) which are the undamped natural frequencies of the system.

Substituting each natural frequency value in (3.1) and solving each of the resulting sets of equations for $\{\Psi\}$ we obtain n possible vector solutions $\{\Psi_j\}$ $(j = 1, 2, ..., n)$, known as the mode shapes of the system under analysis.

The complete free vibration solution is normally expressed in two $n\times n$ matrices

$$[\Lambda] = \begin{bmatrix} \omega_1^2 & 0 & \cdots & 0 \\ 0 & \omega_1^2 & \cdots & 0 \\ \vdots & \vdots & \ddots & \vdots \\ 0 & 0 & \cdots & \omega_n^2 \end{bmatrix} \tag{3.3}$$

and

$$[\Psi] = \begin{bmatrix} \{\Psi_1\} & \{\Psi_2\} & \cdots & \{\Psi_n\} \end{bmatrix} \tag{3.4}$$

which contain a full description of the dynamic characteristics of the structural system. Equations (3.3) and (3.4) constitute what is known as the Modal Model, i.e., they describe the system through its modal properties (natural frequencies and mode shapes). [Ψ] is commonly known as the modal matrix.

The mode shape vectors have very important properties known as the orthogonality properties which are described by

$$\{\Psi_i\}^T [M]\{\Psi_j\} = 0 \quad ; \quad \text{for } i \neq j \tag{3.5}$$

$$\{\Psi_i\}^T [K]\{\Psi_j\} = 0 \quad ; \quad \text{for } i \neq j \tag{3.6}$$

The matrix form of the latter equations is

$$[\Psi]^T [M][\Psi] = \left[m^* \right] \tag{3.7}$$

$$[\Psi]^T [K][\Psi] = \left[k^* \right] \tag{3.8}$$

with

$$k_j^* = \omega_j^2 m_j^*$$

where $[m^*]$ and $[k^*]$ are diagonal matrices known as the modal mass and modal stiffness matrix, respectively.

The amplitudes of the modal shape vectors are only relative values which may be normalized following any convenient procedure. The most common normalization scheme used in modal analysis is to normalize the modes with respect to the mass matrix $[M]$ as follows:

$$\phi_{ij} = \frac{\Psi_{ij}}{\sqrt{\{\Psi_i\}^T [M]\{\Psi_j\}}}$$

(3.9)

or

$$\phi_{ij} = \frac{\Psi_{ij}}{\sqrt{m_j}}$$

(3.10)

in which ϕ_{ij} is the i*th* normalized component of the j*th* modal vector. The orthogonality condition for the mass-normalized modal vectors is given by

$$\{\phi_i\}^T [M]\{\phi_j\} = 1 \qquad ; \text{for } i = j$$

(3.11)

$$\{\phi_i\}^T [K]\{\phi_j\} = \omega_j^2 \qquad ; \text{for } i = j$$

(3.12)

Therefore, the mass-normalized modal matrix orthogonality properties can be expressed as

$$[\Phi]^T [M][\Phi] = [I]$$

(3.13)

$$[\Phi]^T [K][\Phi] = [\Lambda]$$

(3.14)

where $[I]$ is the identity matrix.

In this research, it is assumed that damage in a structure will affect only the stiffness matrix and not the mass matrix in the eigenvalue problem formulation. This assumption is consistent with those used by Yuen (1985) and Pandey (1994).

3.2 DAMAGE EFFECT ON MODAL PARAMETERS

3.2.1 Simply Supported Beam

The free vibration analysis of a simply supported beam with and without damage is performed. Modal responses of the beam are generated using finite element models before and after damaging episode cases. The following dimensions and material properties are used for the beam: length $L=100$ *in* [1 *in=2.54 cm*], height of the cross section $H=4$ *in* , width of the cross section $b=2$ *in*, elastic modulus $E = 29000$ *ksi* [1ksi= 6.895 MPa] and mass density $\rho= 0.00073$ *lbm/ in³* [1 *lbm/ in³ = 0.0277 kg/cm³*]. For Finite Element Analysis purposes the beam is divided into 40 elements.

Here, six damage scenarios are investigated, as summarized in Table 3.1. In the first two cases damage is simulated by reducing the stiffness of assumed elements. In cases 3 to 6, damage is simulated in the form of cracks. The finite element model of the beam uses the stiffness matrix of the cracked element described in the Chapter II. The damage scenarios SD1 and SD2 (listed in Table 3.1) were simulated by reducing the stiffness of an element near the beam's mid-span. The damage cases SC1 and SC2 (listed in Table 3.1) correspond to a crack located near the mid-span. The remaining damage

cases SC3 and SC4 in the same table correspond to a multiple damage scenario and were simulated by introducing cracked elements at two different locations.

For each damage scenario, the dynamic characteristics (frequencies and mode shapes) before and after the damage were numerically evaluated, with programs coded in MATLAB®. The first five frequencies are listed in Table 3.2. According to the results in the table the simulated damage scenarios cause the first modal frequency to shift from 0.4% to 3.4 % of the undamaged frequency. Also, it can be noted that the change in the frequencies for the cases SC1 (single crack) and SC3 (two cracks) is practically the same. The decrease in the natural frequencies of the higher modes range from 0.01 to 2.33 % for the second mode, 0.38 to 4.15 % for mode 3, 0.008 to 0.54 % for mode 4, and 0.36 to 2.21 % for the last mode considered. Thus changes in natural frequencies cannot provide information about the location of structural damage. This conclusion is in agreement with the observations in the studies carried out by Salawu (1994), Pandey (1994) and Kim (2003).

Since the present study is based on the use of the flexural modes, only the translation degrees of freedom along the perpendicular axis to the elements (vertical DOFs in the beams and horizontal DOFs in the columns) were considered in the analysis. This was done because, in general, in experimental works rotations are not obtained because of the difficulty in their measurement.

It was assumed that the modal amplitudes were "read" at 9 locations equally spaced along the longitudinal axis of the beam. The first five displacement mode shapes

are compared in Figures 3.1 to 3.5 for the damage case SC2 (a single crack at the mid-span). All mode shapes considered in this study have been normalized with respect to the mass matrix. Figures 3.6 and 3.7 shows the first two undamaged and damaged mode shapes for the damage case SC4 (two cracks). It is observed from the figures that the amplitude changes in the mode shapes alone are not precise enough to locate the damaged element.

Table 3.1 Damage scenarios: simply supported beam.

Damage scenario	Damaged element	Stiffness reduction (%)	*a*/H
SD1	21 (~L/2)	25	-
SD2	21 (~L/2)	50	-
SC1	21 (~L/2)	-	0.1
SC2	21 (~L/2)	-	0.25
SC3	9(~L/5) , 21 (~L/2)	-	0.1
SC4	9(~L/5) , 21 (~L/2)	-	0.25

Table 3.2. Natural frequencies of the simply supported beam.

Damage	Natural Frequency (rad/sec)				
Scenario	Mode 1	Mode 2	Mode 3	Mode 4	Mode 5
Undamaged	226.8	907.1	2041.0	3628.4	5669.5
SD1	224.9	907.0	2024.7	3627.5	5626.2
SD2	221.3	906.9	1994.5	3625.7	5549.0
SC1	225.9	907.1	2033.2	3628.1	5648.7
SC2	221.2	906.9	1993.9	3626.1	5547.6
SC3	225.6	903.7	2026.8	3625.2	5647.9
SC4	219.2	886.0	1956.1	3608.7	5543.8
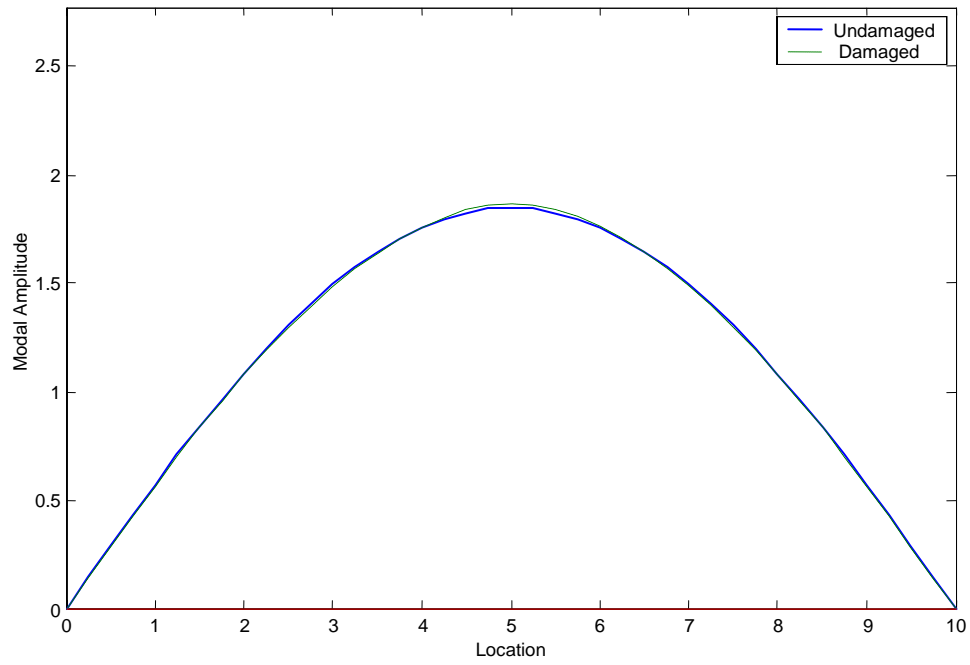
Figure 3.1. First mode of the simply supported beam for case SC2.
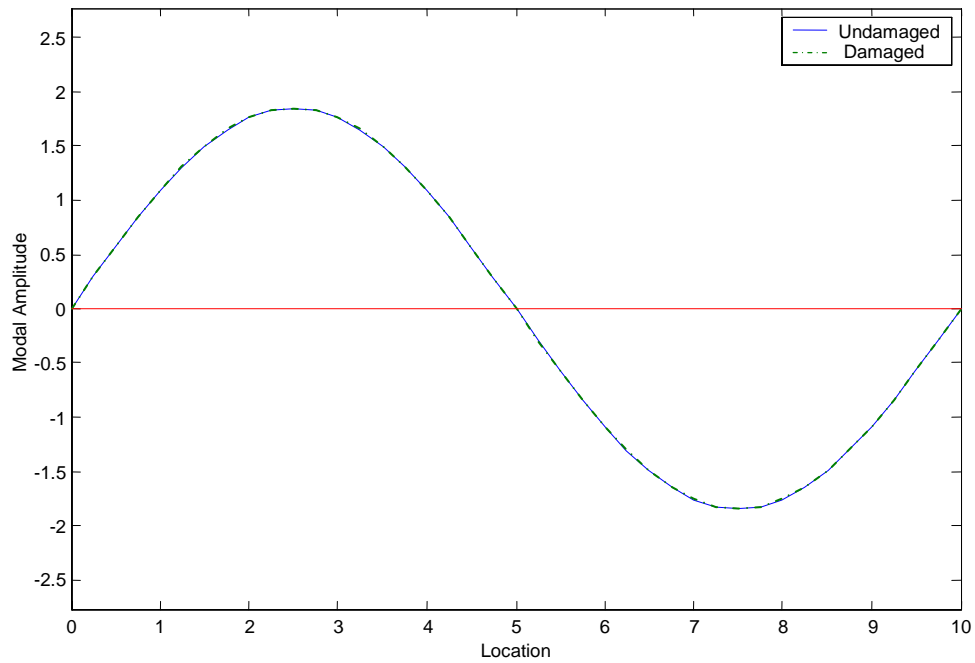
Figure 3.2. Second mode of the simply supported beam for case SC2.
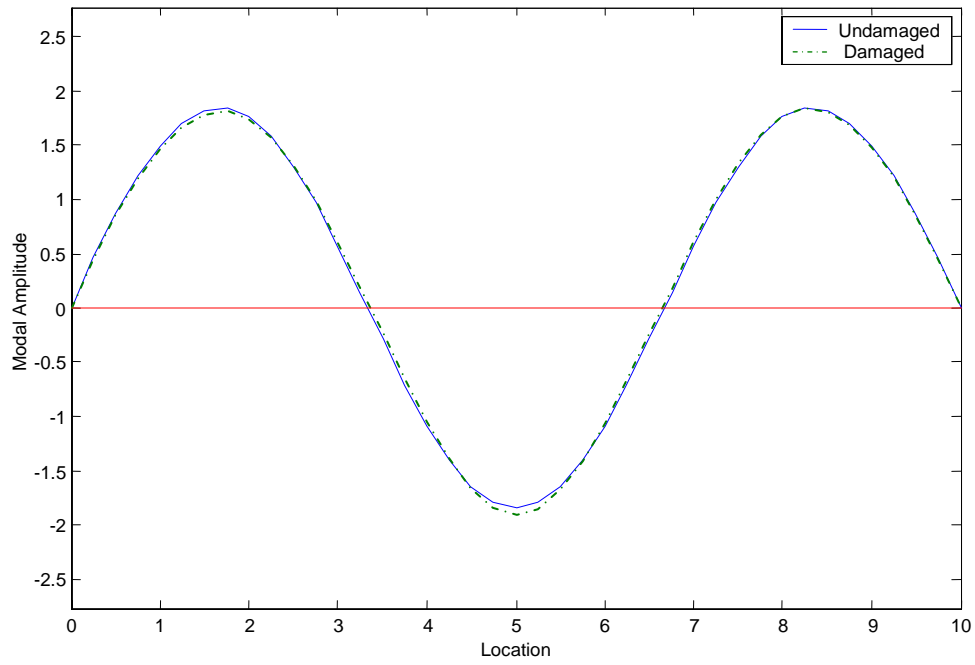
Figure 3.3. Third mode of the simply supported beam for case SC2.
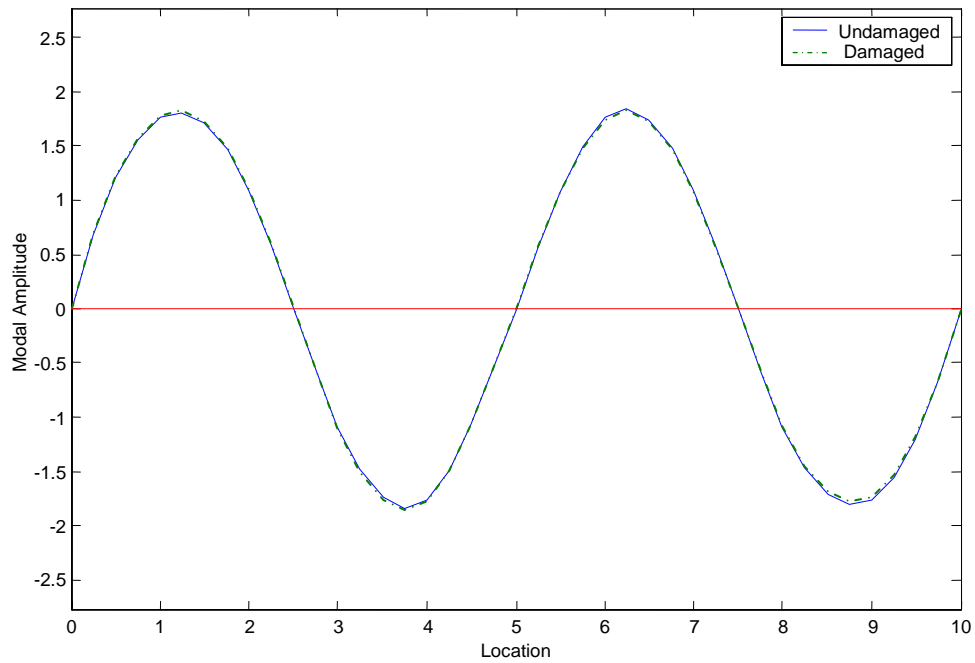
Figure 3.4. Fourth mode of the simply supported beam for case SC2.
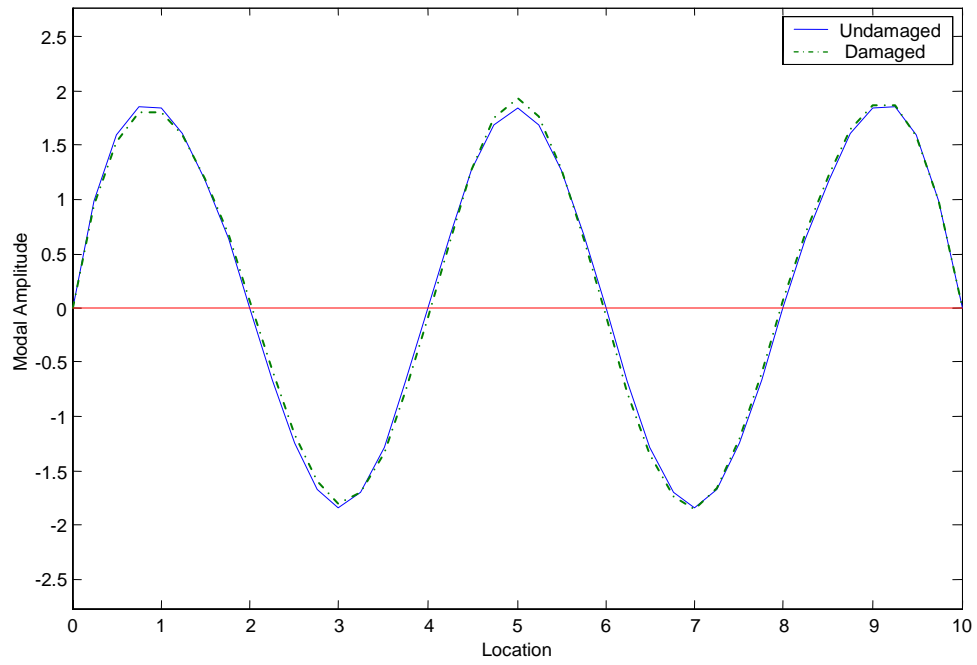
Figure 3.5. Fifth mode of the simply supported beam for case SC2.
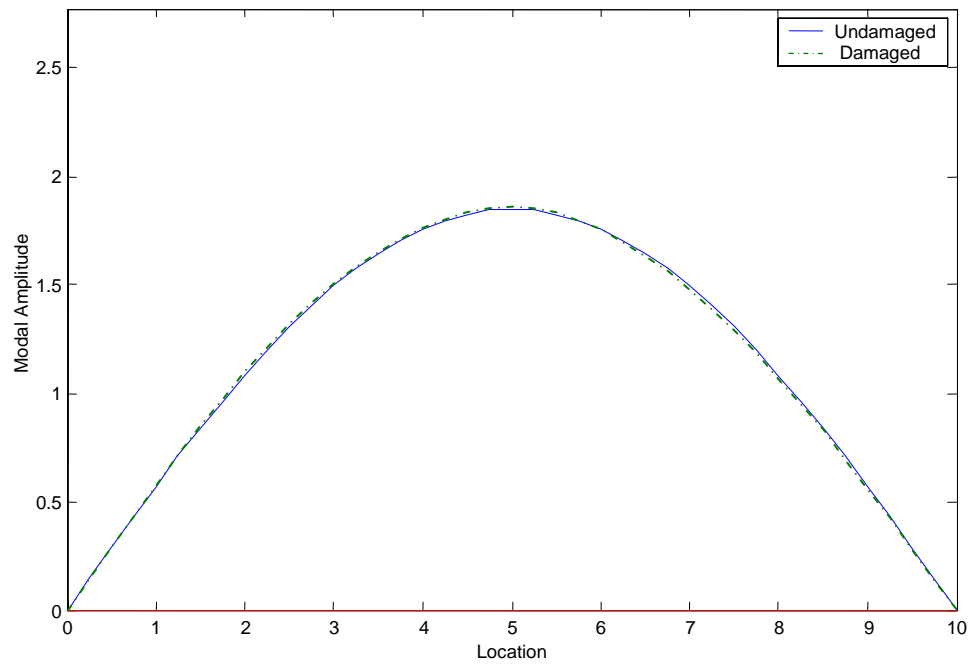
Figure 3.6. First mode of the simply supported beam for case SC4.
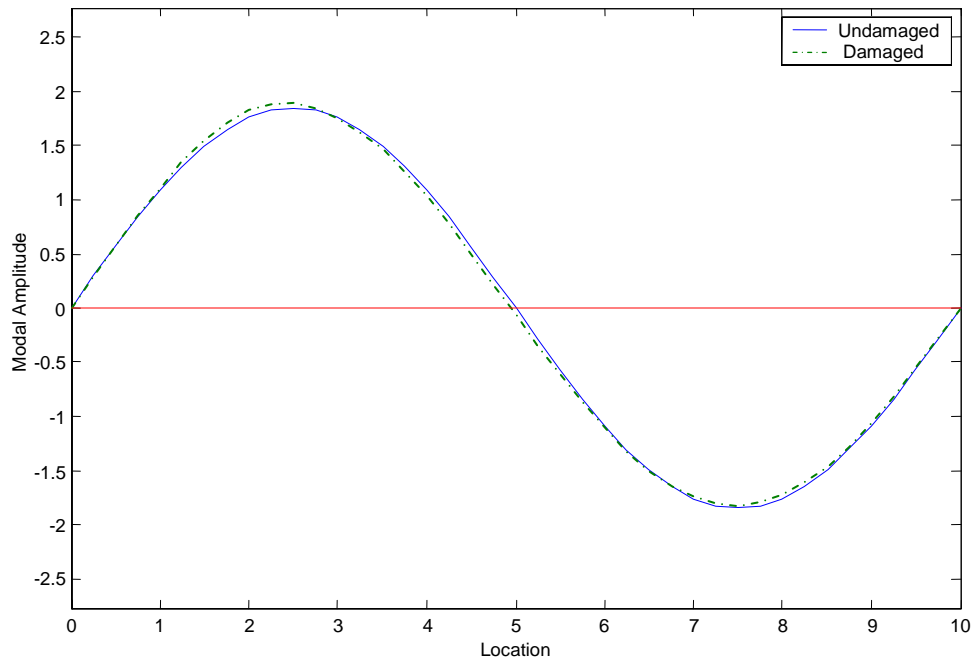
Figure 3.7. Second mode of the simply supported beam for case SC4.

3.2.2 Plane frame

The free vibration analysis of a plane frame with and without damage was performed. The modal quantities of the plane frame were numerically generated using finite element models without and with damage episodes, with routines coded in MATLAB®. The dimensions of the plane frame are listed in Table 3.3. Figure 3.8 illustrates the model of the frame. For modal analysis purposes, the beam and the columns were divided into 40 elements. Six damage scenarios were investigated and are summarized in Table 3.4. In the first two cases the damage is simulated by a crack inflicted at the right column. The damage scenarios PC3 and PC4 (listed in Table 3.4) consist of a single crack near the mid-span of the beam. The remaining damage cases

correspond to two cracks inflicted at two different locations. The crack size was changed during the analysis.

The modal amplitudes were extracted at 19 locations equally spaced along the longitudinal axis of the beam and the right column of the frame. As in the case of the beam, the dynamic characteristics (frequencies and mode shapes) before and after the damage were calculated for each damage scenario. The first five natural frequencies are listed in Table 3.5. It can be observed that the highest variation for the first modal frequency caused by the simulated damage scenarios was 1.7 %. Also, it can be noted that there is no variation in the frequencies for the cases PC3 and PC4. The highest reduction for mode 2, 3, 4 and 5 were 1.4, 1.1, 1.2 and 8.3 %, respectively.

The first three undamaged and damaged modal amplitudes of the frame beam are compared in Figures 3.9 to 3.11 for the damage case PC6 (multiple damage location). The first two undamaged and damaged modal amplitudes of right column of the frame are compared in Figures 3.12 and 3.13 for the damage case PC2. As in the case of the simply supported beam, it is observed from the figures that the amplitude changes in the mode shapes are not adequate to locate the damaged zone of the frame.

Table 3.3. Dimensions and material properties: plane frame.

Bay width (*L*-[*in**])	96
Column height (*Hc*-[*in*])	96
Cross section width (*b*-[*in*])	2
Cross section depth (*H*-[*in*])	5
Elastic modulus *E* [*ksi*$^+$]	29000
Mass density ρ [*lbm/ in*^{3}]**	0.00073

*1 in=2.54 cm, $^+$1ksi=6.895 MPa , **1 *lbm/ in*^{3} = 0.0277 *kg/cm*^{3}

Table 3.4 Damage scenarios: plane frame.

Damage scenario	Damaged member	Damaged element	*a*/H
PC1	Right column	4 (From col. base)	0.1
PC2	Right column	4 (From col. base)	0.2
PC3	Beam	21 (~L/2)	0.1
PC4	Beam	21 (~L/2)	0.2
PC5	Beam	21, 36	0.1
PC6	Beam	21,36	0.2

Table 3.5. Natural frequencies: plane frame

Damage	Natural Frequency (rad/sec)				
Scenario	Mode 1	Mode 2	Mode 3	Mode 4	Mode 5
Undamaged	99.8	394.3	646.4	697.9	1512.6
PC1	99.5	393.9	645.2	697.2	1511.8
PC2	98.1	392.0	639.3	694.4	1507.7
PC3	99.8	391.7	645.8	693.7	1389.7
PC4	99.8	388.7	645.8	691.5	1389.6
PC5	99.7	391.7	645.1	693.3	1388.9
PC6	99.4	388.7	642.9	689.8	1386.4
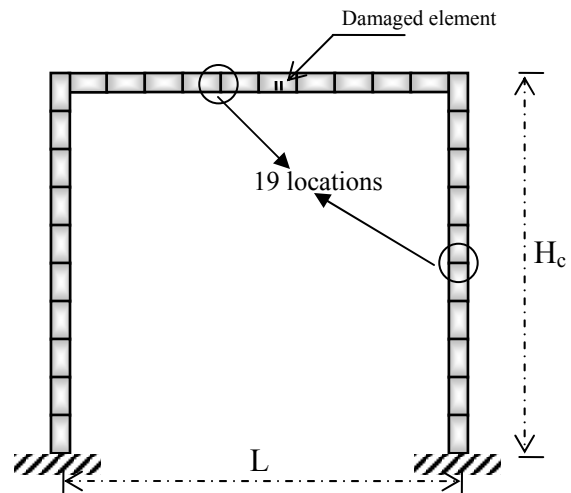
Figure 3.8 Plane frame model.
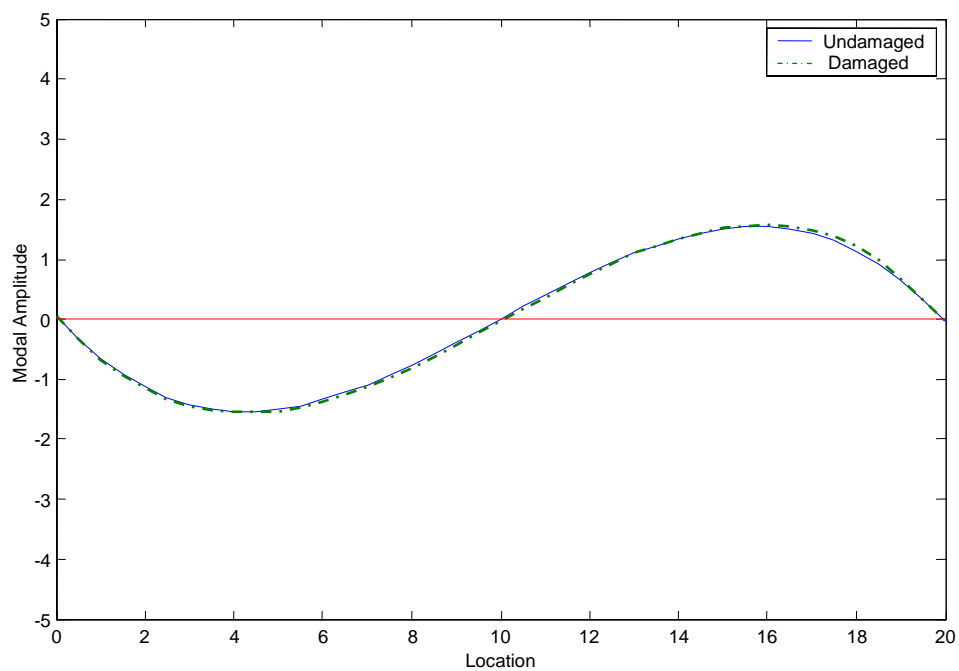
Figure 3.9. First mode of the frame beam for case PC6.
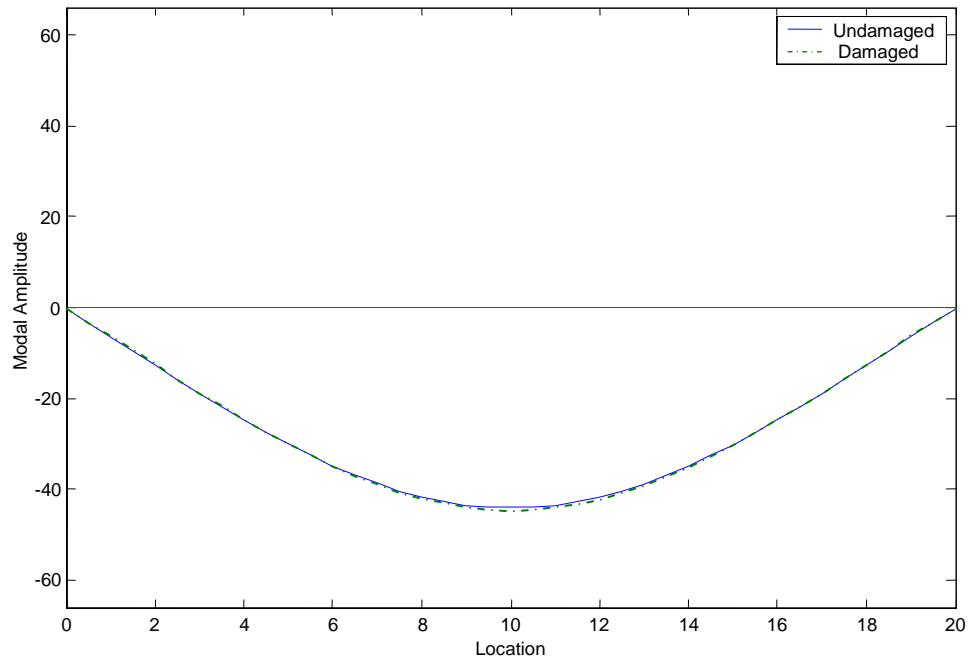
Figure 3.10. Second mode of the frame beam for case PC6.
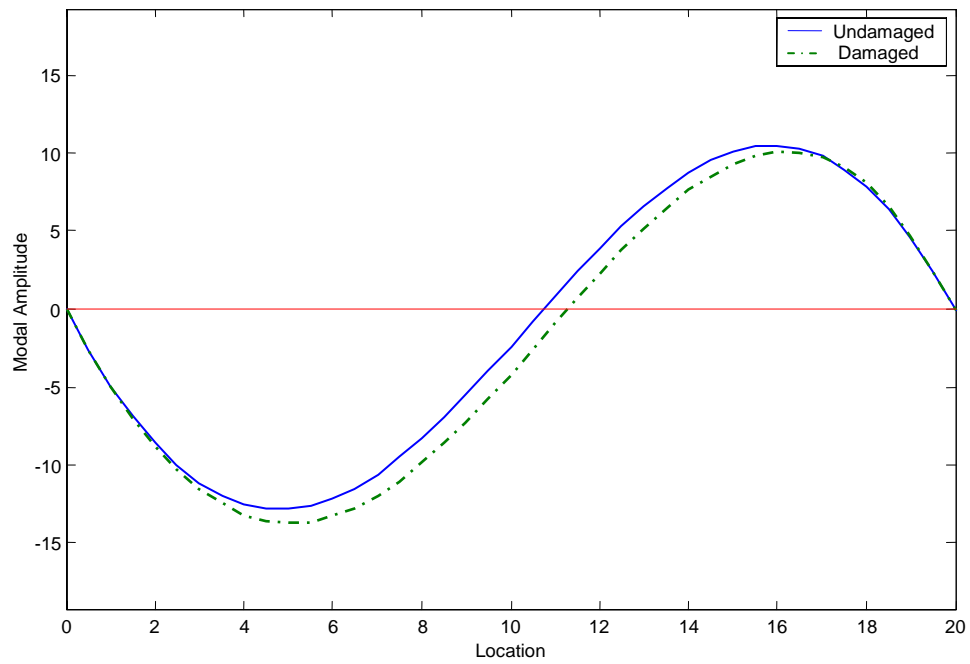
Figure 3.11. Third mode of the frame beam for case PC6.
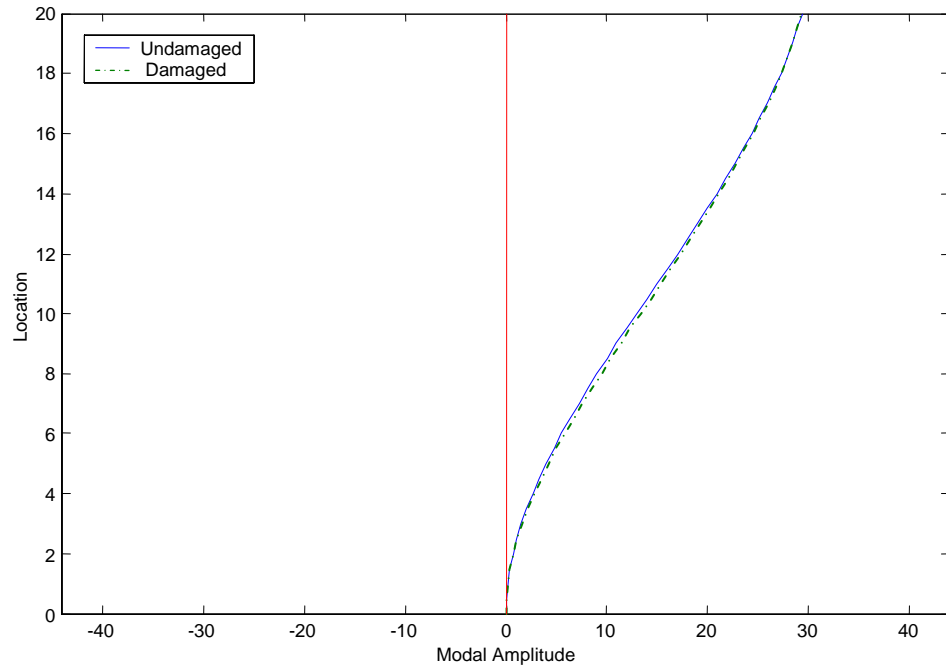
Figure 3.12. First mode of the plane frame for case PC2.
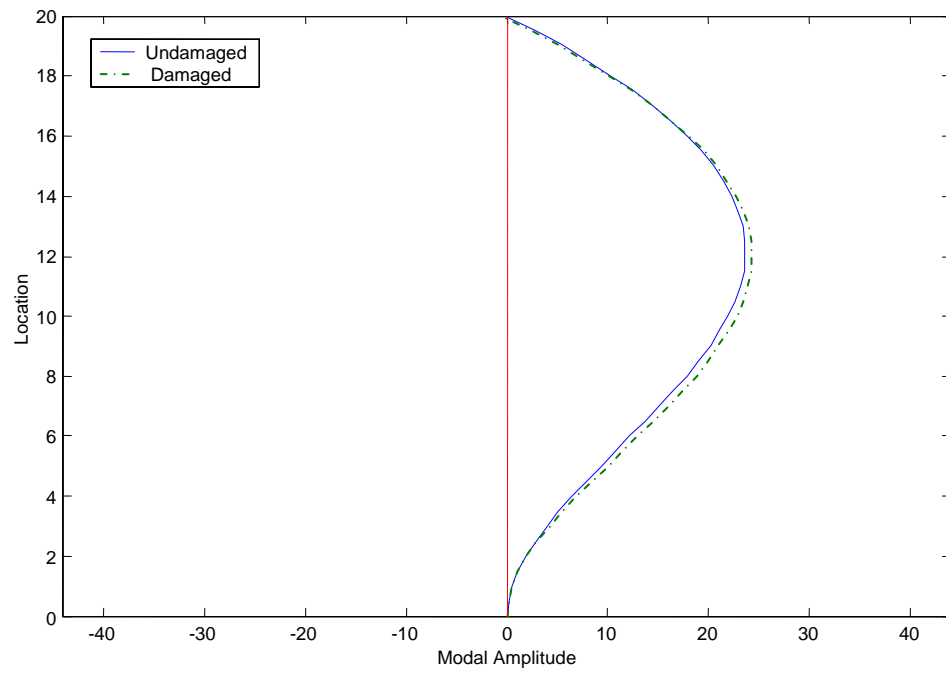
Figure 3.13. Second mode of the plane frame for case PC2.

CHAPTER IV

METHODS BASED ON CHANGES IN MODE SHAPES AND FREQUENCIES

4.1 INTRODUCTION

As mentioned in the previous chapter, in theory it is possible to determine the presence of cracks or damage in a structure from the changes in its natural frequencies. The methods using frequencies only, however, have some limitations. The frequency changes may not be sufficient to locate the precise position of the damage, since similar defects at different places may cause similar amount of frequency changes. In addition, significant damage may cause very small changes in natural frequencies, particularly for larger structures. Because of the small values, these changes may go undetected due to measurement errors (Kim et al. 2003). Moreover, the changes in frequencies cannot distinguish between damage at symmetrical locations in a symmetric structure. In contrast, vibration mode shapes are more strongly influenced by local damage and thus they offer a better means of locating damage (Salawu 1994).

In this chapter, several structural damage identification methods based on changes in displacement mode shapes are presented. Numerical simulations are performed to compare the effectiveness of the existing procedures to locate damage.

4.2 EIGENPARAMETER METHOD

The eigenparameter method was proposed by Yuen (1985) to detect the presence and location of damage in a cantilever beam. It was also evaluated by Salawu and Williams (1993) and Dong et al. (1994). This method utilizes only mode shape data. It is based on the premise that the mode displacements associated with each of the dynamic degrees of freedom would be affected differently by the presence of damage and the changes in the mode shapes should reflect the location and extent of the damage.

The parameters used are the frequencies and mode shapes associated with the eigenvalue problem of the undamaged structure,

$$\left([K] - \lambda_i [M] \right) \{\phi\}_i = 0 \tag{4.1}$$

and the damaged structure

$$\left([K^*] - \lambda_i^* [M] \right) \{\phi^*\}_i = 0 \tag{4.2}$$

A parameter that accounts for the changes in the frequencies and mode shapes of the structure is proposed to be used for damage detection. For the i-*th* mode shape, the eigenparameter is defined by

$$\{U\}_i = \frac{\{\phi^*\}_i}{\omega_i^{*2}} - \frac{\{\phi\}_i}{\omega_i^2} \tag{4.3}$$

The square of the natural frequency (the eigenvalue) is chosen as a normalization factor because it is another dynamic property affected by the introduction of damage in the structure.

4.3 NUMERICAL SIMULATIONS

The simply supported beam and the portal frame described in Chapter III were used as test structures to investigate the performance of the eigenparameter as damage indicator. It was assumed that the beam and frame were subjected to the different damage scenarios presented in Chapter III.

- Simply-supported beam.

The values of the eigenparameter for the damage scenarios SD1 to SC4 are illustrated in Figures 4.1 to 4.6. The eigenparameter was calculated for the first two mode shapes. The parameter for the first mode shows the largest change at the location of the damage, i.e. the peak value occurs in the damaged region. Also at this location the slope changes sign. The damage scenarios SD1, SD2, SC1 and SC2 correspond to a single crack at the mid-span. It can be observed that the absolute value of the parameter increases with an increase in the severity of damage. The eigenparameter for the second mode displays a positive peak at the location of the damage but also other two negative

peaks. These two changes are of the same magnitude than the peak value at L/2, thus indicating a wrong location of damage. In the cases of two cracks (cases SC3 and SC4 in Figures 4.5 and 4.6), the method can locate the damage at the mid-span. As it can be observed the method was not able to clearly indicate simultaneously the location of the two damaged zones of the beam.
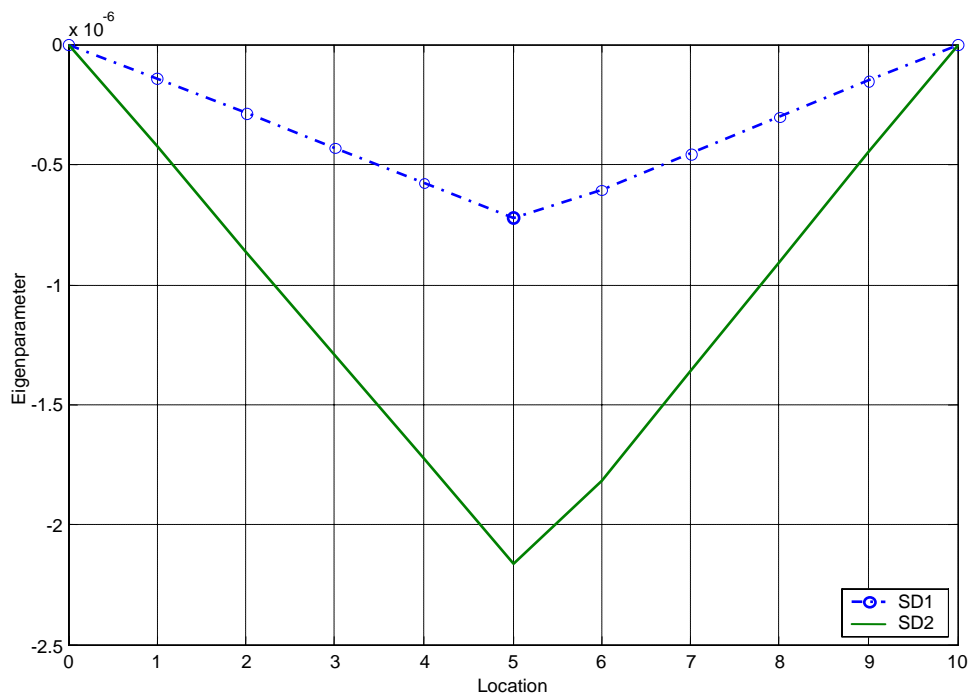
Figure 4.1 Eigenparameter for the first mode of the beam with damage scenarios SD1 and SD2.
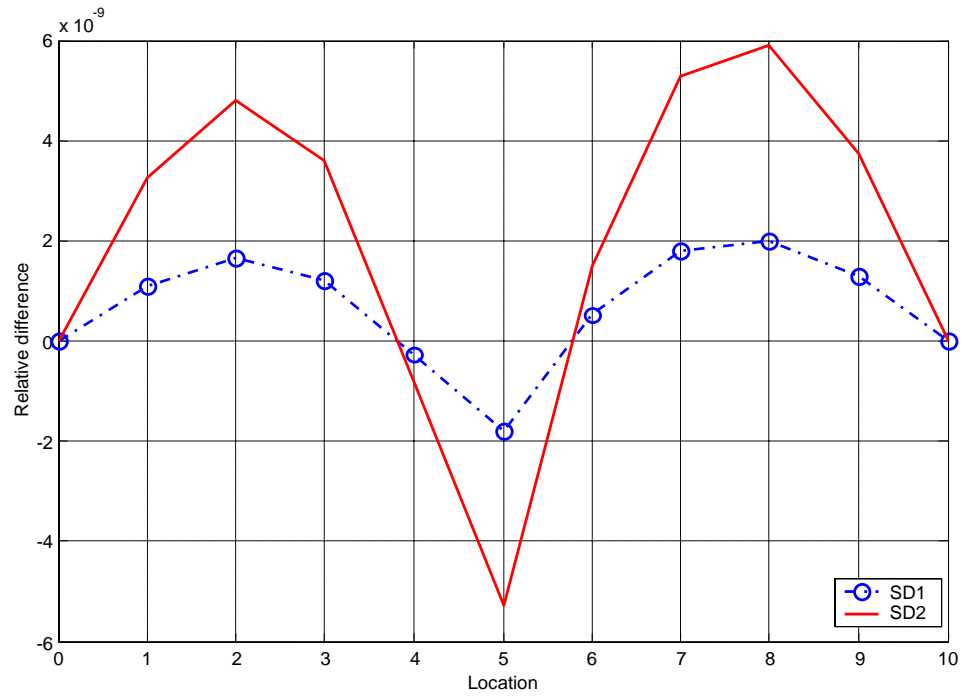
Figure 4.2 Eigenparameter for the second mode of the beam with damage scenarios SD1 and SD2.
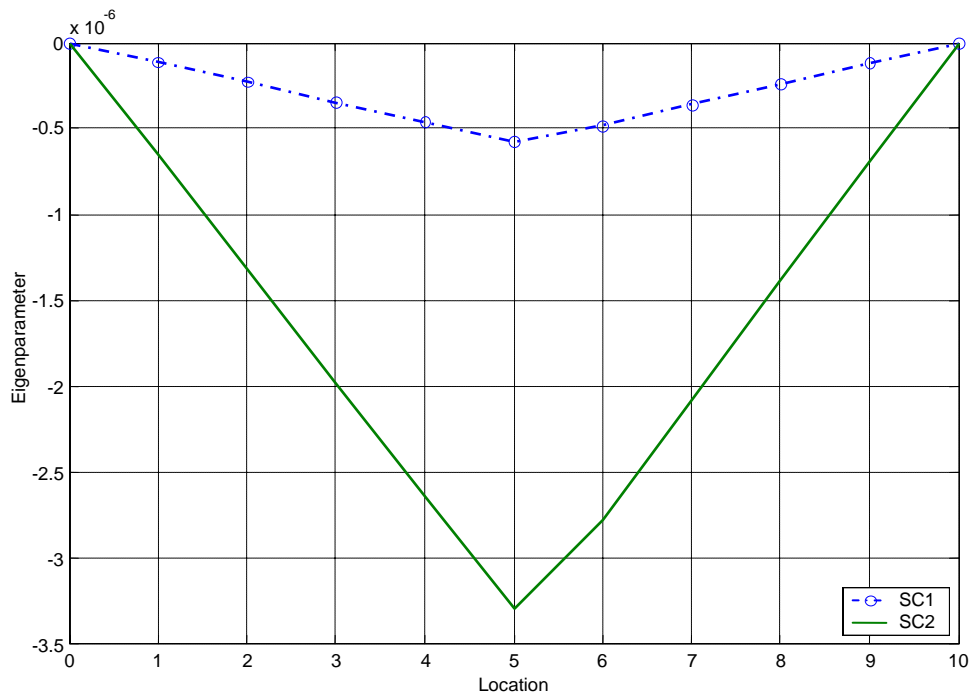
Figure 4.3 Eigenparameter for the first mode of the beam with damage scenarios SC1 and SC2.
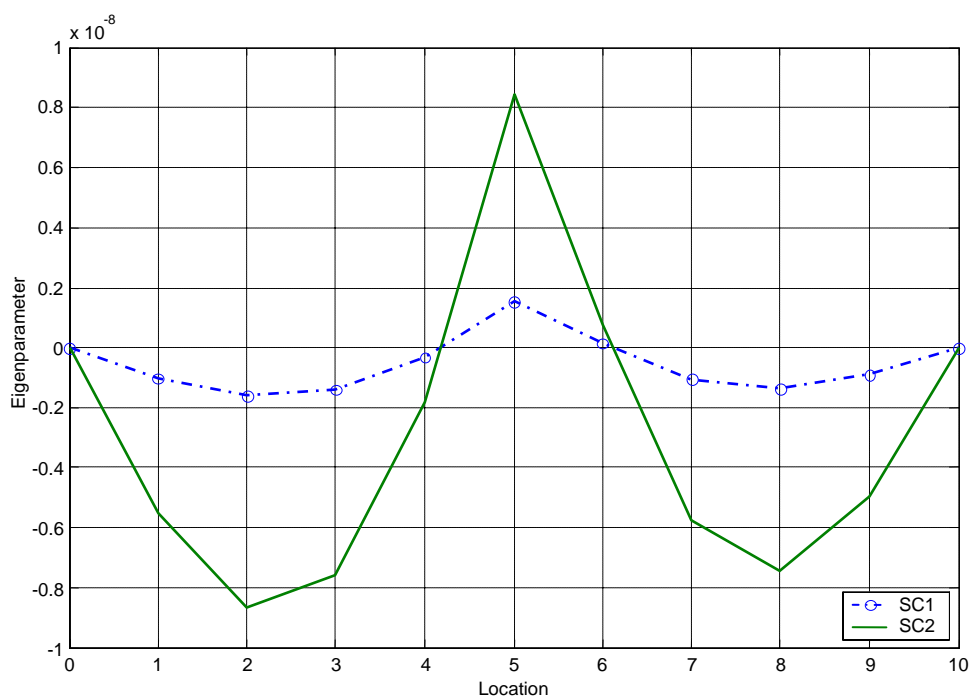
Figure 4.4 Eigenparameter for the second mode of the beam with damage scenarios SC1 and SC2.
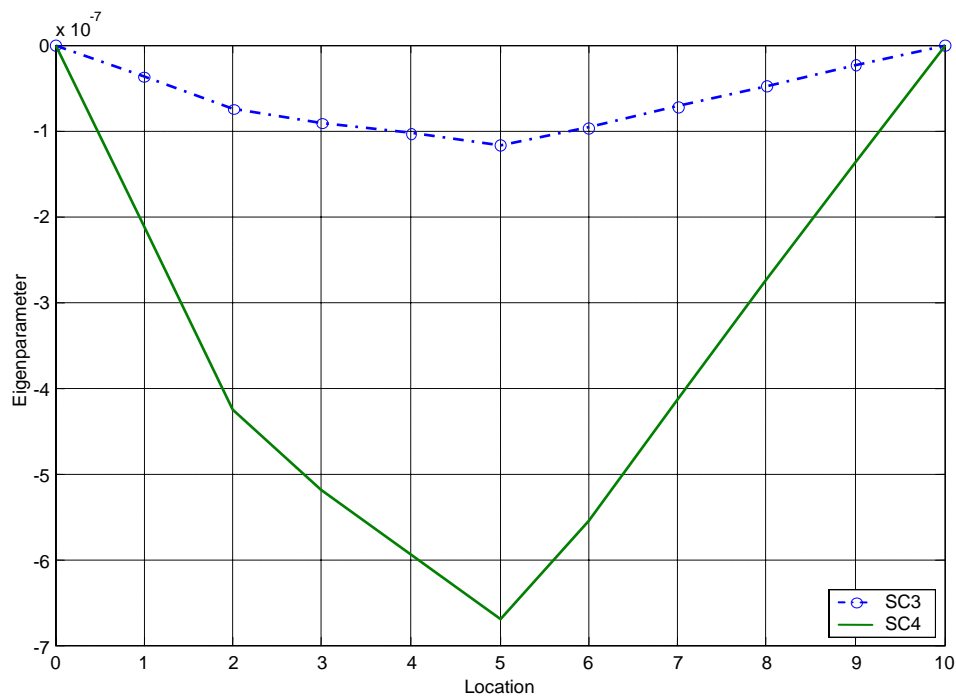
Figure 4.5 Eigenparameter for the first mode of the beam with damage scenarios SC3 and SC4.
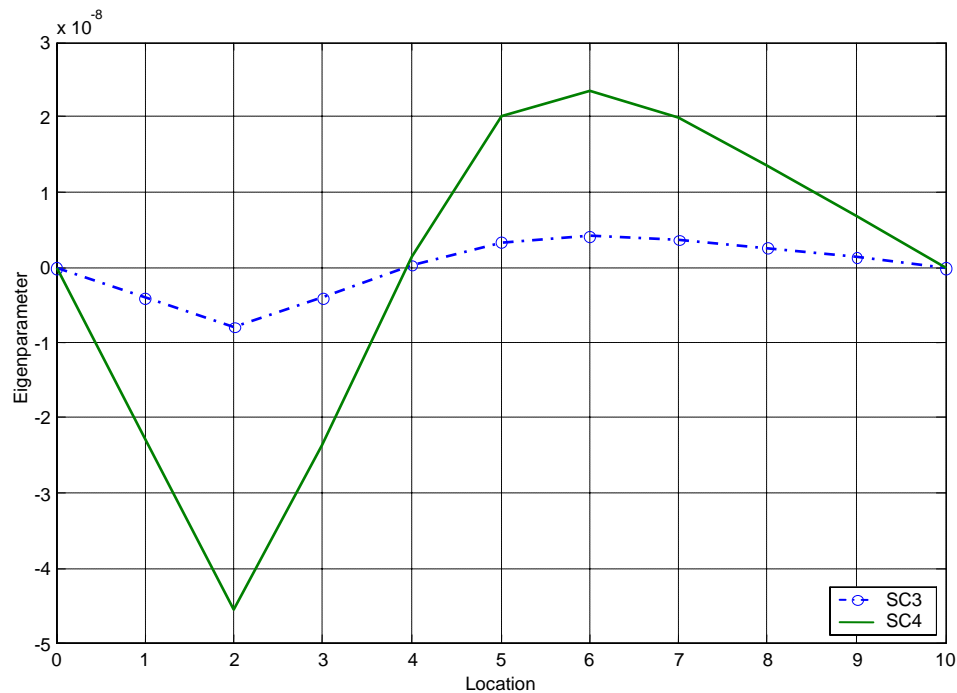
Figure 4.6 Eigenparameter for the second mode of the beam with damage scenarios SC3 and SC4.

- Plane frame

The values of the eigenparameter for the damage scenarios PC1 to PC6 in the plane frame are illustrated in Figures 4.7 to 4.12. For each damage case, the eigenparameter for the first two vibration modes are displayed. In the damage cases PC1 and PC2, it is not clear which is the location of the damage predicted by the method. This is so because the peak in the eigenparameter is spread over part of the column length. In the damage scenarios PC3 to PC6, a clear maximum value of the eigenparameter occurs at the damaged region and thus the localization of the crack is straightforward. In the two cases of multiple damage scenarios (PC5 and PC6 in Figures 4.11 and 4.12), the eigenparameter was able to indicate damage at one location.
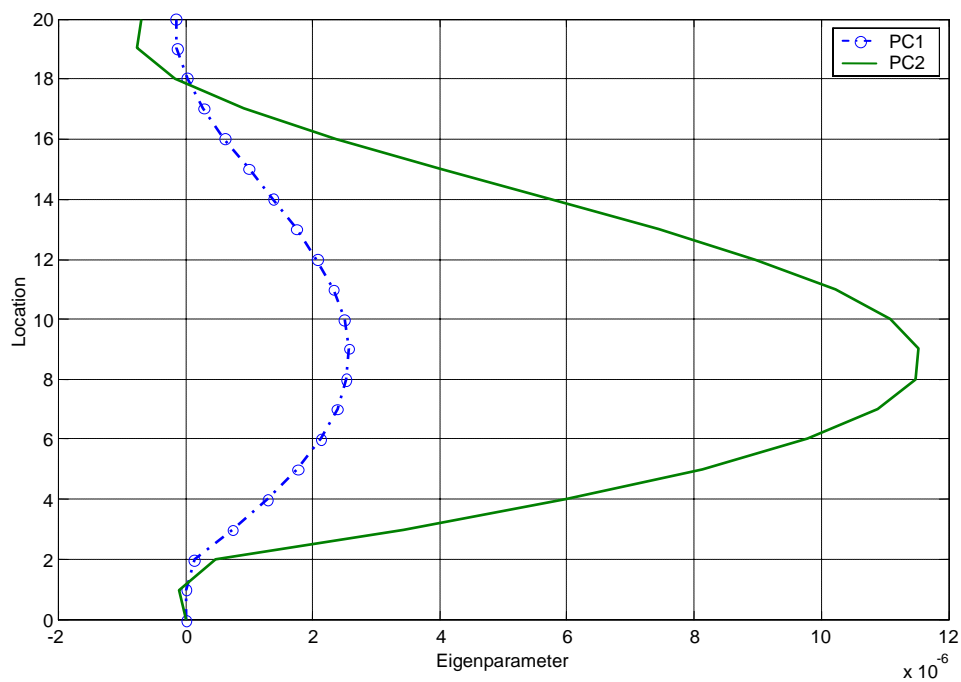
Figure 4.7 Eigenparameter for the first mode of the frame with damage scenarios PC andPC2.
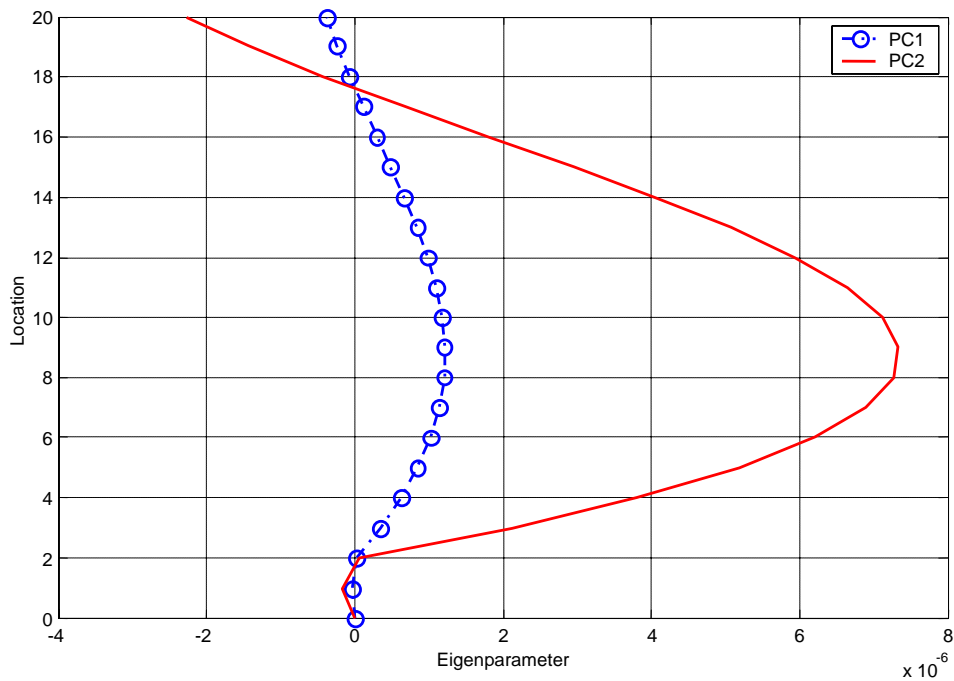
Figure 4.8 Eigenparameter for the second mode of the frame with damage scenarios PC1 and PC2.
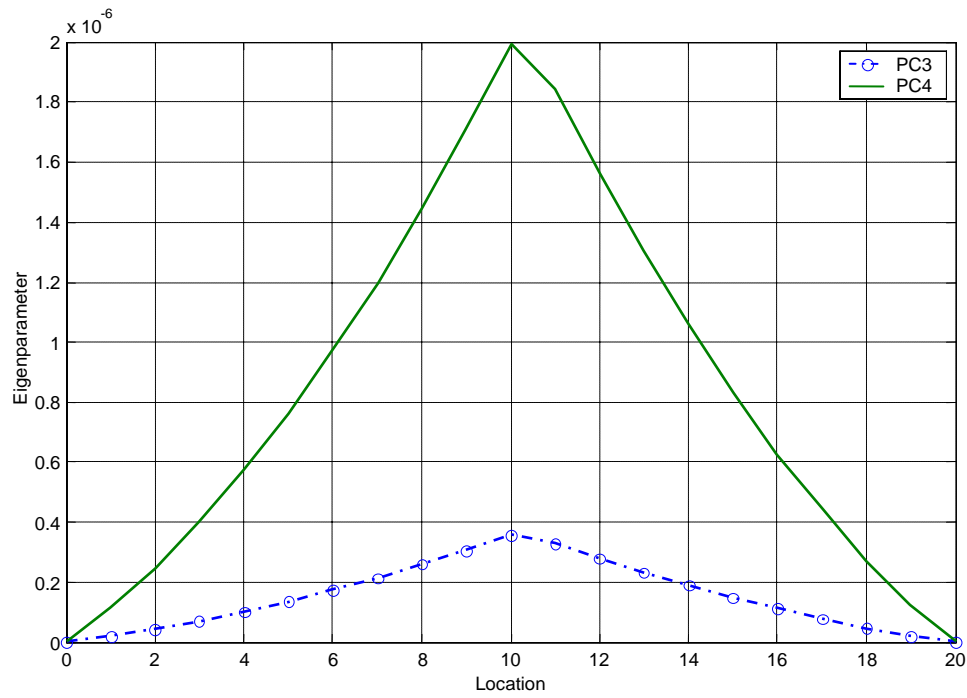
Figure 4.9 Eigenparameter for the first mode of the frame with damage scenarios PC3 and PC4.
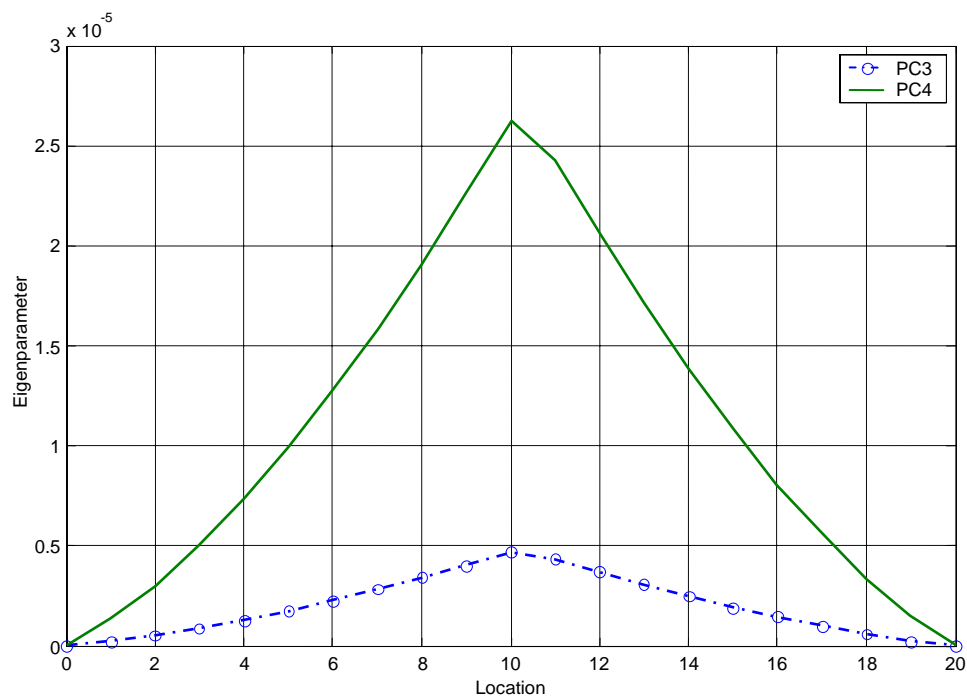
Figure 4.10 Eigenparameter for the second mode of the frame with damage scenarios PC3 and PC4.
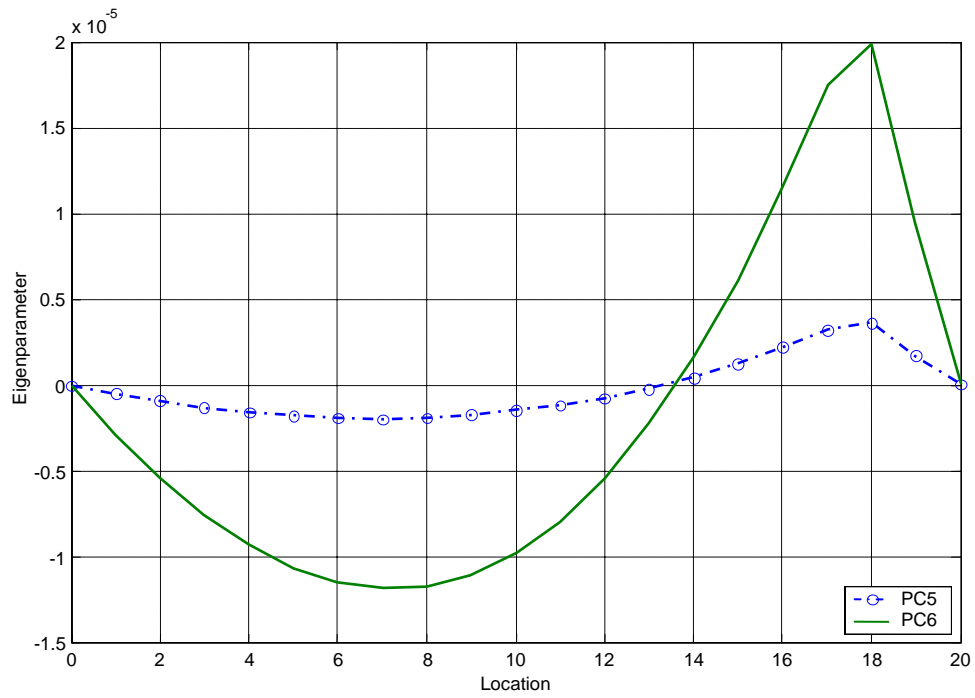
Figure 4.11 Eigenparameter for the first mode of the frame with damage scenarios PC5 and PC6.
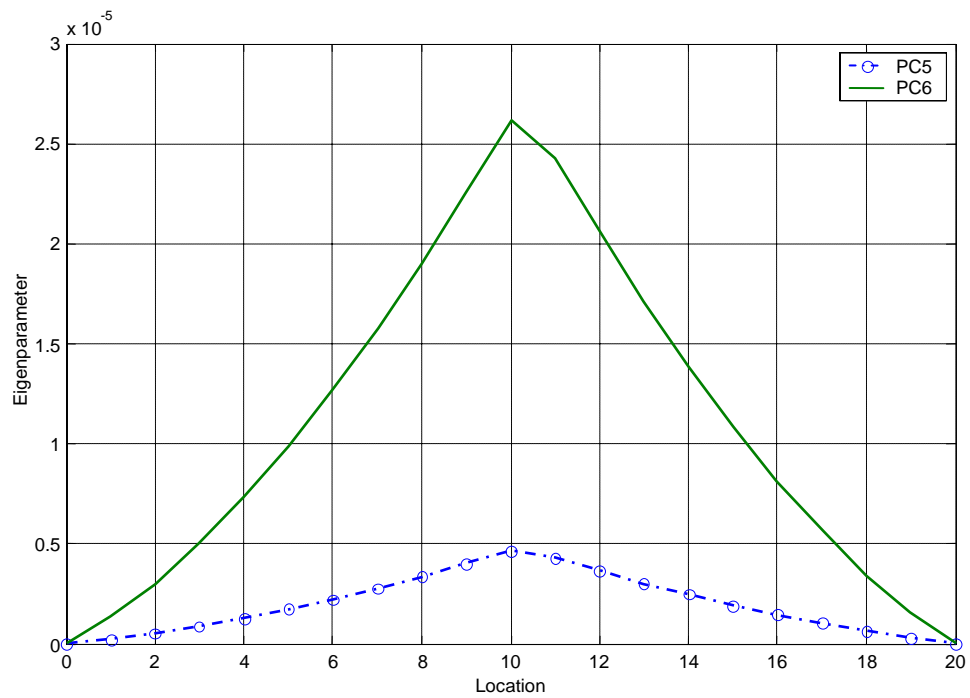
Figure 4.12 Eigenparameter for the second mode of the frame with damage scenarios PC5 and PC6.

4.4 MODE SHAPE RELATIVE DIFFERENCE METHOD.

In this formulation, a graphical comparison of the displacement mode shapes is used as an indicator of the damage location. The parameter used is the relative difference (RD) between the mode shapes for the undamaged and damaged structure. For the i-*th* mode shape the parameter is a vector defined as (Fox 1992):

$$\{RD\}_i = \frac{\{\phi\}_i - \{\phi^*\}_i}{\{\phi\}_i} \qquad (4.4)$$

In theory a plot of the vector {RD} as a function of the measurement locations should show a definite trend with distinct discontinuity at the damage locations. The displacement mode shapes most affected by the damage are more likely to indicate the location of the damaged regions of the structure.

4.5 NUMERICAL SIMULATIONS

The relative difference between the mode shapes of the undamaged and damaged structures are applied to find the locations of the cracks in the simply-supported beam and the plane frame considered before. The same damage scenarios described in Chapter III were simulated in the two structures.

- Simply-supported beam

The values of the relative difference for the first two mode shapes and for damage scenarios SD1 to SC4 are graphically presented in Figures 4.13 to 4.18. For the second mode, to avoid division by zero because a node of the mode is localized at 0.5L, the difference between the modes has been normalized with respect to the maximum absolute value of the undamaged mode shape. For the first mode of the beam with a single crack (cases SD1, SD2, SC1 and SC2) there is a negative peak at the location of the damage and there are other two peaks near the ends. Therefore, the localization of the damage cannot be clearly identified. The situation is even worse for the two cases of multiple damage (SC3 and SC4 in Figures 4.17 and 4.18): the method cannot locate the damaged zones in the beam because the width of the peaks is large and not all of them are at or near the cracks.

- Plane frame

The values of the relative difference between the modes of the original and damaged structure for damage scenarios PC1 to PC6 are shown in Figures 4.19 to 4.24. The values of the parameter RD were calculated for the first two mode shapes. In the damage cases PC1 and PC2, there is a peak near the damaged element (location 2). In the damage scenarios PC3 to PC4, the maximum value of the parameter occurs at the damaged region of the frame's beam. In Figures 4.21 and 4.23 the mode difference was normalized with respect to the maximum absolute value of the mode shape of the undamaged system. For the cases of multiple damage scenarios PC5 and PC6 illustrated

in Figures 4.23 and 4.24, the relative difference parameter showed a performance similar to the eigenparameter method.
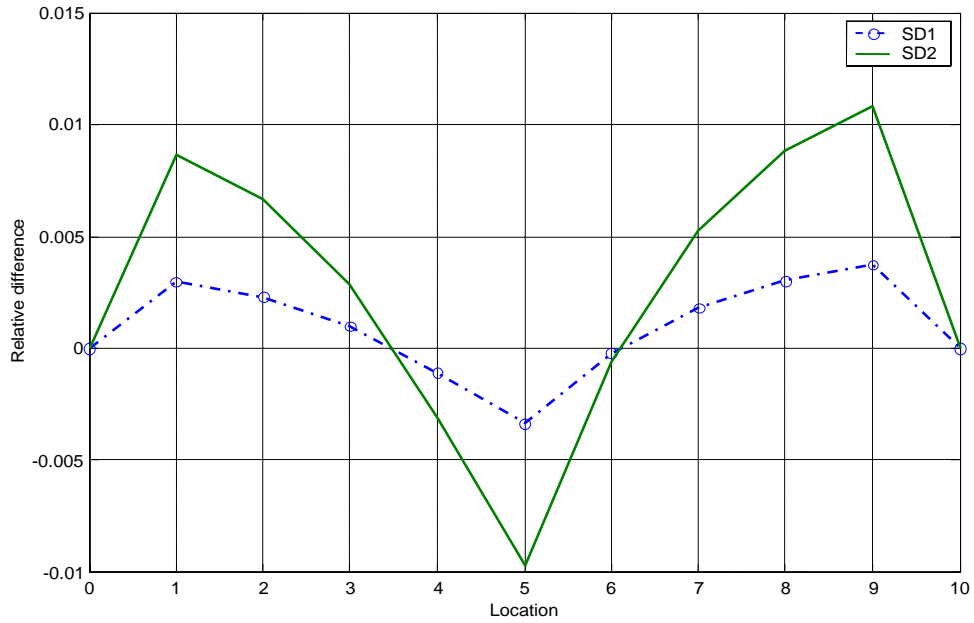
Figure 4.13 Relative difference for the first mode of the beam with damage scenarios SD1 and SD2.
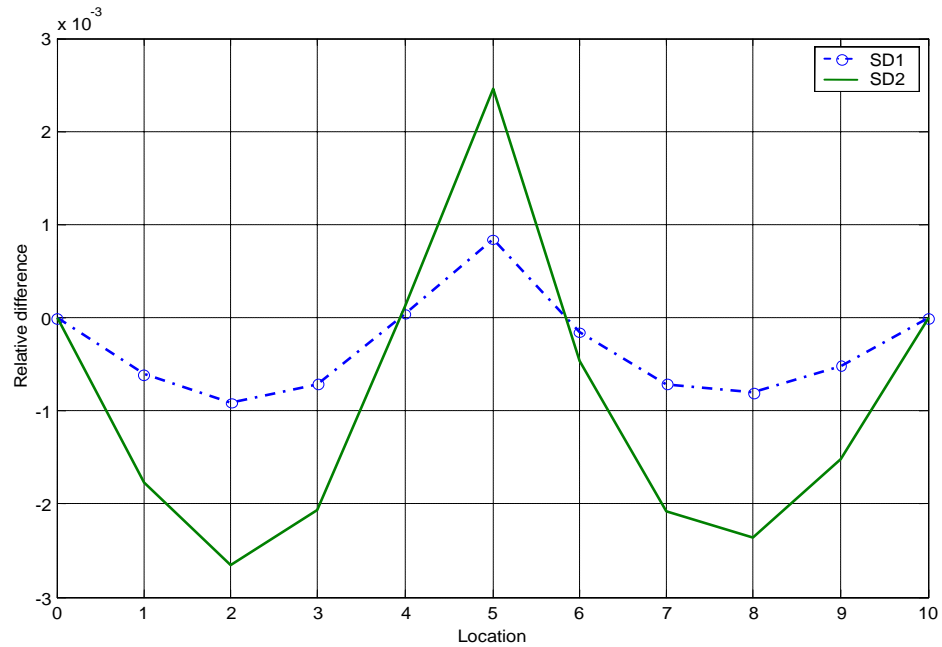
Figure 4.14 Relative difference for the second mode of the beam with damage scenarios SD1 and SD2.
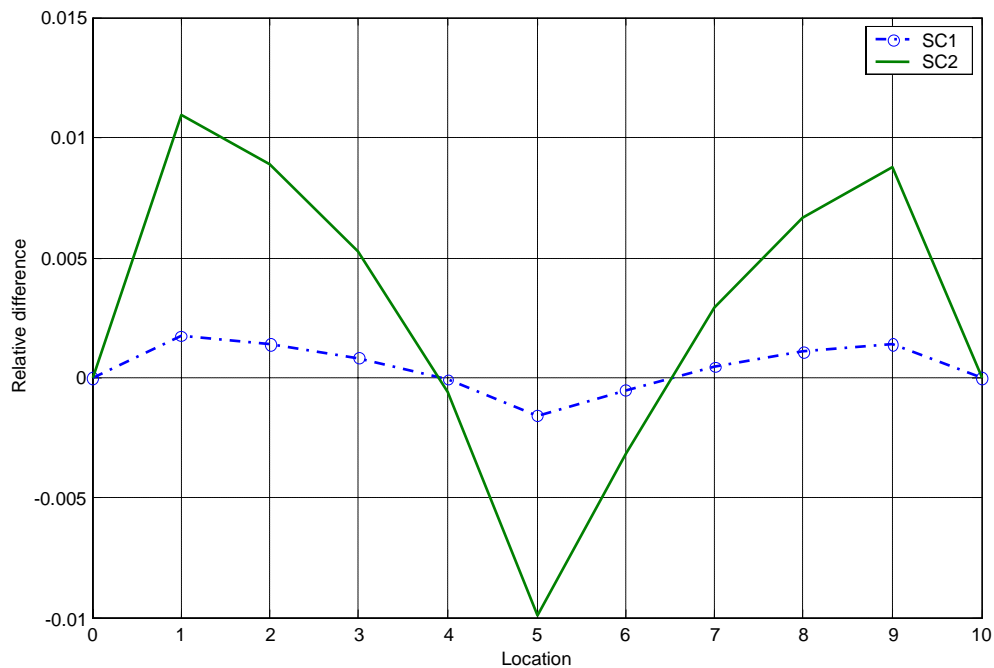
Figure 4.15 Relative difference for the first mode of the beam with damage scenarios SC1 and SC2.
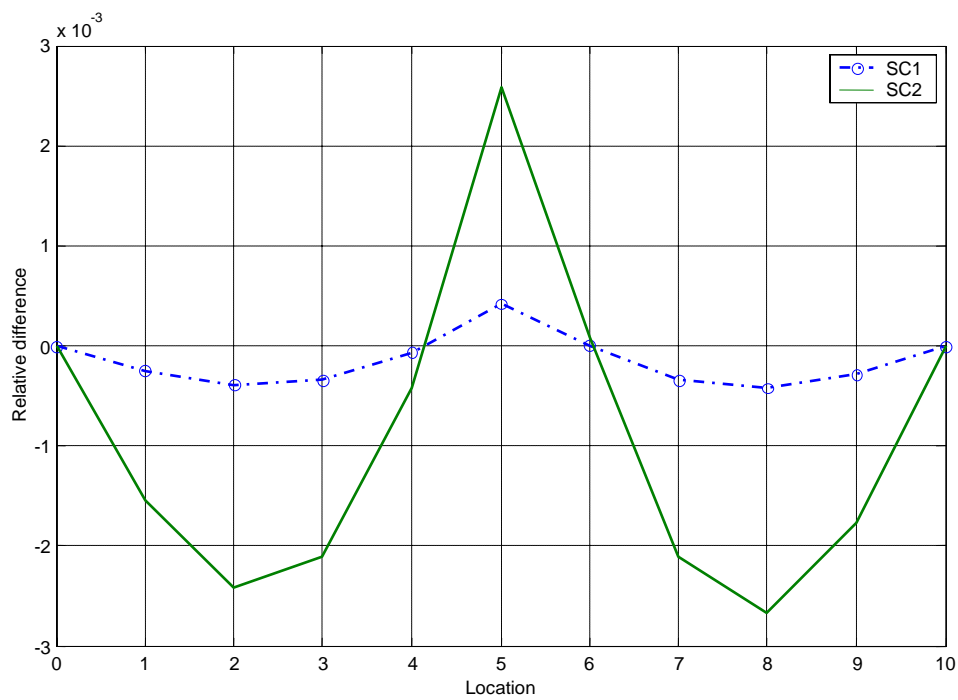
Figure 4.16 Relative difference for the second mode of the beam with damage scenarios SC1 and SC2.
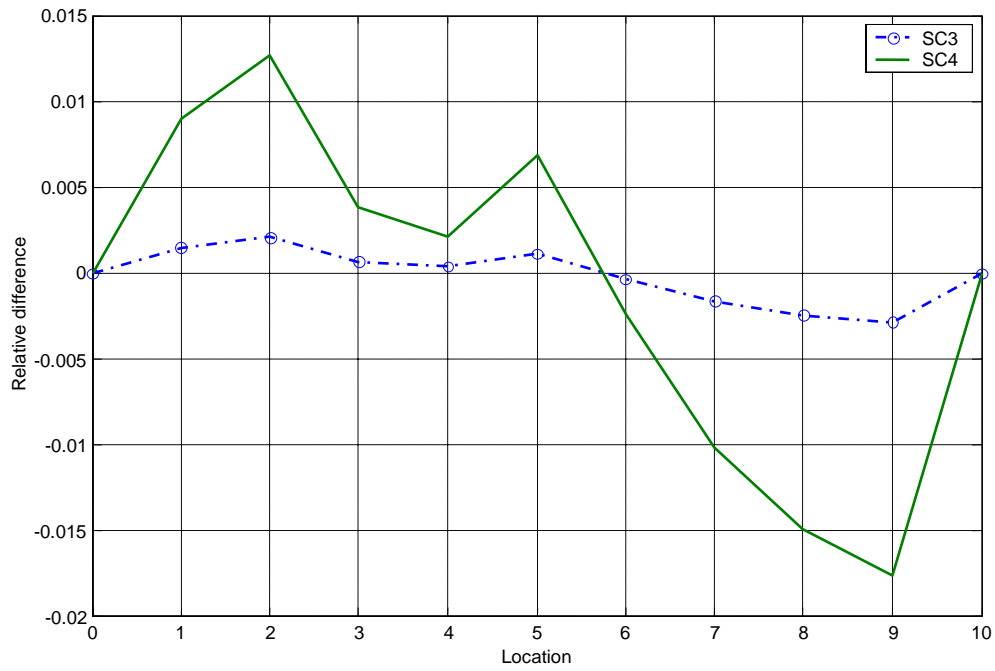
Figure 4.17 Relative difference for the first mode of the beam with damage scenarios
SC3 and SC4.
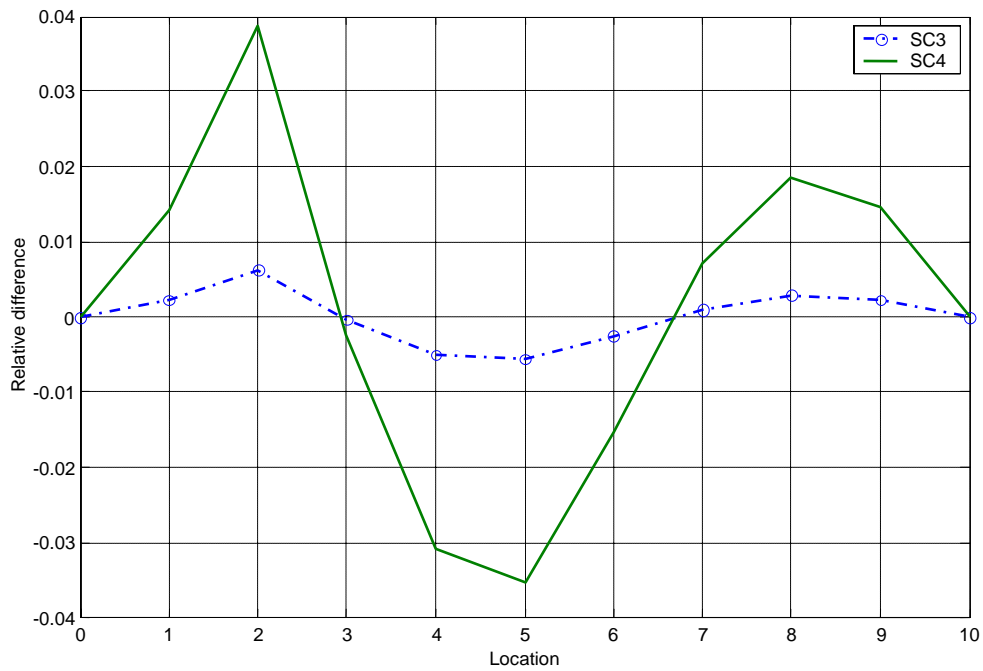
Figure 4.18 Relative difference for the second mode of the beam with damage scenarios
SC3 and SC4.
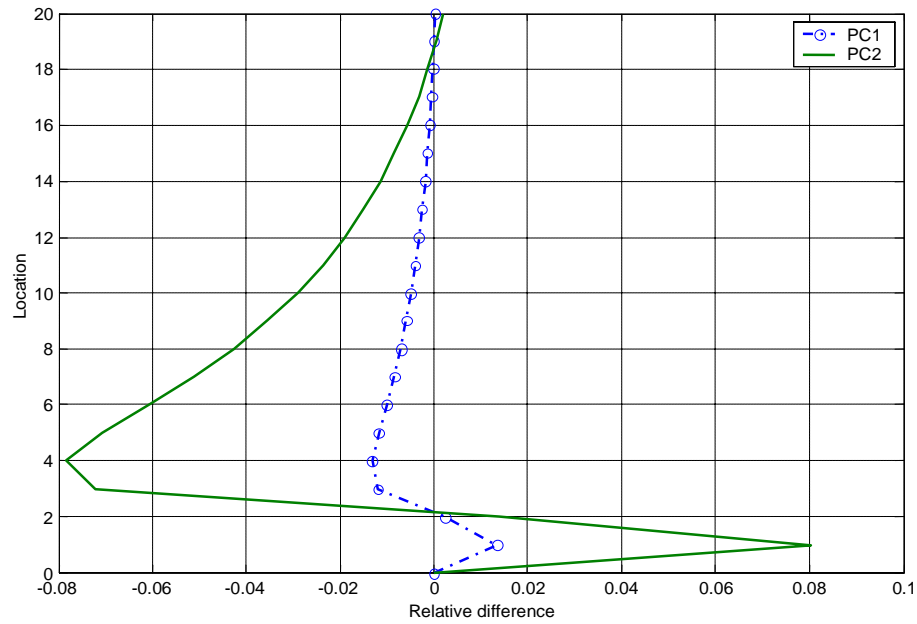
Figure 4.19 Relative difference for the first mode of the frame with damage scenarios PC1 and PC2.
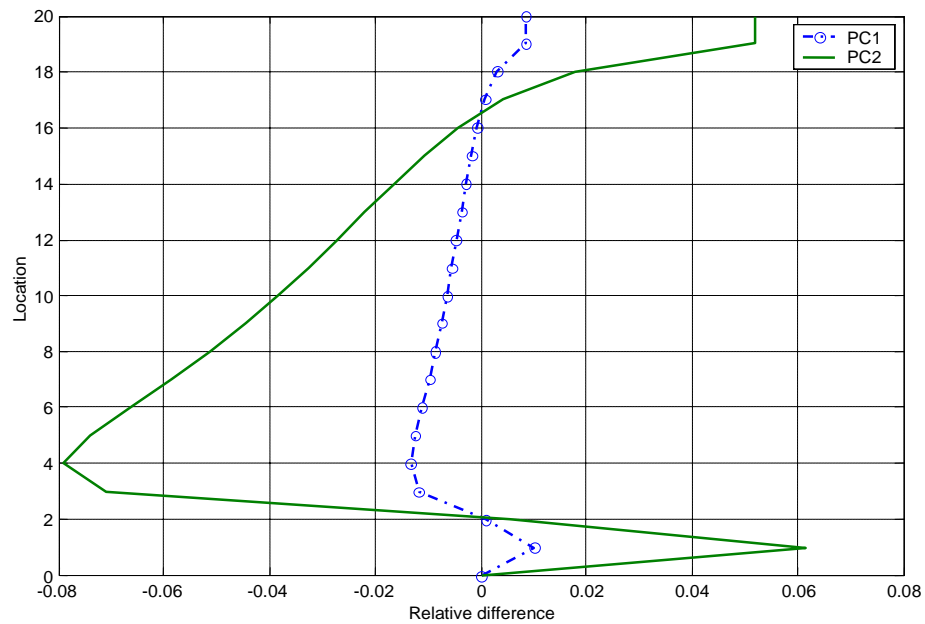
Figure 4.20 Relative difference for the second mode of the frame with damage scenarios PC1 and PC2.
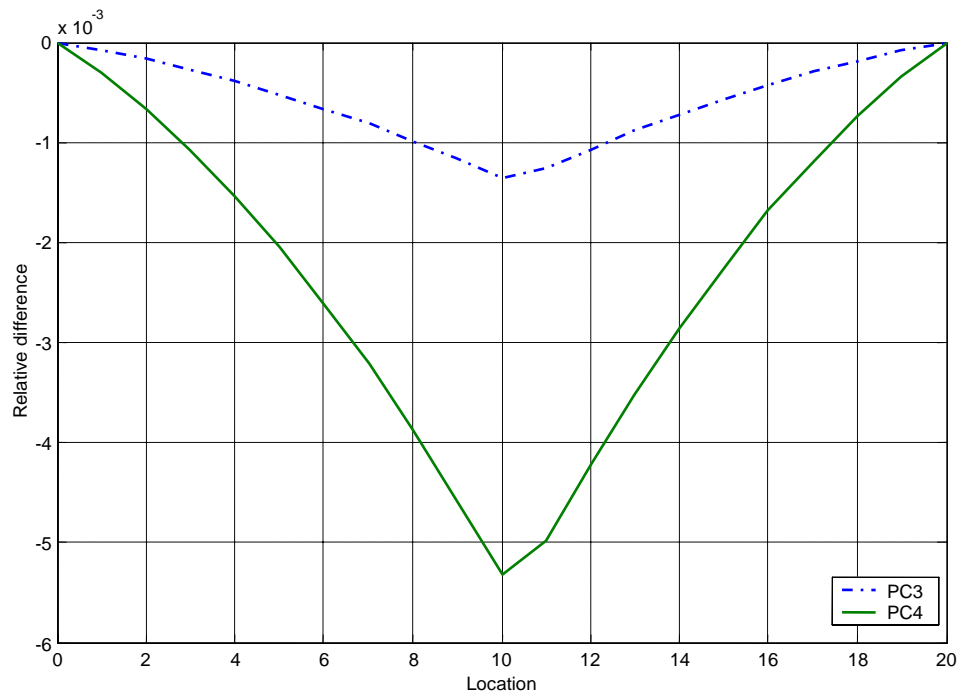
Figure 4.21 Relative difference for the first mode of the frame with damage scenarios PC3 and PC4.
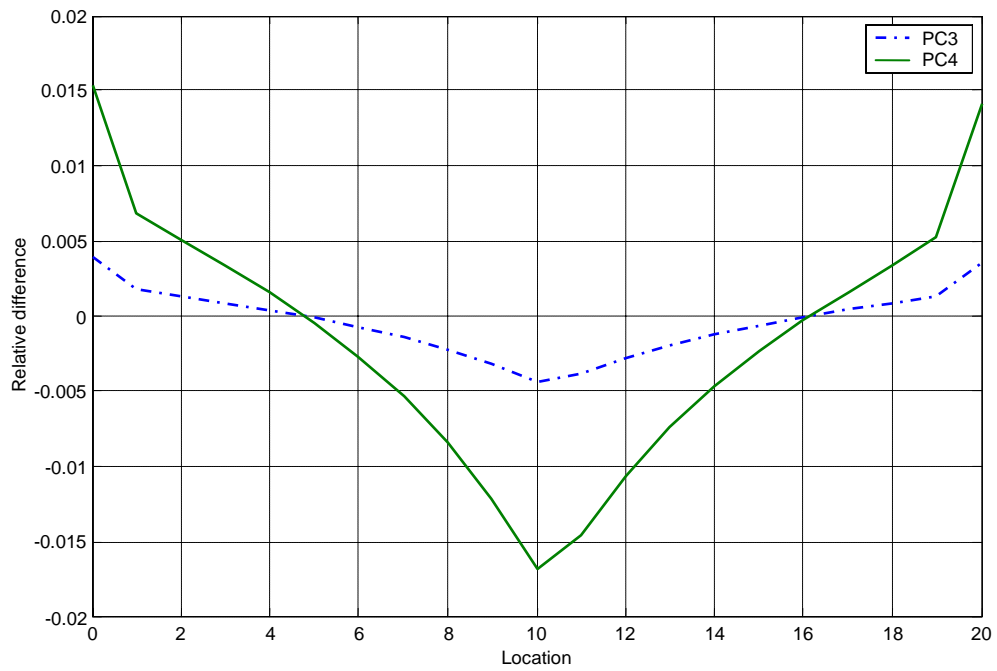
Figure 4.22 Relative difference for the second mode of the frame with damage scenarios PC3 and PC4.
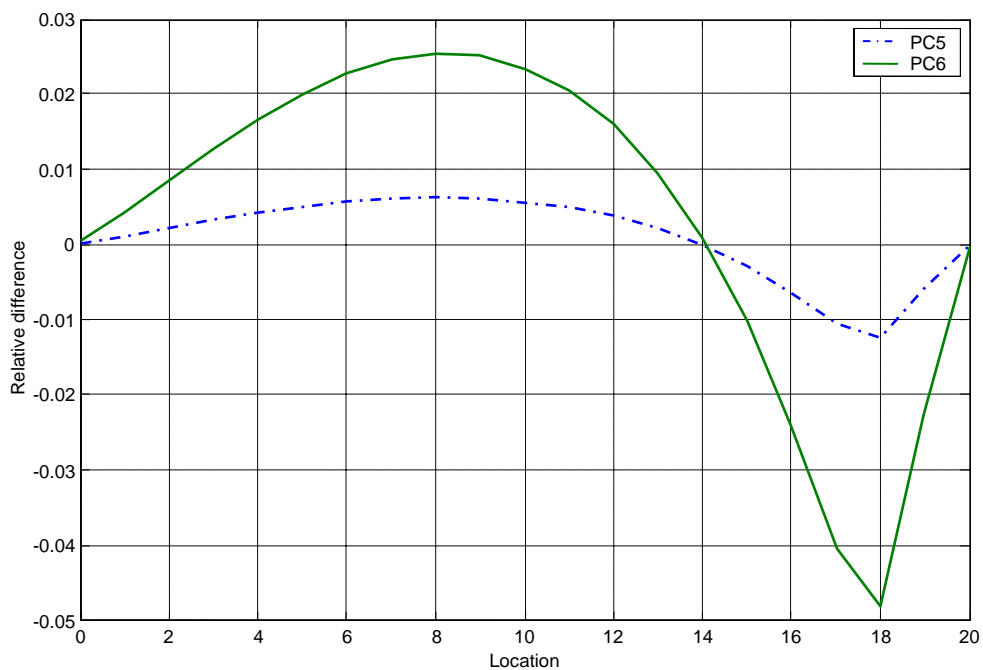
Figure 4.23 Relative difference for the first mode of the frame with damage scenarios PC5 and PC6.
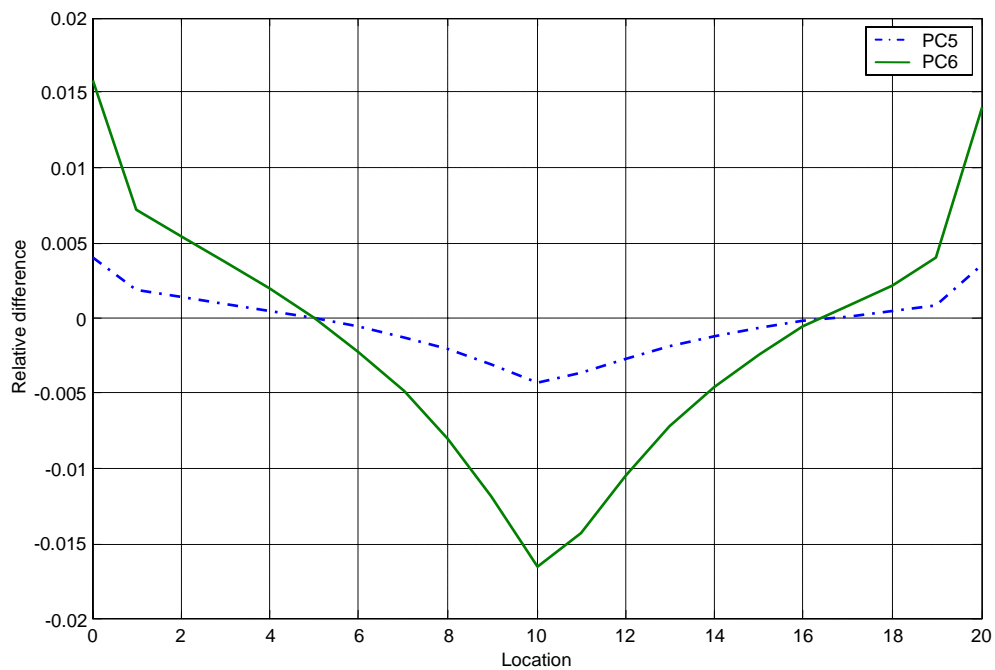
Figure 4.24 Relative difference for the second mode of the frame with damage scenarios PC5 and PC6.

4.6 ELEMENT DAMAGE INDEX EQUATION

De Roeck (2002) proposed a mode shape-based method, to predict the damage location and severity. The performance of this method will be studied here by applying it to the beam used for other procedures. A conventional finite-element discretization is used for the structural modeling. The modal properties considered are the natural frequencies and mode shapes of the undamaged and damaged structure.

In De Roeck study the damage in the structure is represented by a decrease in the stiffness of the individual finite elements. The damage identification is carried out at the element level. It is assumed that the stiffness matrix of the whole element decreases uniformly. The change in stiffness of an element is expressed by the damage index D_e

$$\Delta k_e = k_e - k_e^* = D_e k_e \tag{4.5}$$

where

k_e : element stiffness matrix of the undamaged structure.

k_e^* : element stiffness matrix of the damaged structure.

Δk_e : the stiffness reduction of the element.

A positive value of D_e will indicate a loss of the element stiffness. The e*th* element is undamaged when $D_e = 0$ and the stiffness of the e*th* element is completely lost when $D_e = 1$. Therefore, the damaged element stiffness matrix can be represented by

$$k_e^* = k_e \left(1 - D_e \right)$$ (4.6)

For planar beam elements in bending k_e is the stiffness matrix defined in Equation (2.17). In this case the element damage index is the ratio of the damaged to the undamaged bending stiffness

$$D_e = \frac{(EI)_e^*}{(EI)_e}$$ (4.7)

For a structural system with N elements ($e = 1,2,…,N$), n undamaged mode shapes ($i = 1,…, n$) and m damaged mode shapes ($j = 1,…, m$), the element damage index equations can be formulated as

$$\sum_{e=1}^{N} \phi_{je}^{*T} k_e \phi_{ie} D_e = \left(1 - \frac{\omega_j^{*2}}{\omega_i^2} \right) \phi_j^{*T} K \phi_i$$ (4.8)

where

K : stiffness matrix of the undamaged structure.

ϕ_i : mode shape of the ith modal vector for the undamaged structure.

ϕ_j^* : mode shape of the jth modal vector for the undamaged structure.

ω_j^*, ω_i : natural frequencies of the damaged and undamaged structure.

Equations can be written in the compact matrix notation

$$[S]\{D\} = \{R\} \tag{4.9}$$

where the coefficients of the system matrix [S] are

$$S_{ije} = \phi_{je}^{*T} k_e \phi_{ie} \tag{4.10}$$

and the elements of the vector on the right-hand side are

$$R_{ij} = \left(1 - \frac{\omega_j^{*2}}{\omega_i^2}\right) \phi_j^{*T} K \phi_i \tag{4.11}$$

The system matrix and the residual vector on the right-hand side of Equation (4.8) involve both undamaged and damaged mode shapes. The expanded damage equations (4.9) are

$$
\begin{bmatrix}
S_{111} & \cdots & S_{11N} \\
\vdots & \vdots & \vdots \\
S_{1m} & \cdots & S_{1mN} \\
S_{211} & \cdots & S_{21N} \\
\vdots & \vdots & \vdots \\
S_{2m1} & \cdots & S_{2mN} \\
\vdots & \vdots & \vdots \\
S_{(n-1)11} & \cdots & S_{(n-1)1N} \\
\vdots & \vdots & \vdots \\
S_{(m-1)m1} & \cdots & S_{(n-1)mN} \\
S_{n11} & \cdots & S_{n1N} \\
\vdots & \vdots & \vdots \\
S_{nm1} & \cdots & S_{nmN}
\end{bmatrix}_{(n\times m)\times N}
\begin{Bmatrix}
D_1 \\
D_2 \\
D_3 \\
\vdots \\
\vdots \\
\vdots \\
\vdots \\
\vdots \\
\vdots \\
\vdots \\
\vdots \\
D_{N-1} \\
D_N
\end{Bmatrix}_{N\times 1}
=
\begin{Bmatrix}
R_{11} \\
\vdots \\
R_{1m} \\
R_{21} \\
\vdots \\
R_{2m} \\
\vdots \\
R_{(n-1)1} \\
\vdots \\
R_{(n-1)m} \\
R_{n1} \\
\vdots \\
R_{nm}
\end{Bmatrix}_{(n\times m)\times 1}
\tag{4.12}
$$

The system matrix [S] of damage Equation (4.12) is not always square. It is square if the product of the number of undamaged and damaged mode shapes is the same as the number of elements (or sensors in an actual application). In general the element damage equations may be determined, overdetermined, or underdetermined depending on the number of undamaged modes n, damaged modes m, and elements N chosen. When a direct inverse solution is not possible because $n \ x \ m \ < \ N$, the Moore–Penrose pseudoinverse $[S^{+}]$ can be used. The pseudoinverse can be calculated by solving the singular value decomposition of [S]. Another possible approach to solve the damage equations is to use the non-negative least-squares technique – NNLS (Lawson and Hanson 1974).

4.7 NUMERICAL SIMULATIONS

The damage index equations presented before were implemented to detect damage in a simply-supported beam. Due to the definition of damage of this method, in this numerical example the beam was divided into 15 elements. Three damage scenarios were investigated. In the first case the damage was simulated by reducing by 50% the stiffness of an element located at the mid-span. In the second case, the reduction was done at two elements. In the third case considered, a crack at L/2 was introduced to the beam by means of the element developed in Chapter II. The crack size corresponds to the damage scenario SC2.

Next, the proposed damage index equations are solved by using the NNLS technique, available in MATLAB. The predicted distributions of element damage indices for the simulated damage scenarios are shown in Figures 4.25 to 4.27. The indices were obtained by using the first three mode shapes of the beam. It can be seen that for these particular damage scenarios the damage identification method was able to indicate the location and severity of the damaged elements. In the present simulation the complete stiffness matrix of the beam was used to compute the values of the coefficients R_{ij}. This is a disadvantage of the method in its current form because it uses the rotational degrees of freedom to generate the equations (4.12). However, in general, in experimental modal analysis the rotations are not measured.
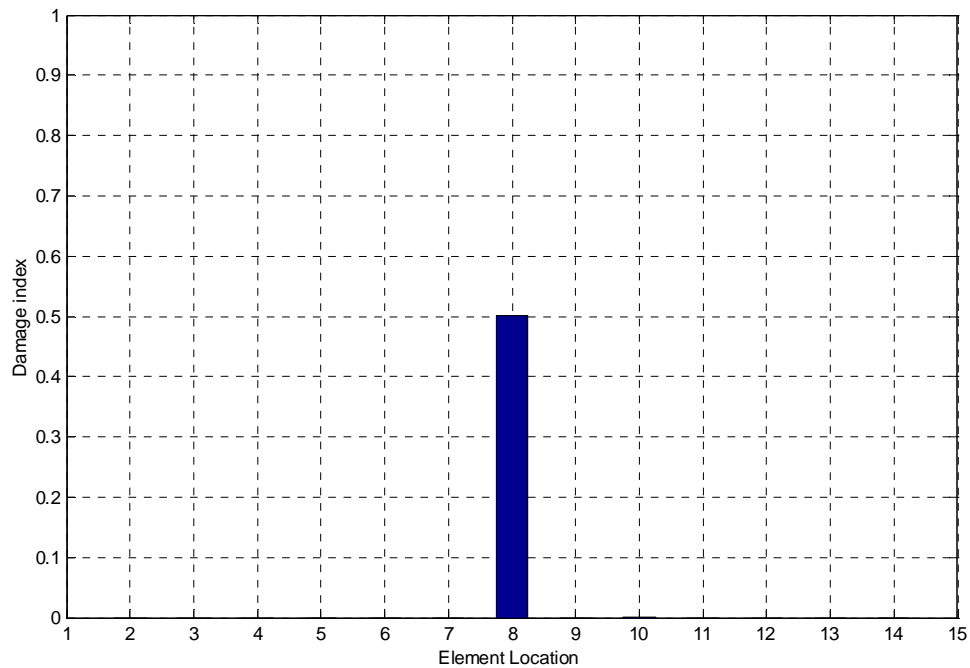
Figure 4.25 Element damage index for the beam single damage scenario.
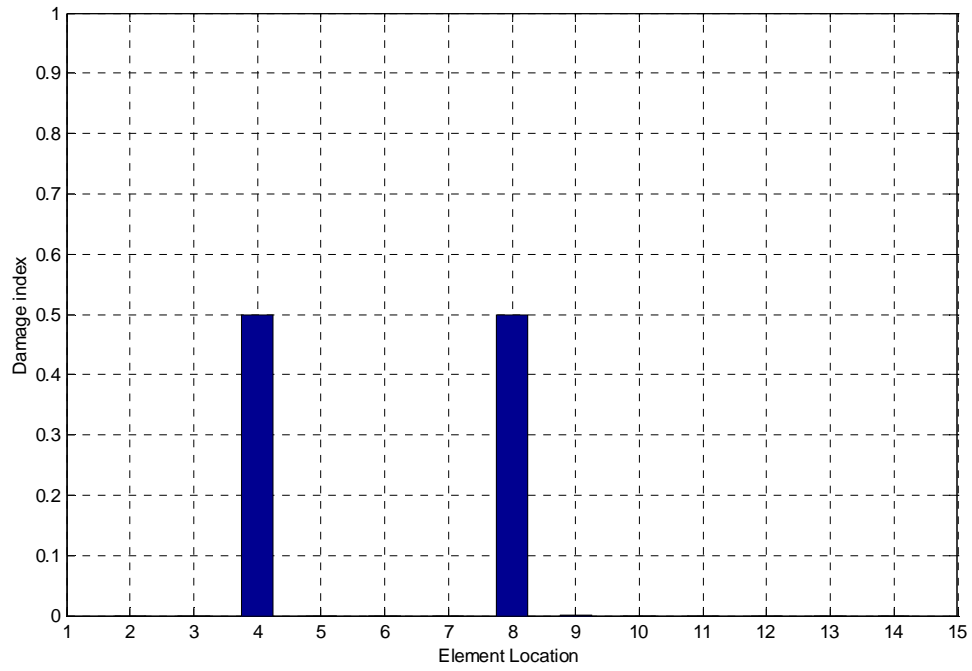
Figure 4.26 Element damage index for the beam with multiple damage scenario.
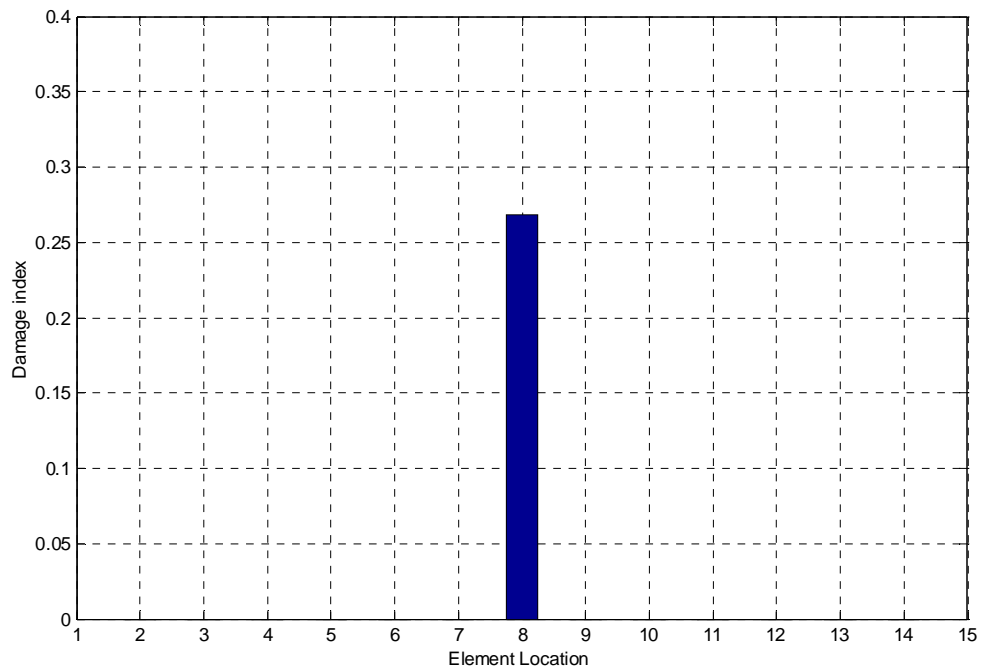
Figure 4.27 Element damage index for the beam with a cracked element.

4.8 SUMMARY

In this chapter, several structural damage identification methods based on changes in the mode shapes and frequencies are presented. Numerical examples are performed to compare the effectiveness of the methods studied, to indicate and locate the damage in simple structures. Six damage scenarios were analyzed for the simply-supported beam and plane frame.

In the cases of the eigenparameter method, it was found that this method can indicate the location of the region damaged of the simply-supported beam, when the first mode shapes is used in damage scenarios that simulate one damaged element. For multiple damage scenarios the parameter was not able to locate clearly the damaged zones. In the plane frame, the damage simulated at the column was not located. In the cases of multiple damage the parameter cannot locate the positions of the cracks simultaneously. In the mode shape relative difference method, the results obtained indicate that the parameter introduces factors of uncertainty about the correct locations of damage.

The element damage index method was evaluated for three damage scenarios. Since this method uses the modal forces and the rotational degrees of freedom to generate the equations, and in experimental modal analysis, rotations are not measured, presents limitations respect to others methods.

CHAPTER V

METHOD BASED ON DYNAMICALLY MEASURED FLEXIBILITY

5.1 INTRODUCTION

As mentioned earlier, the presence of damage in a structure changes its dynamic characteristics. Changes also occur in some of the structural parameters: the damping, stiffness and flexibility matrices of the structure. There are a few methods based on this concept, which use a dynamically measured flexibility matrix to calculate changes in the performance of the structures [Pandey and Biswas (1994), Raghavendrachar and Aktan (1992)]. By definition, the flexibility matrix relates the applied forces and the resulting structural displacements. Thus, each column of the flexibility matrix represents the displacement pattern of the structure associated with a unit force applied at the associated DOF. The measured flexibility matrix can be estimated from the measured mass-normalized mode shapes and frequencies. Typically, to detect damage using a flexibility matrix, the flexibility matrix obtained using the modes of the damaged structure is compared with the matrix calculated using the modes of the undamaged structure or the analytical flexibility matrix from the FEM.

5.2 THE DELTA METHOD.

This method was proposed by Pandey and Biswas (1994). The method is based on the changes in the flexibility matrices of the undamaged and damaged structure. The flexibility matrix obtained by this method is approximate due to the fact that only the first few modes of the structure (associated with the lowest frequencies) are measured. The synthesis of the complete flexibility matrix would require the measurement of as many mode shapes and frequencies as dynamic degrees of freedom are being measured. In the method proposed by Pandey and Biswas the development of an analytical model of the structure is not required. All the predictions of the state of damage can be made using the data experimentally collected on the structure.

If the mode shapes are normalized with respect to the mass matrix, the stiffness matrix [K] and flexibility matrix [F] are related to the modal properties as

$$[K] = [M]_{n \times n} [\Phi]_{n \times n} [\Lambda]_{n \times n} [\Phi]_{n \times n}^{T} [M]_{n \times n} \qquad (5.1)$$

$$[F] = [\Phi]_{n \times n} [\Lambda]_{n \times n}^{-1} [\Phi]_{n \times n}^{T} = \sum_{i=1}^{n} \frac{\phi_i \phi_i^T}{\omega_i^2} \qquad (5.2)$$

If all the *n* normal modes and their respective natural frequencies are used, equation (5.2) defines the flexibility matrix of the structure. If only a number *m < n* of modes are used, a *singular* matrix is obtained. This is known as the *pseudo-flexibility* matrix or the *raw flexibility* matrix, and is defined as

$$[F] = [\Phi]_{n \times m} [\Lambda]^{-1}_{m \times m} [\Phi]^{T}_{m \times n}$$

(5.3)

From equation (5.2), it can be observed that the modal contribution to the flexibility matrix decreases as the frequency increases, i.e., the flexibility matrix converges rapidly with increasing values of frequency. Therefore, a good estimate of the flexibility matrix can be obtained with only a few of the lower frequency modes.

In practice, the flexibility matrices for the undamaged structure and the damaged structure are obtained by using equation (5.3). Knowing these flexibility matrices, the change in the flexibility matrix $[\Delta]$ can be calculated

$$[\Delta] = [F] - [F_*]$$

(5.4)

where $[F]$ is the flexibility matrix for the undamaged structure,

$$[F_*] = [\Phi_*]_{n \times m} [\Lambda_*]^{-1}_{m \times m} [\Phi_*]^{T}_{m \times n}$$

(5.5)

For each degree of freedom j of the structure, the maximum absolute value of the elements in the corresponding column of $[\Delta]$ is defined by

$$\delta_j = \max_i |\delta_{ij}|$$

(5.6)

where δ_{ij} are the elements of $[\Delta]$.

The parameter δ_j which is a measure of change of flexibility for each measurement location can be used to detect and locate damage in a structure.

A variation on the method based on the dynamically measured flexibility matrix is the use of the dynamically measured stiffness matrix. This matrix is defined as the pseudoinverse of the dynamically measured flexibility matrix. A brief discussion of these methods is presented in Appendix A.

5.3 NUMERICAL SIMULATIONS

The procedure presented above was used to calculate the pseudo-flexibility matrices of the undamaged and damaged structures with the different damage scenarios presented in Chapter III. The modal amplitudes obtained from the free vibration analysis are used to construct the mode shape matrices. Next, the parameter δ_j is computed for each one of damage scenarios.

- Simply-supported beam

Six scenarios of damage for the beam are studied. The flexibility changes for the damage scenarios SD1 to SC4 are illustrated in Figures from 5.1 to 5.3, using the first three displacement mode shapes. These flexibility changes were normalized with respect to the maximum value. The point in the graphs where the slope changes sign, indicates the damaged region. For the damage cases shown in Figures 5.1 and 5.2, a single crack was induced at the mid-span. It is recalled that the difference between cases SD1 and

SD2, and SC1 and SC2 is the amount of damage. It is interesting to observe that the curves are similar to the bending moment diagrams obtained for a vertical force applied at the location of damage. Moreover, it can be observed that, as expected, the change in the flexibility increases with an increase in the severity of damage. From Figure 5.1 it can be seen that the change in flexibility for case SD2 is three times the change for case SD1, whereas the severity of damage inflicted in case SD2 is twice that of case SD1. Figure 5.3 displays the change in flexibility for a multiple damage case, namely two cracks at locations 2 and 5. It is evident that the method does not possess the capability of detecting the two damaged zones of the beam: it just tells that there is some damage in the beam.
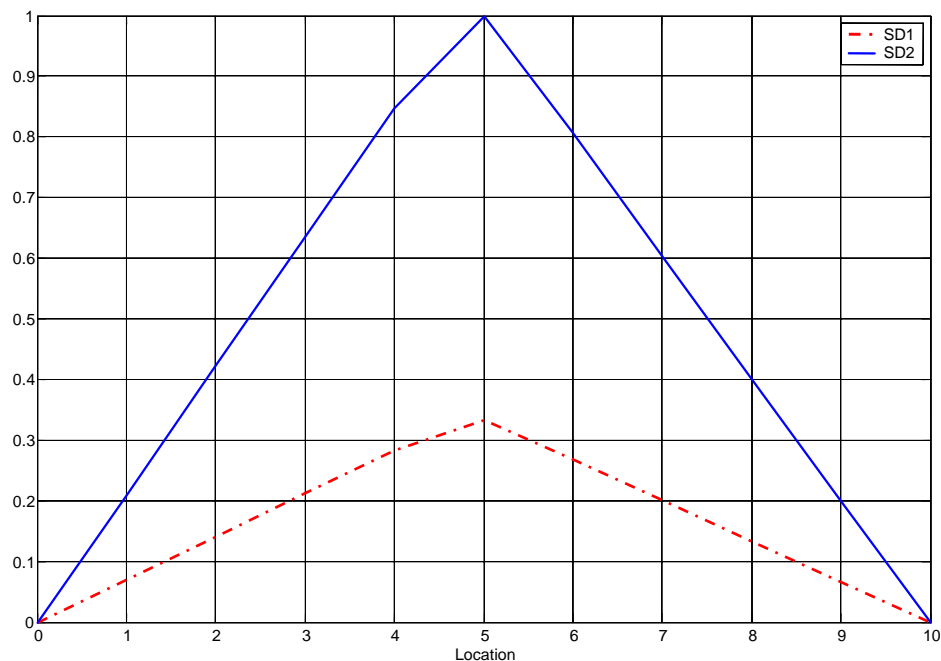
Figure 5.1 Normalized flexibility change for the beam with damage scenarios SD1 and SD2.
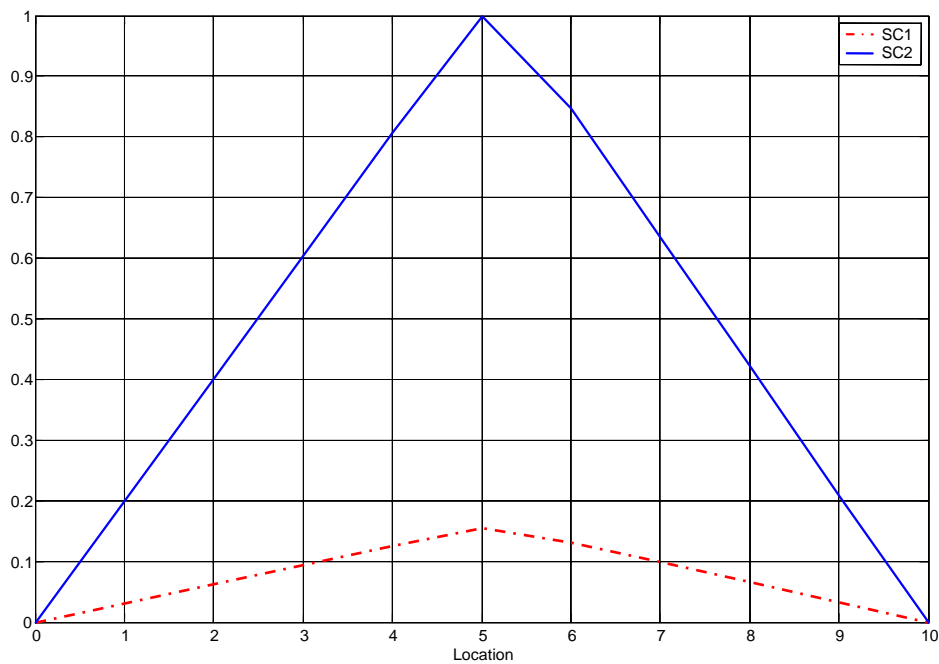
Figure 5.2 Normalized flexibility change for the beam with damage scenarios SC1 and SC2.
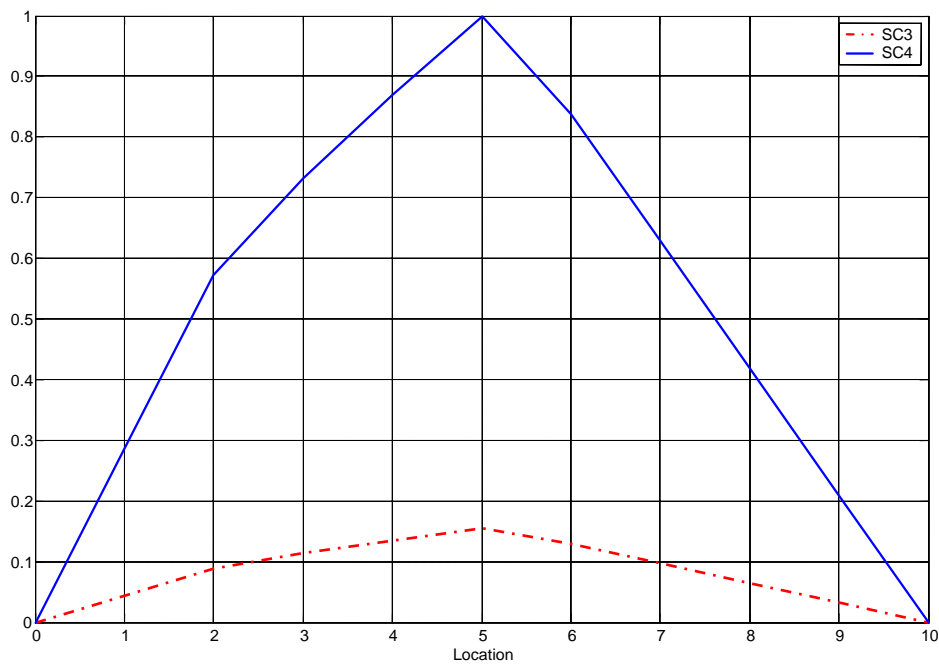
Figure 5.3 Normalized flexibility change for the beam with damage scenarios SC3 and SC4.

- Plane frame

The flexibility-based methodology is next tested on the plane frame of Figure 3.8. For this structure three pairs of damage scenarios are considered. The flexibility changes for the damage scenarios PC1 to PC6 are shown in Figures 5.4 to 5.6. In all the cases the first two mode shapes were used to define the flexibility matrix. In the cases PC1 and PC2 where the crack is near the base of the column, the location of the damage is not clear, although at location 2 the slope changes value.

In damage scenarios PC3 and PC4 (a single crack in the beam of the frame), the identification was successful since the maximum flexibility change occurs in the damaged region. However, as in the cases of the beam, this method cannot locate the damaged zones in the cases of multiple damage. This is evidenced by the results displayed in Figure 5.6. The damage cases denoted as PC5 and PC6 correspond to the beam with two cracks. The parameter δ_j only indicated that there is damage at the mid-span of the beam. Note that the results for damage scenarios PC3 and PC5, and PC4 and PC6, are practically identical.
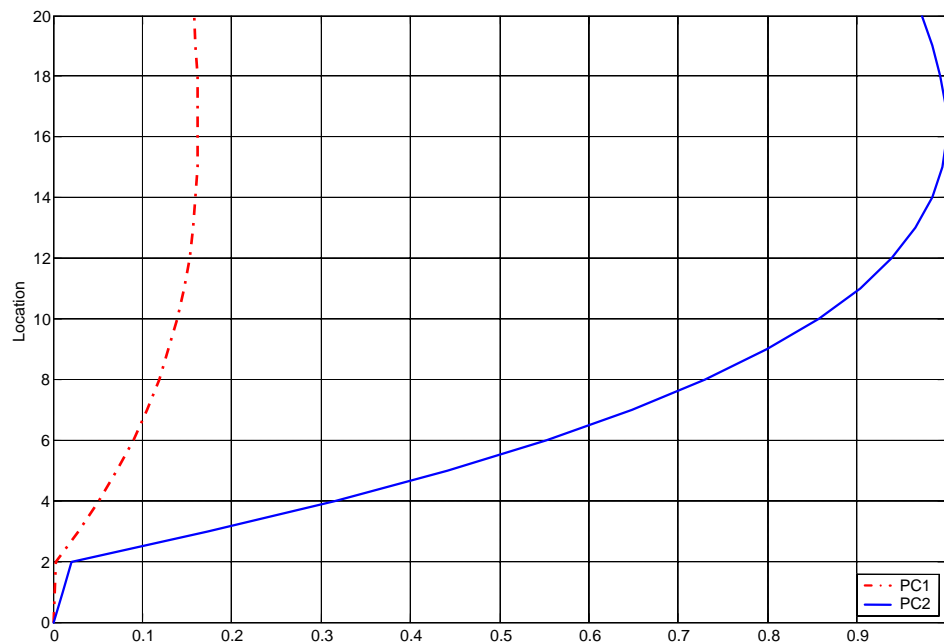
Figure 5.4 Normalized flexibility change for the frame with damage scenarios PC1 and PC2.
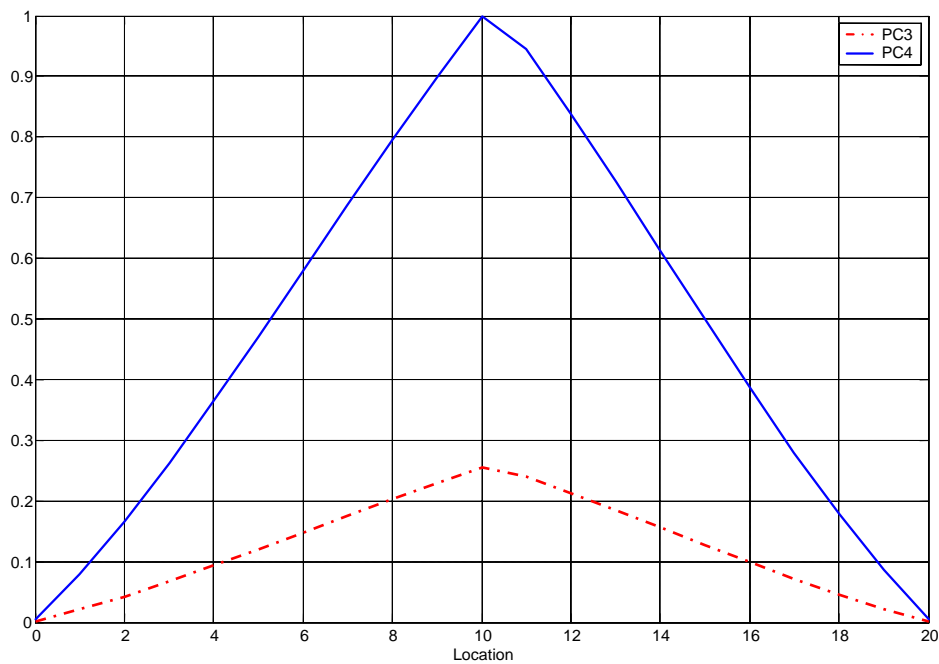
Figure 5.5 Normalized flexibility change for the frame with damage scenarios PC3 and PC4.
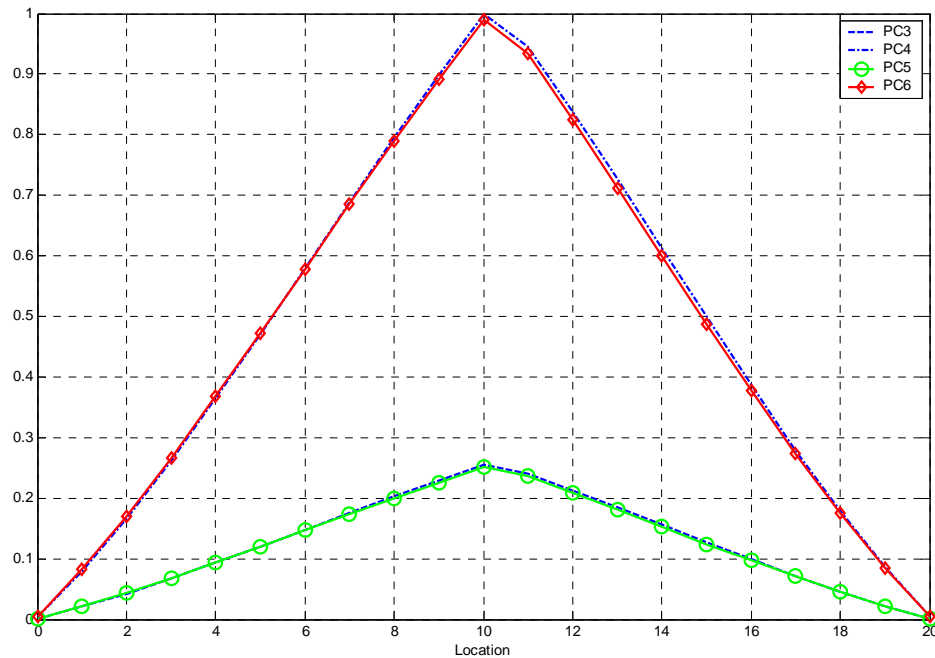
Figure 5.6 Normalized flexibility change for the frame with damage scenarios PC3 to PC6.

5.8 SUMMARY

In this chapter, a structural damage identification method based on changes in the flexibility matrix is presented. By means of numerical examples the effectiveness of the method to indicate the presence of damage in simple structures and to locate its position was examined.

The first structure analyzed was a simply-supported beam. Six damage scenarios were studied. For each of these cases, the values of the localization index δ_j were calculated. It was found that this method was able to pinpoint the location of the region damaged in the beam when the first two or three mode shapes were used and when the

damage was restricted to a single crack. However, when the beam had more than one crack, the method failed to clearly locate the damaged zones.

In the other structure considered, a plane frame, six scenarios of damage were also studied. The flexibility-based localization index only indicated the damaged region in the cases of single damage scenarios in the beam of the frame. The damage inflicted at the right end of the beam was not detected. Moreover, when the crack was placed at one of columns of the frame, the results were ambiguous.

It was found that in both structures the change in flexibility is sensible to the severity of the damage inflicted to the structure, and thus it could be used to indicate relative degrees of damage. An advantage of the method is that to locate the damage it requires only a few modes (two or three) because the measured flexibility matrix is mostly influenced by the lower-frequency modes of the structure. However, based on the numerical simulations performed here it is not recommended for practical, real applications.

CHAPTER VI

METHODS BASED ON THE MODE SHAPE CURVATURE.

6.1 INTRODUCTION

Changes in mode shapes are much more sensitive to local damage when compared with changes in natural frequencies. However, using mode shapes also has some limitations. As damage is a local phenomenon, it may not significantly influence the mode shapes of the lower modes, that are usually those measured from vibration tests of large structures.

As mentioned earlier, the existence of damage at a given section of a structure reduces the stiffness, especially in the neighborhood of that section. This reduction leads to an increase in the magnitude of the curvature at the section. Since the changes in the curvatures are local and depend on the extent of reduction in the structural stiffness, the curvature changes can be used to detect and locate damage.

In this chapter, a damage identification method based on the modal curvature is proposed, and two existing methodologies are presented. Numerical simulations are performed to compare the effectiveness of the existing and proposed procedures to locate the damage.

6.2 CURVATURE MODE SHAPE

This method was proposed by Pandey et al. (1991) to identify and locate damage in a structure. It has been also evaluated by Salawu and Williams (1994). Curvature mode shape is related to the flexural stiffness of beam cross-sections. By definition, the curvature at a point of an element with bending deformation is given by

$$\upsilon'' = \frac{M}{EI}$$

(6.1)

in which v'' is the curvature at a section, M is the bending moment at a section, E is the modulus of elasticity and I is the second moment of the cross-sectional area.

If a crack or other damage is introduced in a structure, it reduces the flexural stiffness EI of the structure at the cracked section or in the damaged region. This in turn increases the magnitude of curvature at that section of the structure. The changes in the curvature are local in nature and therefore they can be used to detect and locate a crack or other damage in the structure. The change in curvature increases with the reduction in the value of the flexural stiffness EI.

Starting with the displacement mode shapes obtained from the finite element analysis, the curvature mode shapes for the undamaged structure can be obtained numerically by using a central difference approximation as

$$\phi_i'' = \frac{\phi_{i-1} - 2\phi_i + \phi_{i+1}}{h^2}$$

(6.2)

where,

h : distance between the measurement points *(i)* and *(i+1)*

ϕ_i : mass normalized mode shape of the undamaged structure associated with a given

frequency

Similarly, the curvature mode shapes for the damaged structure can be obtained as

$$\phi_{*,i}'' = \frac{\phi_{i-1}^* - 2\phi_i^* + \phi_{i+1}^*}{h^2}$$

(6.3)

where,

ϕ_i^* : mass normalized mode shape of the damaged structure corresponding to a specific

natural frequency.

For mode *j* the absolute difference between the curvatures of the damaged and undamaged structure is calculated as

$$\{\Delta\phi''\}_j = \left| \{\phi_*''\}_j - \{\phi''\}_j \right|$$

(6.4)

6.3 NUMERICAL SIMULATIONS

The procedure described before was used to calculate the absolute differences between the curvature mode shapes of undamaged and damaged structures. The same simply-supported beam and plane frame as well as the damage scenarios presented in Chapter III are considered again here to evaluate the method. The modal amplitudes obtained from the free vibration analysis are used to numerically compute the modal curvatures.

- Simply-supported beam

The absolute differences between the curvature mode shapes of the undamaged and the damaged beam for damage scenarios SD1 and SD2 are plotted in Figures 6.1 to 6.3 for the first three displacement mode shapes. The discrete points in the horizontal axis correspond to the position of the sensors along the span of the beam. The maximum difference for each curvature mode shape occurs in the damaged region, which is between locations 5 and 6 for this damage case. The larger differences in the curvature mode shapes are localized near the damaged zone and they are much smaller outside the damaged region. Figures 6.4 to 6.6 show the results for damage scenarios SC1 and SC2. It is recalled that these correspond to a single crack at the mid-span with ratios between crack depth and section height of 0.1 and 0.25, respectively. The absolute differences between the curvature mode shapes of the undamaged and the cracked beam are plotted over the beam's length for the first three displacement mode shapes. As it can seen in Figures 6.4 to 6.6, the maximum difference for each curvature mode shape occurs in the

damaged region, which is between locations 5 and 6 for these damage scenarios. As expected, the differences are larger for damage case SC2, since this correspond to a larger crack depth for the same cross section

Figures 6.7 to 6.9 show the results for the multiple damage scenarios SC3 and SC4 (two cracks at 1/5 and 1/2 of the length with increasing depths). The cracks are at positions 2 and 5. The absolute differences between the curvature mode shapes for the first three modes of the undamaged and the cracked beam are plotted as a function of the sensor position. As it can be observed, only with the curvatures of the first mode shape it is possible to clearly detect the damaged zones. From the modal curvatures of modes 2 and 3, it is possible to identify only one of the damaged elements. Although for the damage case SC3 the results are somewhat better than for case SC4, the resolution is not good enough nevertheless. Hence the curvature mode method does not exhibit a good performance for multiple damage scenarios.
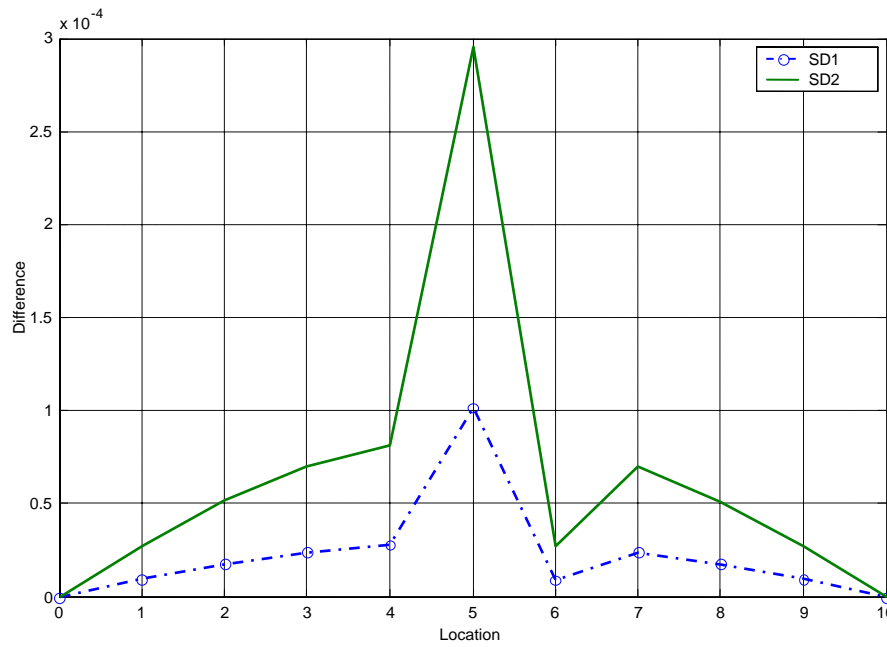
Figure 6.1. Absolute difference between the curvature mode shapes for mode 1 of the beam for damage scenarios SD1 and SD2.
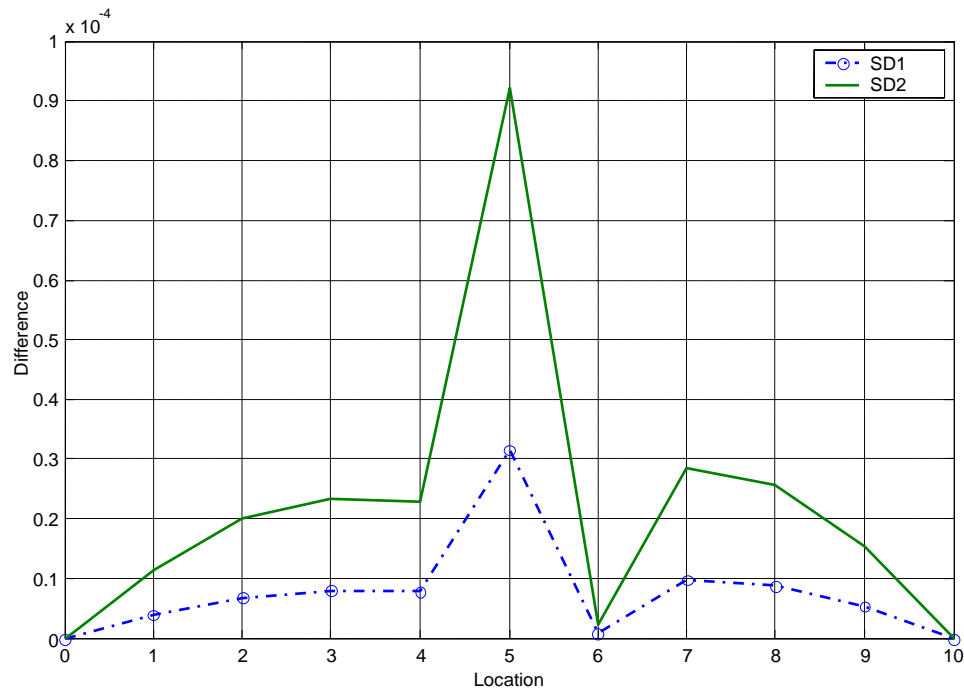
Figure 6.2. Absolute difference between the curvature mode shapes for mode 2 of the beam for damage scenarios SD1 and SD2.
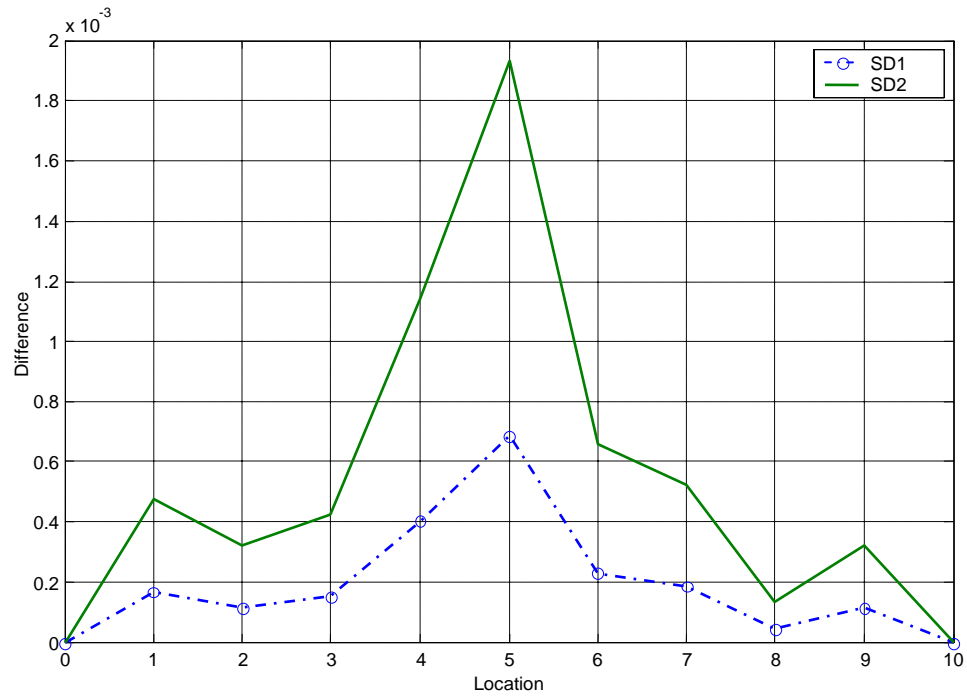
Figure 6.3. Absolute difference between the curvature mode shapes for mode 3 of the beam for damage scenarios SD1 and SD2.
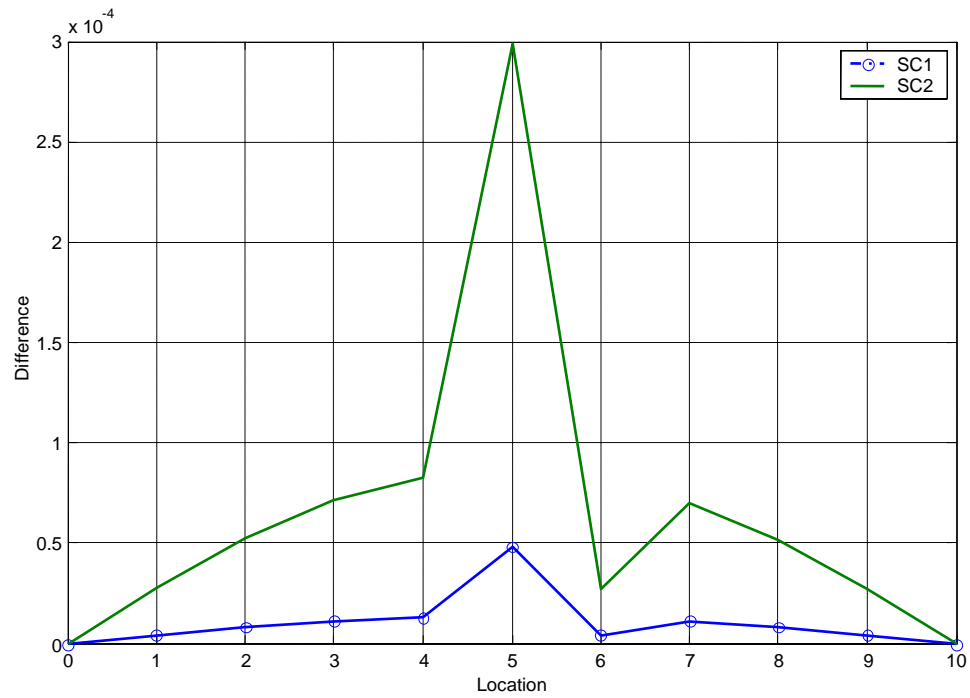
Figure 6.4. Absolute difference between the curvature mode shapes for mode 1 of the beam for damage scenarios SC1 and SC2.
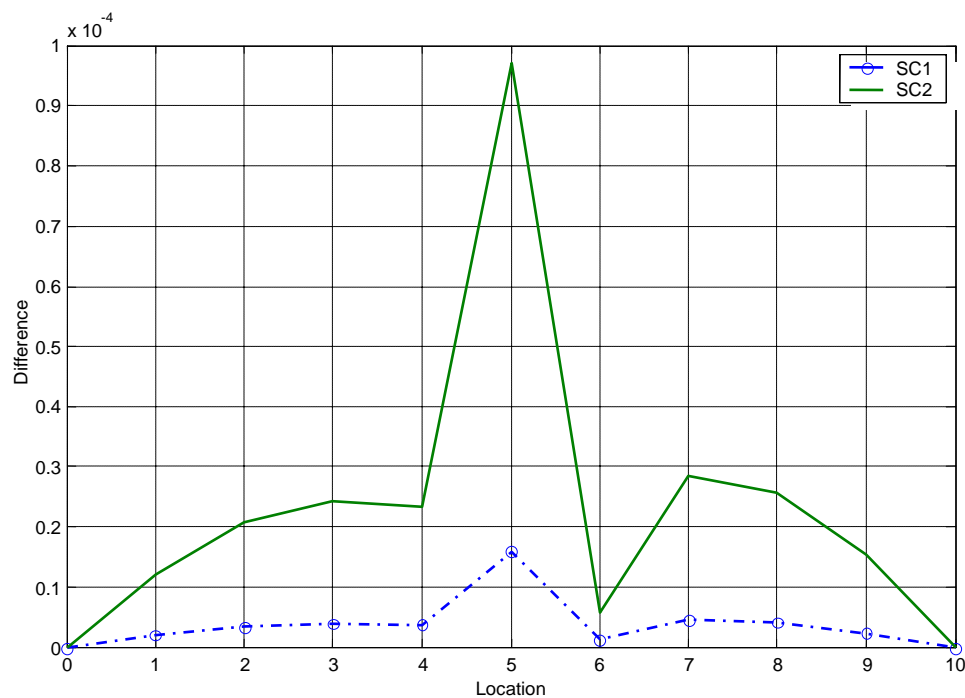
Figure 6.5. Absolute difference between the curvature mode shapes for mode 2 of the beam for damage scenarios SC1 and SC2.
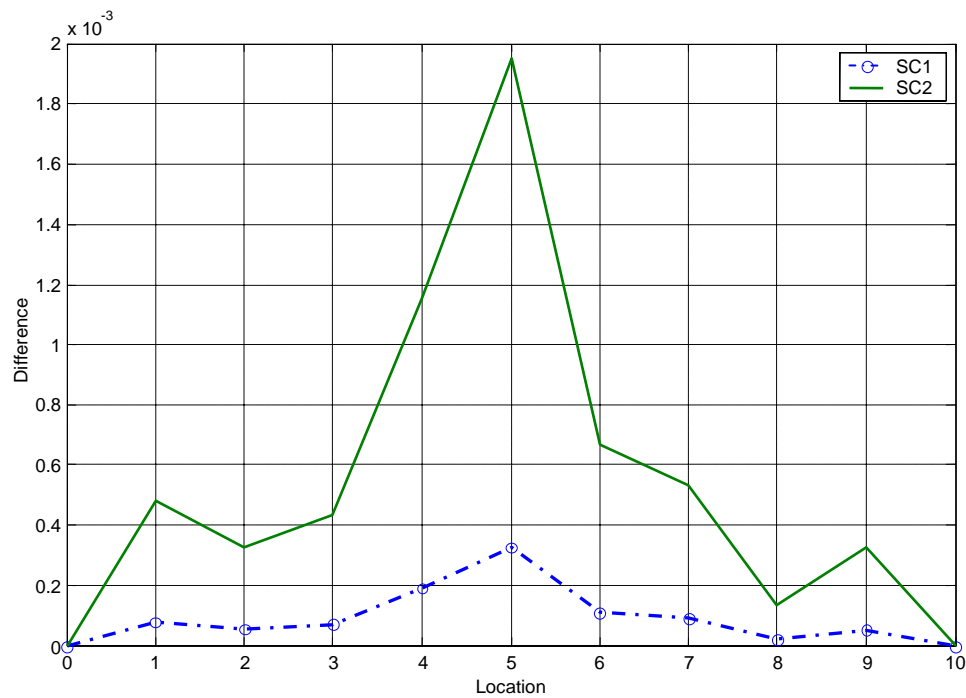
Figure 6.6. Absolute difference between the curvature mode shapes for mode 3 of the beam for damage scenarios SC1 and SC2.
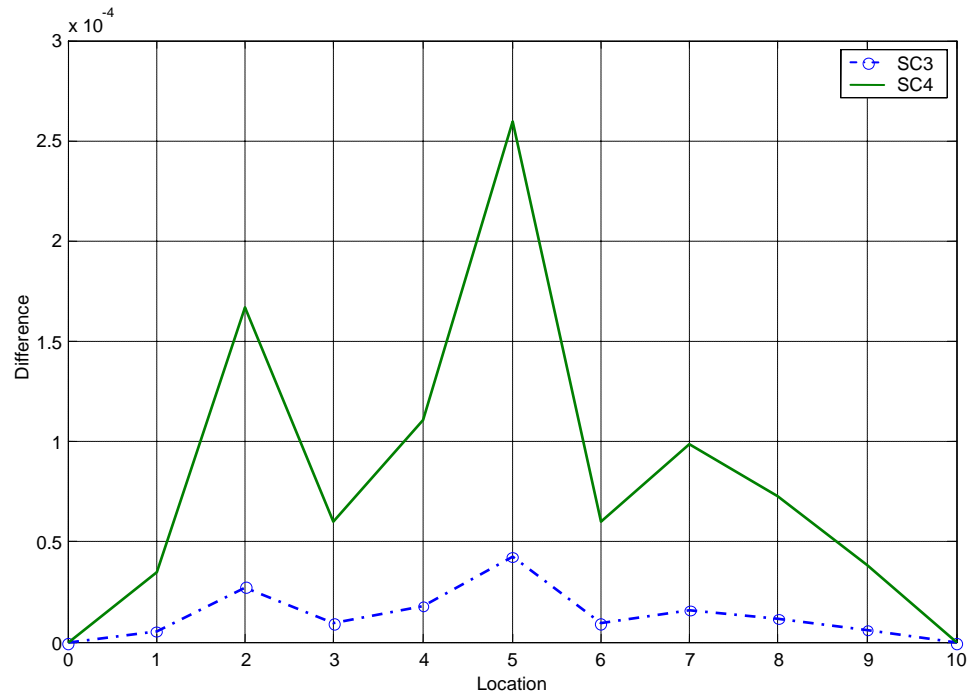
Figure 6.7. Absolute difference between the curvature mode shapes for mode 1 of the beam for damage scenarios SC3 and SC4.
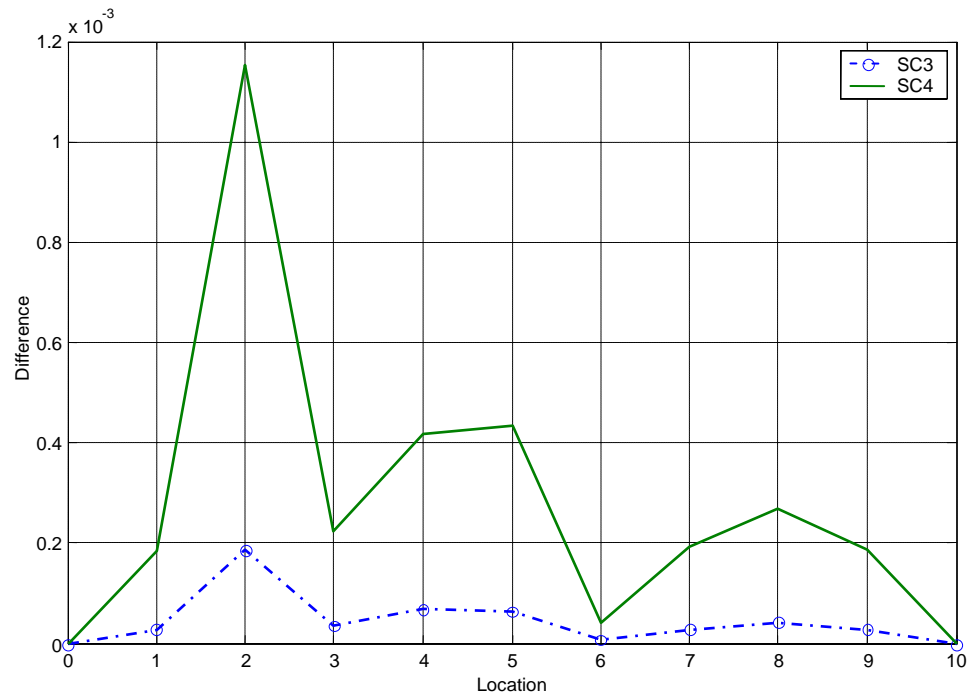
Figure 6.8. Absolute difference between the curvature mode shapes for mode 2 of the beam for damage scenarios SC3 and SC4.
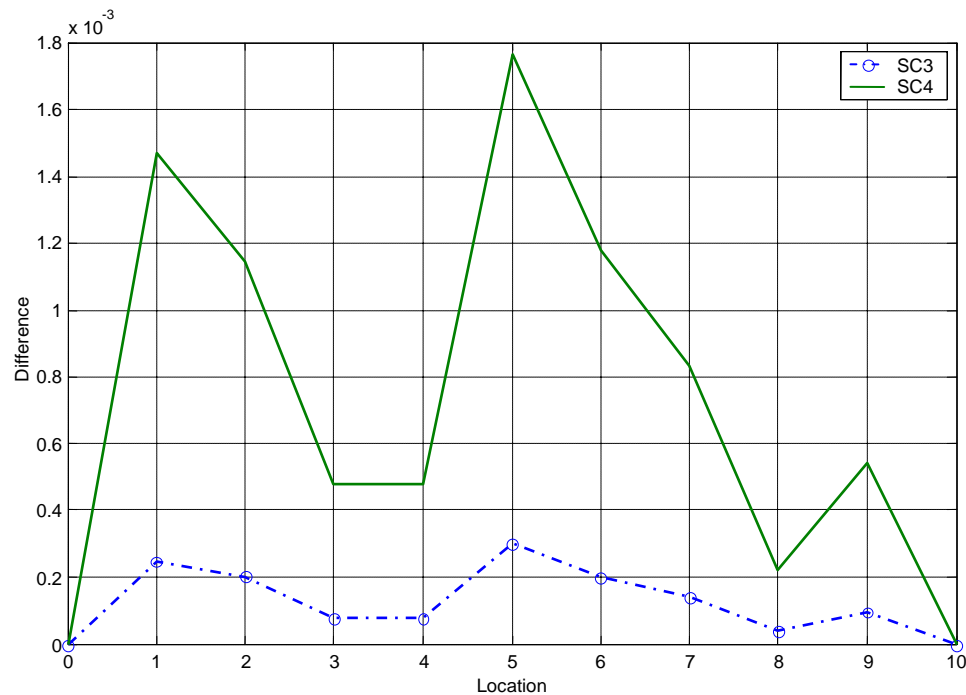
Figure 6.9. Absolute difference between the curvature mode shapes for mode 3 of the beam for damage scenarios SC3 and SC4.

- Plane frame

The performance of the mode shape curvature criterion to detect damage is examined by applying it to the plane frame in Figure 3.8. In damage scenarios PC1 and PC2 the crack-like damage is located near the right fixed support (between location points 1 and 2). The depth of the crack for case PC2 is twice that of case PC1. The absolute differences between the curvature mode shapes corresponding to the undamaged and cracked right column are shown in Figures 6.10 to 6.12. The figures display the modal curvatures for the first three displacement mode shapes. The method was able to pinpoint the damaged zone in the right column using the three modal curvatures.

In the next damage scenarios PC3 and PC4 a single crack is introduced at the mid-span of the beam (between location points 10 and 11). Figures 6.13 and 6.14 show the absolute differences between the curvature mode shapes corresponding to the undamaged and the damaged beam of the frame, for the first two mode shapes. As it can be observed by inspecting the figures, the method was able to indicate the presence of damage and the location of the damaged region of the frame.

In the multiple damage scenarios (PC5 and PC6), the presence of two cracks at the beam is simulated. The defects are at positions 10 and 18 measured from the left end of the beam. The results in terms the absolute differences between the curvature mode shapes corresponding to the undamaged and the damaged beam are shown in Figures 6.15 to 6.17, for the first three modes. It is evident from the graphs displayed in Figures 6.15 and 6.16 that the method could not indicate simultaneously the location of the two damaged regions of the beam using the curvatures of the first two modes. Notice, however, that is possible to detect one of the damaged zones using the difference in the first mode shape curvatures and the other one using the corresponding quantity for the second mode. The difference between the modal curvatures of the third undamaged and damaged modes for the case of the bigger crack (PC6) yielded better results. However, even in this case there is some ambiguity in the results in the left region of the beam.
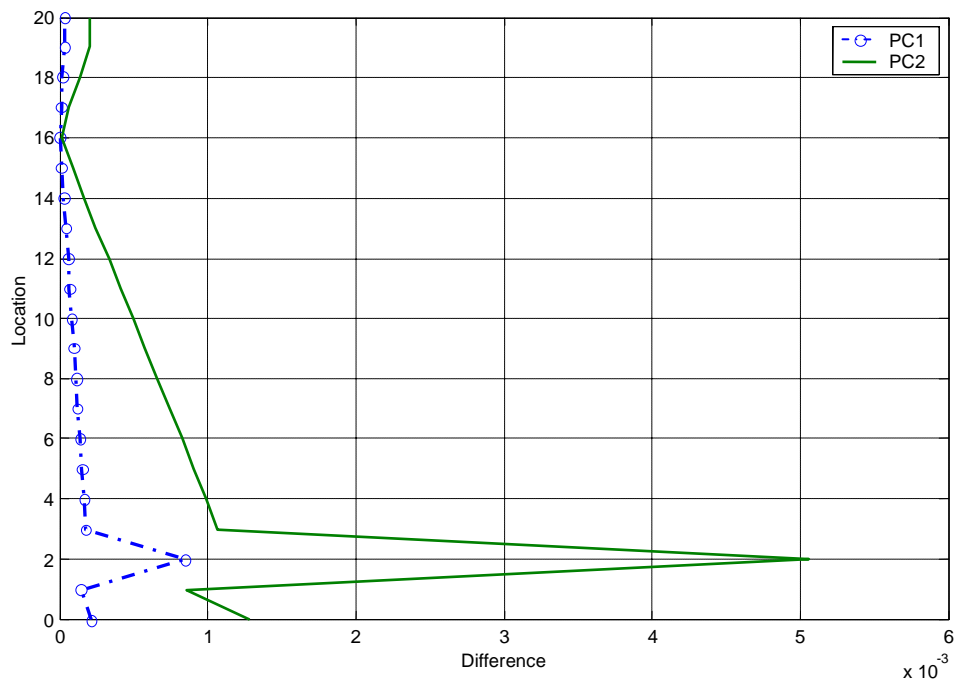
Figure 6.10. Absolute difference between the curvature mode shapes for mode 1 of the frame for damage scenarios PC1 and PC2.
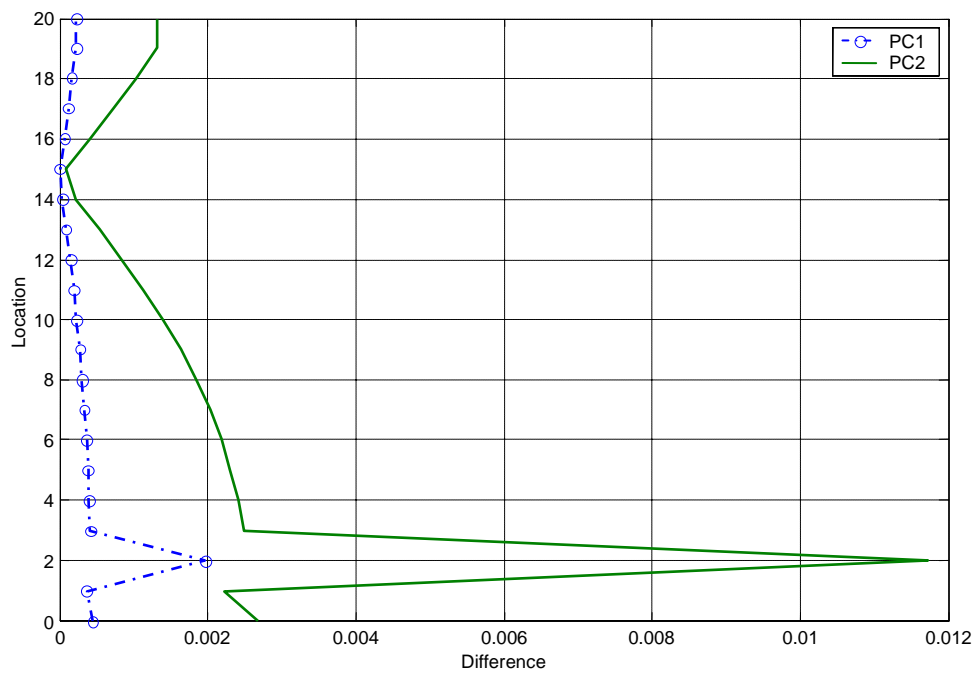
Figure 6.11. Absolute difference between the curvature mode shapes for mode 2 of the frame for damage scenarios PC1 and PC2.
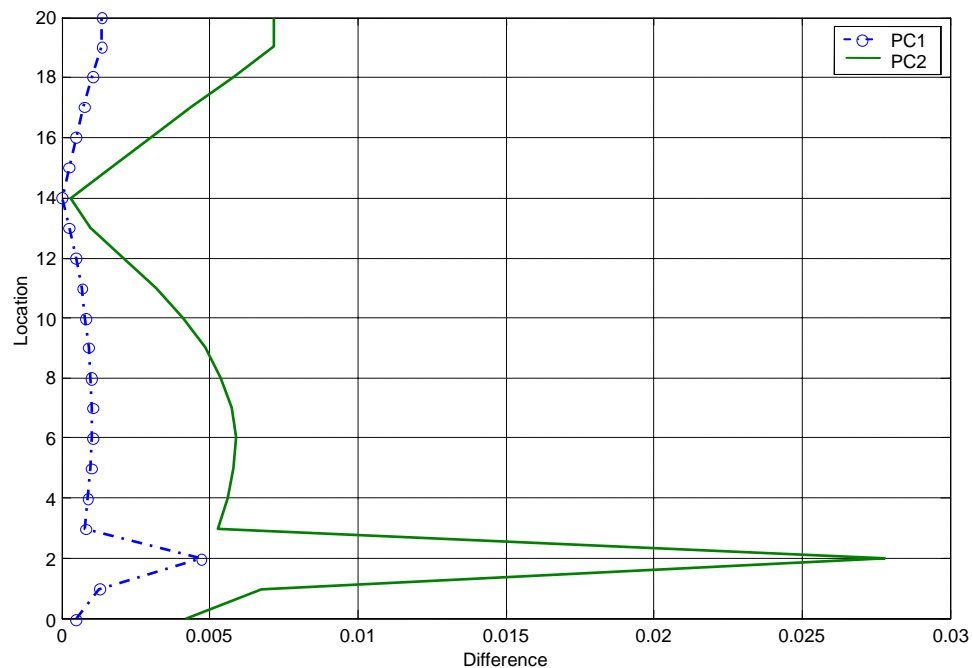
Figure 6.12. Absolute difference between the curvature mode shapes for mode 3 of the frame for damage scenarios PC1 and PC2.
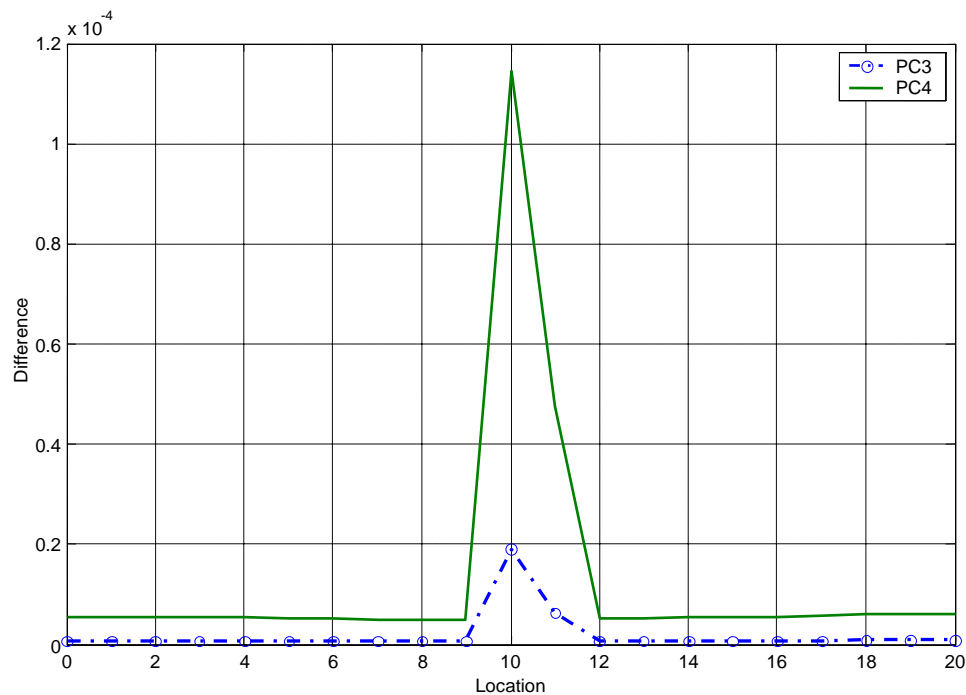
Figure 6.13. Absolute difference between the curvature mode shapes for mode 1 of the frame for damage scenarios PC3 and PC4.
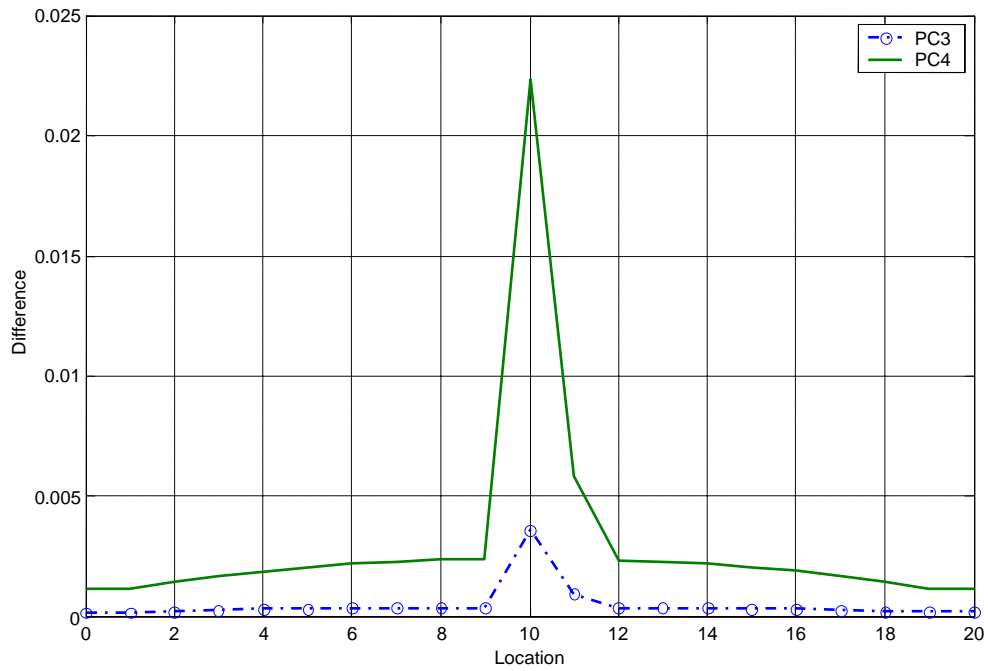
Figure 6.14. Absolute difference between the curvature mode shapes for mode 2 of the frame for damage scenarios PC3 and PC4.
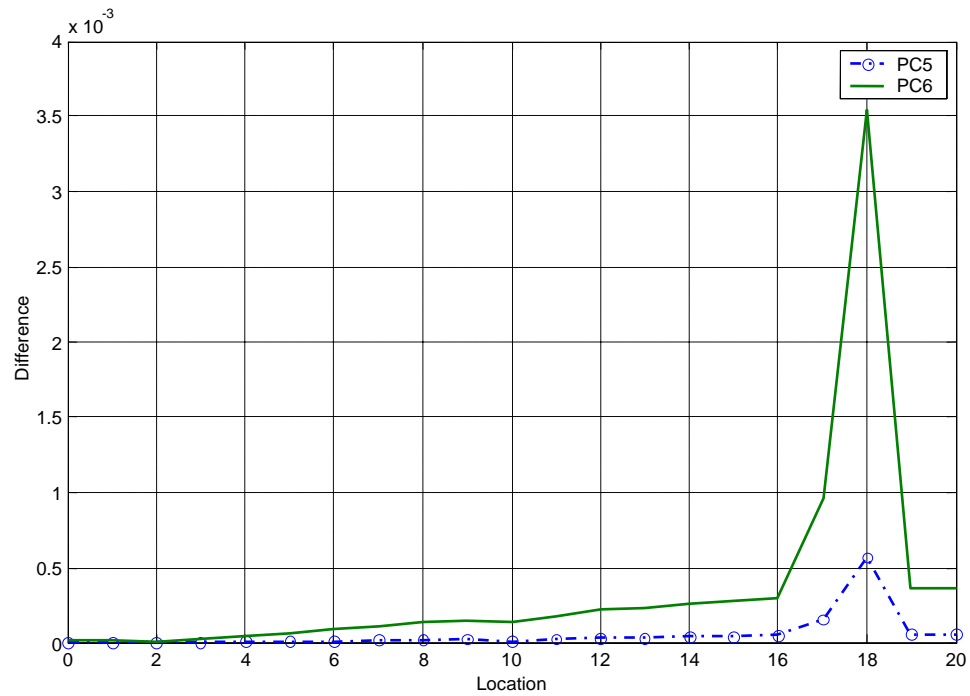
Figure 6.15. Absolute difference between the curvature mode shapes for mode 1 of the frame for damage scenarios PC5 and PC6.
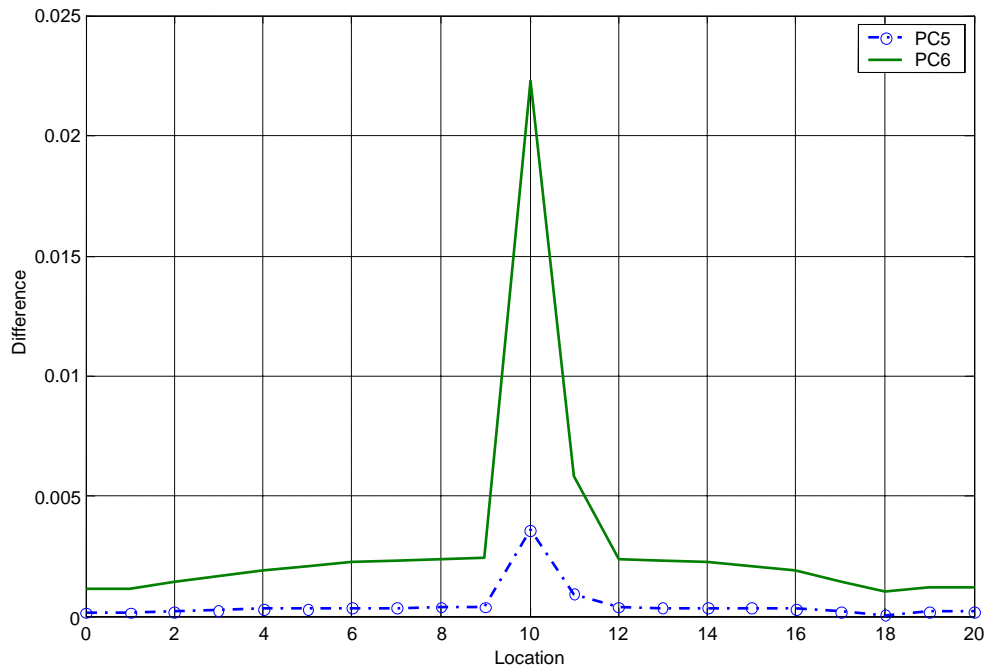
Figure 6.16. Absolute difference between the curvature mode shapes for mode 2 of the frame for damage scenarios PC5 and PC6.
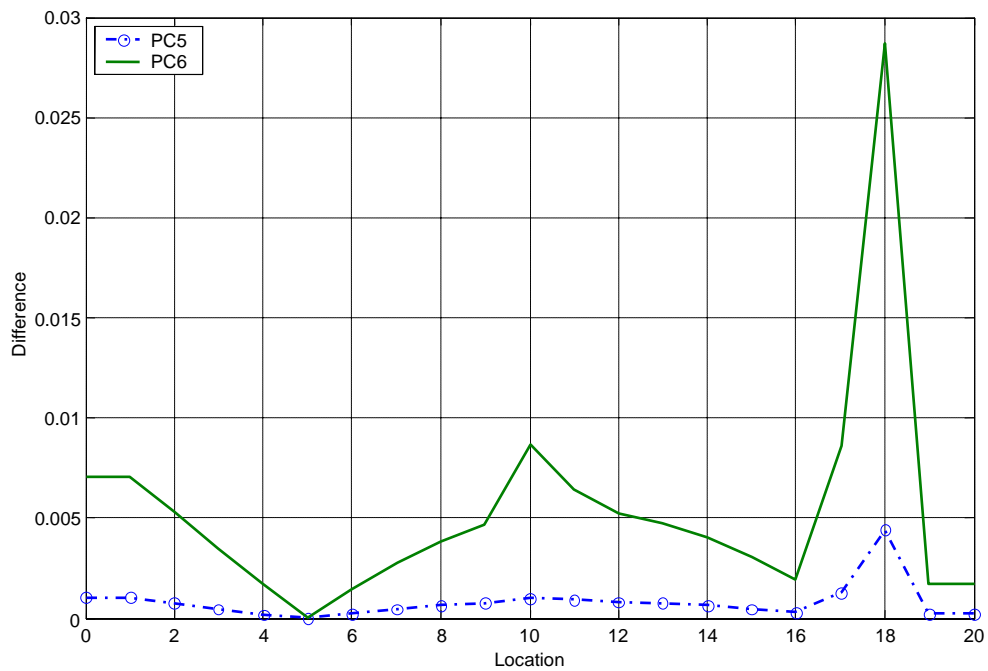
Figure 6.17. Absolute difference between the curvature mode shapes for mode 3 of the frame for damage scenarios PC5 and PC6.

6.4 DAMAGE INDEX β

This method was proposed by Kim et al. (2003), and is designed to yield information on the location and the severity of damage in a structure directly from measured changes in the modal characteristics of the structure. The modal characteristics of interest are natural frequencies and mode shapes. Once several sets of modal parameters are measured, for the undamaged structure and the damaged state, the damage indices developed are used to predict the damage location and to estimate the severity of the damage at that location.

The damage indices are based on the variation of the fraction of modal energy at the elements of the structure for a particular mode.

The method considers a structural system with *ne* elements (*j=1,2,…,ne*) and a measured set of *nm* vibration modes (*i* =1,…, *nm*). For several measurable and identifiable modes, the damage localization index for the *j*th location, is given by:

$$\beta_j = \frac{\sum_i \gamma_{ij}^*}{\sum_i \left(\gamma_i \eta_i + \gamma_{ij}\right)} \qquad (6.5)$$

where η_i is the relative change in the eigenvalues of the damaged and undamaged system:

$$\eta_i = \frac{\Delta \omega_i^2}{\omega_i^2} = \frac{\omega_i^{*2} - \omega_i^2}{\omega_i^2}$$

(6.6)

with

ω_i^*, ω_i: natural frequencies of the damaged and undamaged structure

$$\gamma_{ij}^* = \int_{x_k}^{x_k + \Delta x} \left[\phi_i^{"*}(x) \right]^2 dx$$

$$\gamma_{ij} = \int_{x_k}^{x_k + \Delta x} \left[\phi_i^{"}(x) \right]^2 dx$$

(6.7)

$$\gamma_i = \int_0^L \left[\phi_i^{"}(x) \right]^2 dx$$

$\phi_i^{"*}(x), \phi_i^{"}(x)$: curvature mode shape of the *ith* modal vector for the damaged and undamaged structure.

in which x_k and $x_k + \Delta x$ are the local coordinates of two consecutive nodes of element *j*. Note that an asterisk is used to denote the modal parameters associated with the damaged system.

The damage index defined in equation (6.5) is the original definition as proposed by Kim et al. (2003). However, when this damage index was implemented to evaluate damage via numerical simulations, it did not give the results expected. The reasons for this are not clear; it is possible that there was a misprint problem in the original expressions. Therefore, in this work it is proposed an alternative damage localization index with a format similar to the original one. The new index is defined as

$$\beta_j = \frac{\sum_i \gamma_{ij}^*}{\sum_i \gamma_{ij}\left(1+\eta_i\right)} \qquad (6.8)$$

This index is defined in terms of the first two integrals in Equations (6.7), over the same element j of the structure. After the damage localization index of element j is computed for the damage cases, the values of the indicator are normalized according to the following rule:

$$Z_j = \frac{\beta_j - \mu_{\beta j}}{\sigma_{\beta j}} \qquad (6.9)$$

where

$\mu_{\beta j}$: mean of the damage index

$\sigma_{\beta j}$: standard deviation of the damage index

The structural elements are next assigned to a damage class via a statistical-pattern-recognition technique that utilizes hypothesis testing. The null hypothesis, referred to as H_0, corresponds to the structure *not* damaged at the *jth* location and the alternate hypothesis, denoted as H_1, means that the structure *is* damaged at the *jth* location. To assign damage to a particular location, the following decision rule is used: (1) select H_0 if $Z_j < 2$ or (2) select the alternate H_1 if $Z_j \geq 2$. This test corresponds to a confidence level of 97.7 %.

6.5 NUMERICAL SIMULATION

It is recalled that the modal amplitudes were obtained at a reduced number of locations. To obtain a better approximation in the evaluation of equations (6.7), from the i*th* modal vector, modal coordinates at the 41 nodal points (corresponding to 40 elements) of the damage detection model were calculated by using cubic spline interpolation functions. Using the interpolated modal coordinates, the curvature mode shapes were generated numerically via a central difference approximation. To evaluate the integrals, the function *quad,* (included in MATLAB) was used. This function evaluates numerically the integral using a recursive adaptive Simpson quadrature.

- Simply-supported beam

The damage index for the damage scenarios SD1 to SC4 using the first two displacement mode shapes are illustrated in Figures 6.18, 6.20 and 6.22. It can be seen that for all the damage scenarios the damage index displays a peak in the damaged region. In Figures 6.18 and 6.20 the damage was simulated at the mid-span of the beam. As it happened with the modal curvature method studied before, the damage index was also able to clearly identify the damage. However, as it can be observed in Figure 6.22, the new method can indicate simultaneously the location of the two damaged regions of the beam. The damage index β_j for the damage scenarios SD2, SC2 to SC4 are used to calculate the normalized index Z_j defined in equation (6.9). The predicted damaged elements using the normalized indicator index Z_j are shown in Figures 6.19, 6.21 and 6.23

respectively. As it is evident from these figures, the predicted damaged elements correspond to peak values of the damage localization index.
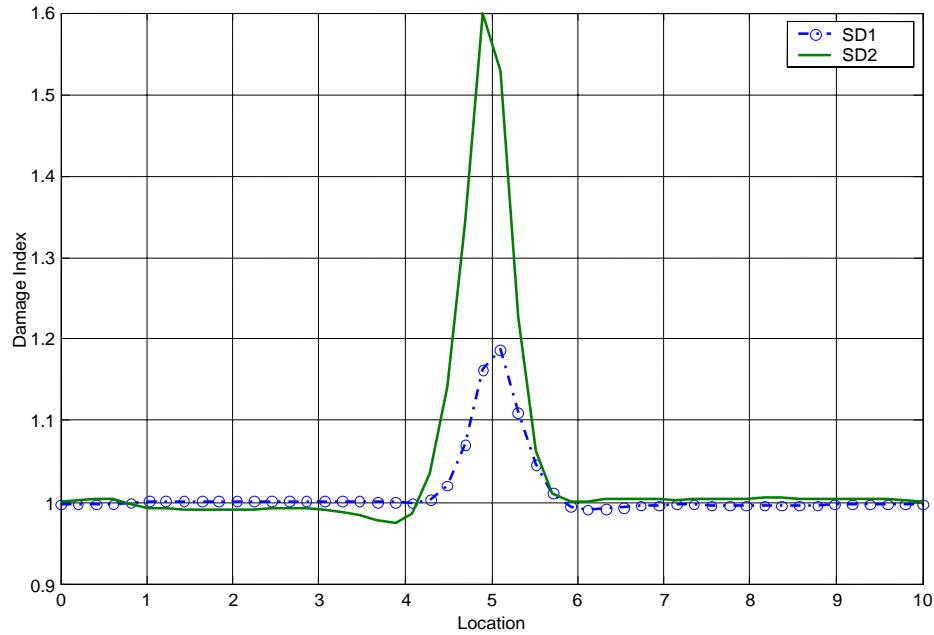
Figure 6.18. Damage Index for the beam with damage scenarios SD1 and SD2
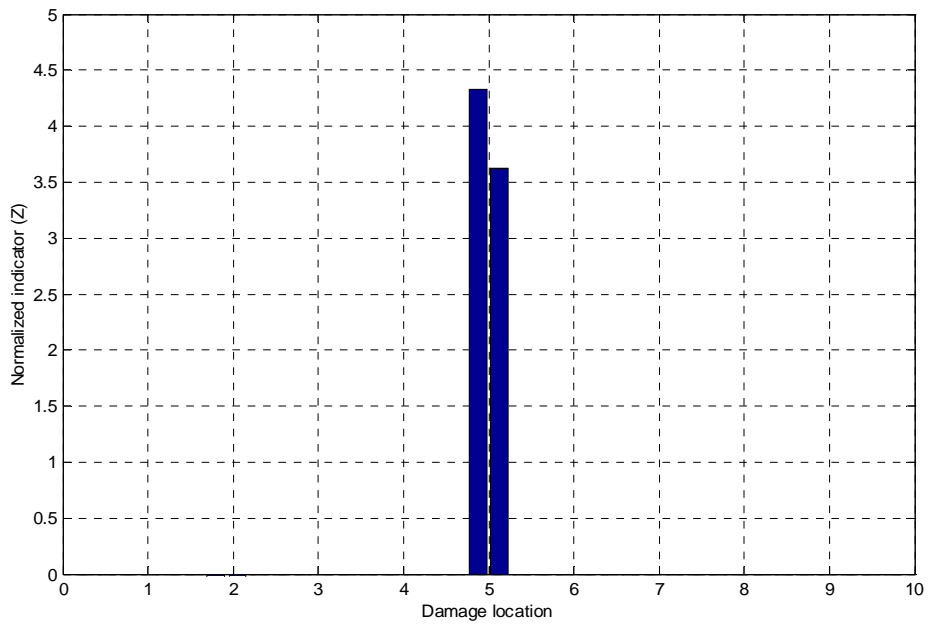
Figure 6.19. Normalized indicator for damage scenario SD2.
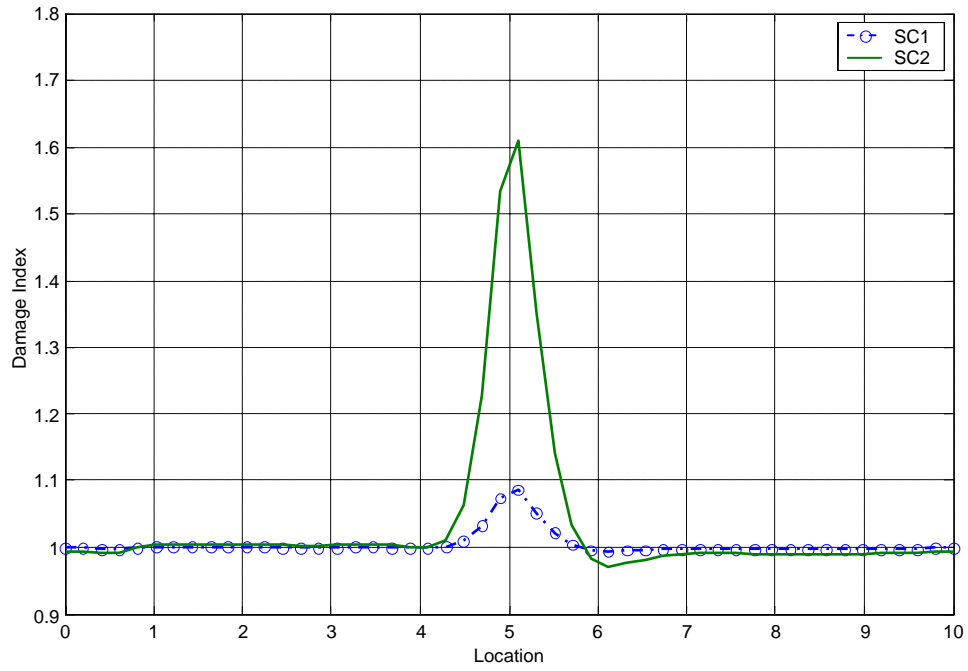
Figure 6.20 Damage Index for the beam with damage scenarios SC1 and SC2.
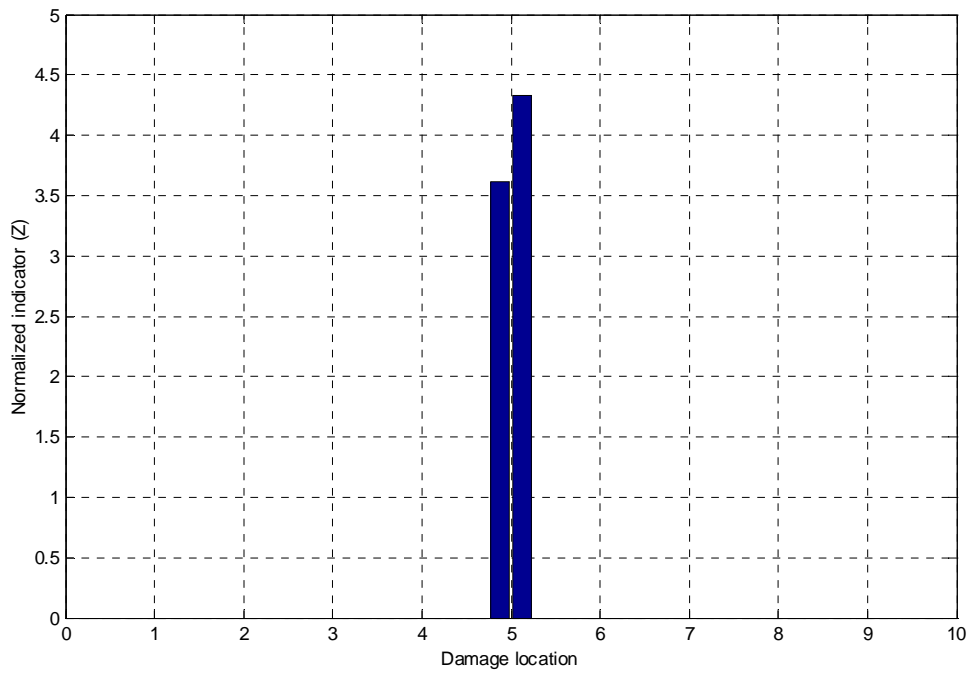
Figure 6.21 Normalized indicator for damage scenario SC2.
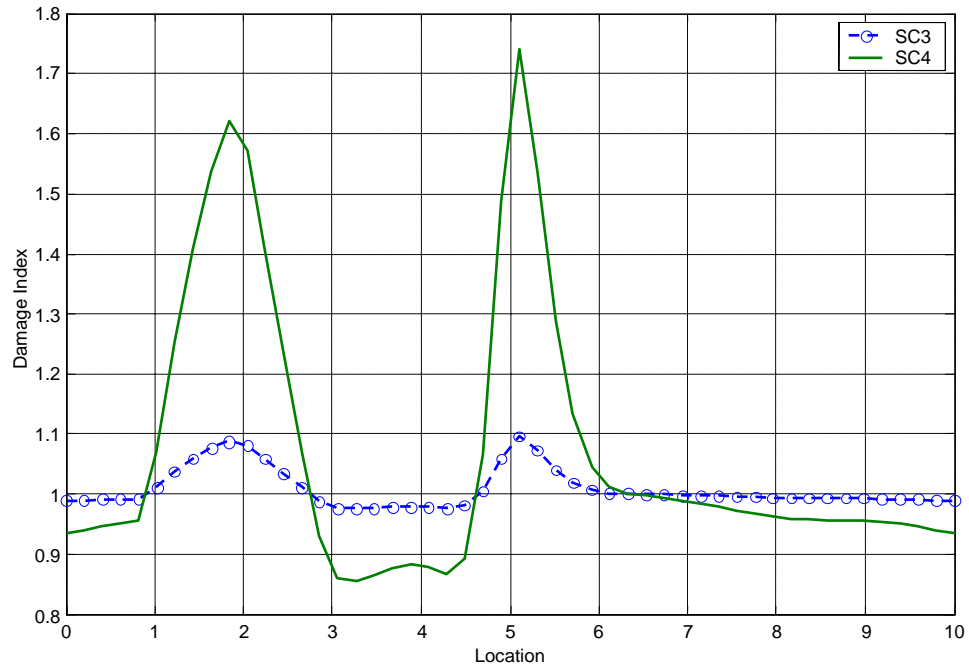
Figure 6.22 Damage Index for the beam with damage scenarios SC3 and SC4.
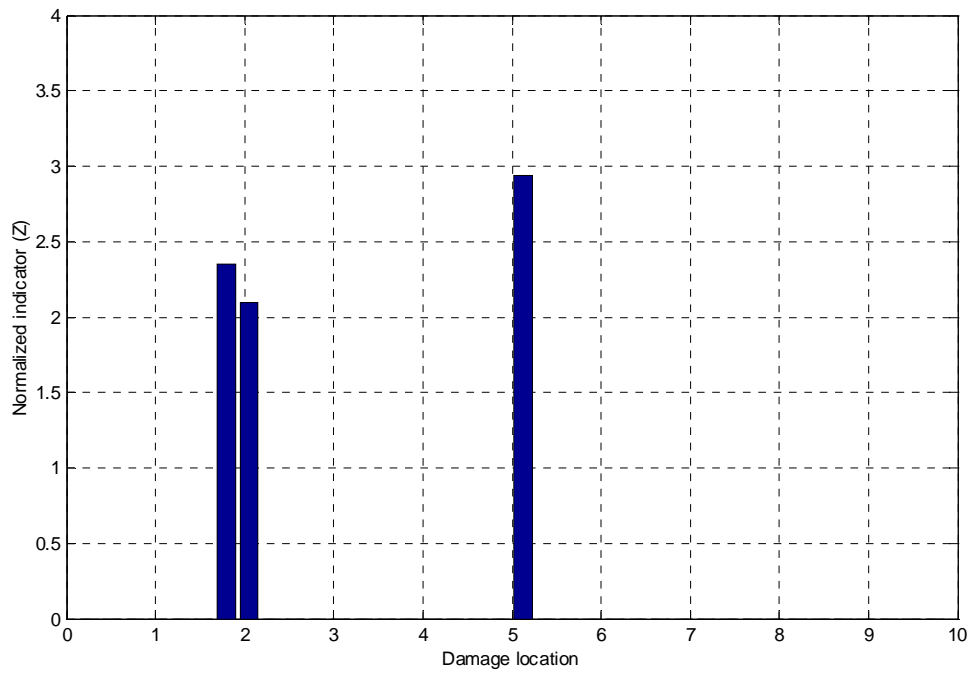
Figure 6.23 Normalized indicator for damage scenario SC4.

- Plane frame

Similar sets of results are presented next for the plane frame. The damage localization index β_j for the damage scenarios PC1 to PC6 are shown in Figures 6.24, 6.26 and 6.28. The index is defined using the first two mode shapes. Again, the peak values are in correspondence with the damaged regions. Figure 6.24 and 6.26 show the results when the damage is a single crack in the column and beam, respectively. Figure 6.28 corresponds to the case where there are two cracks in the beam of the frame. In a similar way as for the simply supported beam with multiple damage, the plot of the damage indexes was able to locate the damaged spots.

The predicted location of the damaged elements using the normalized indicator index Z_j for the damage scenarios PC2, PC4 and PC6 are shown in Figures 6.25, 6.27 and 6.29 respectively. As it can be seen, the predicted damaged elements correspond to peak values of the damage localization index.
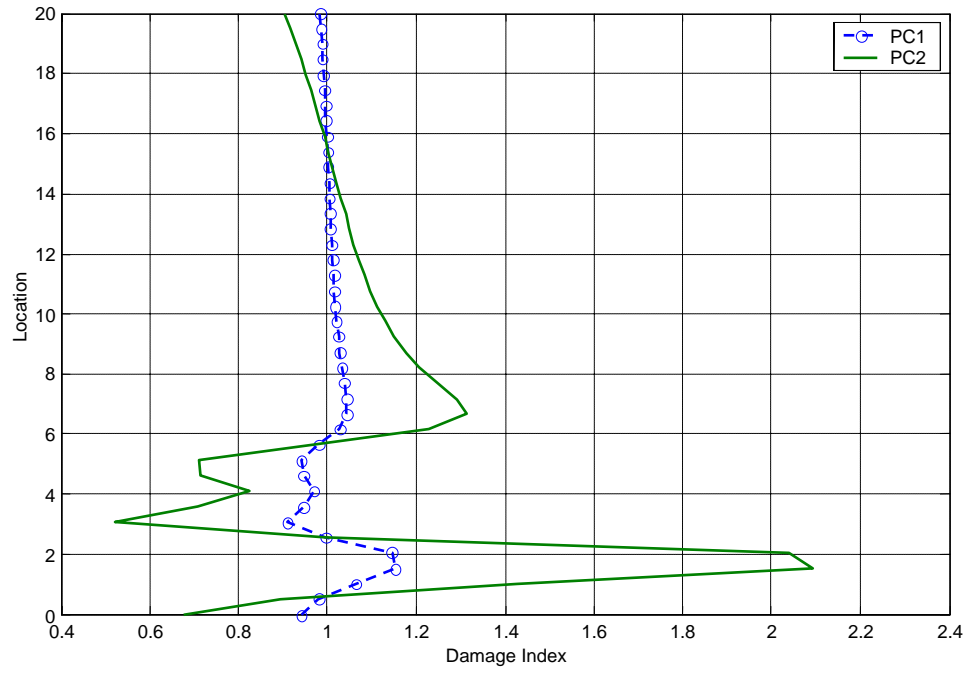
Figure 6.24 Damage Index for the frame with damage scenarios PC1 and PC2.
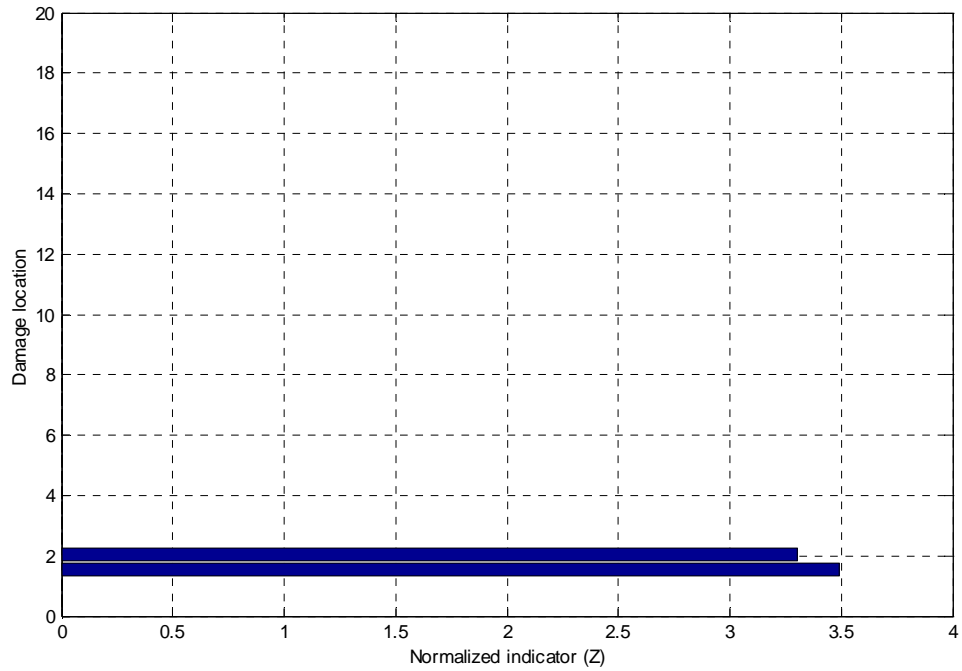
Figure 6.25 Normalized indicator for damage scenario PC2.
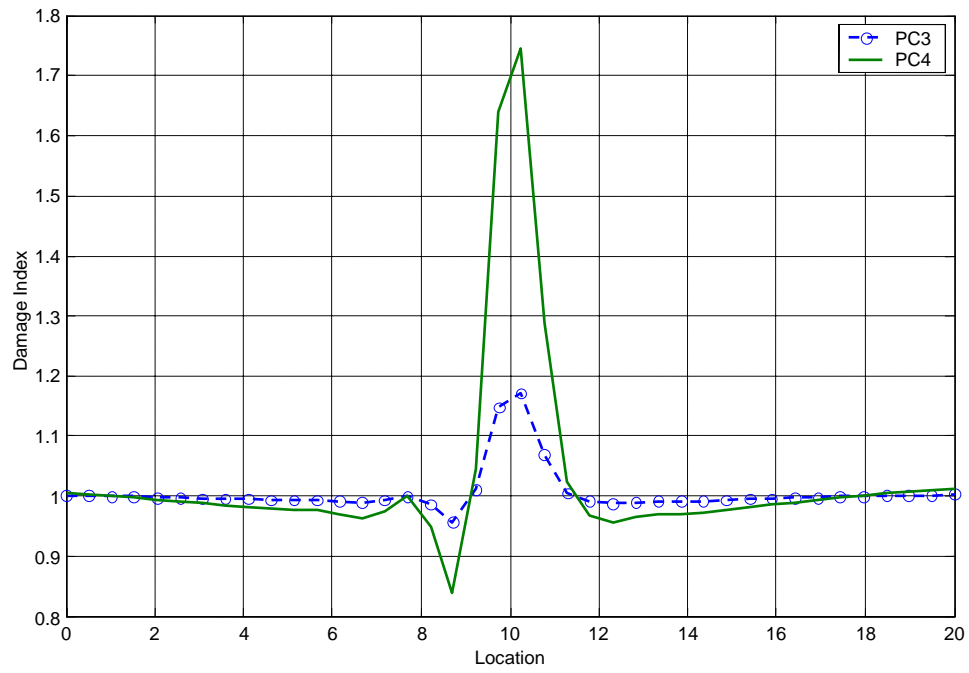
Figure 6.26. Damage Index for the frame with damage scenarios PC3 and PC4.
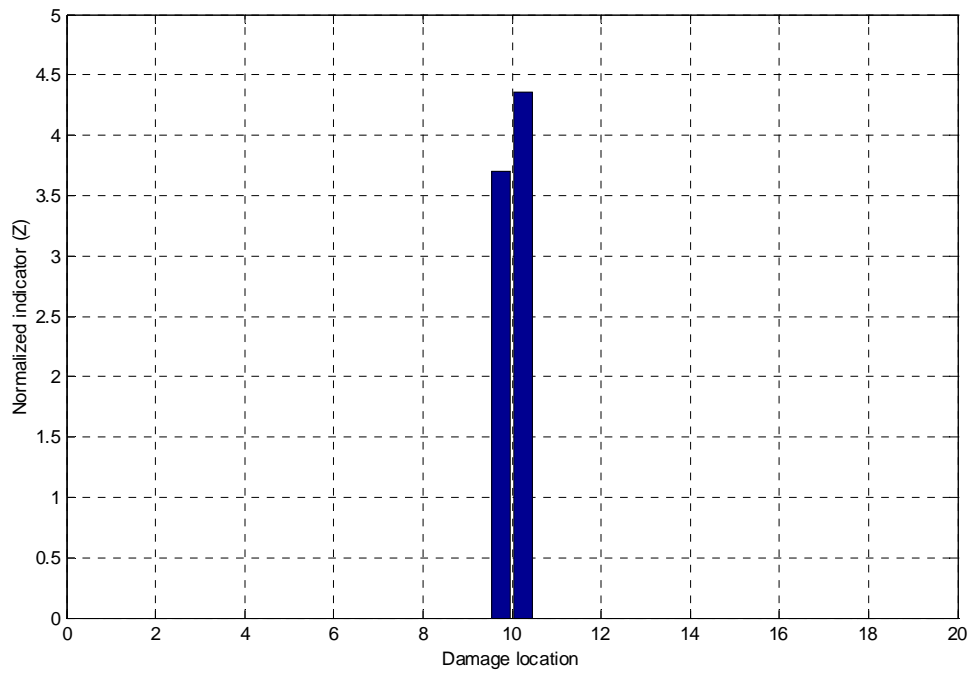
Figure 6.27 Normalized indicator for damage scenario PC4.
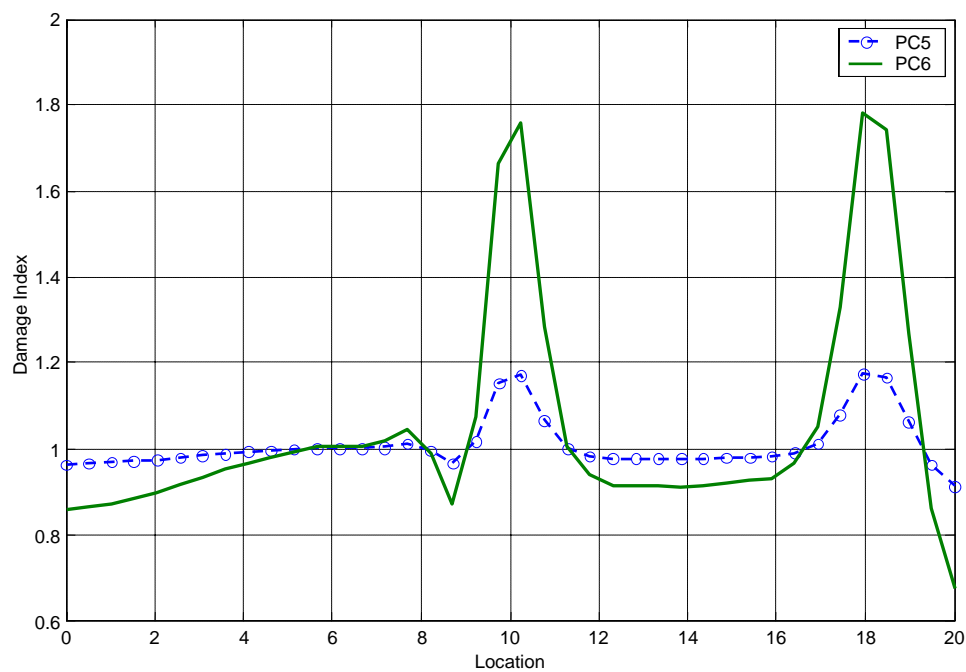
Figure 6.28 Damage Index for the frame with damage scenarios PC5 and PC6.
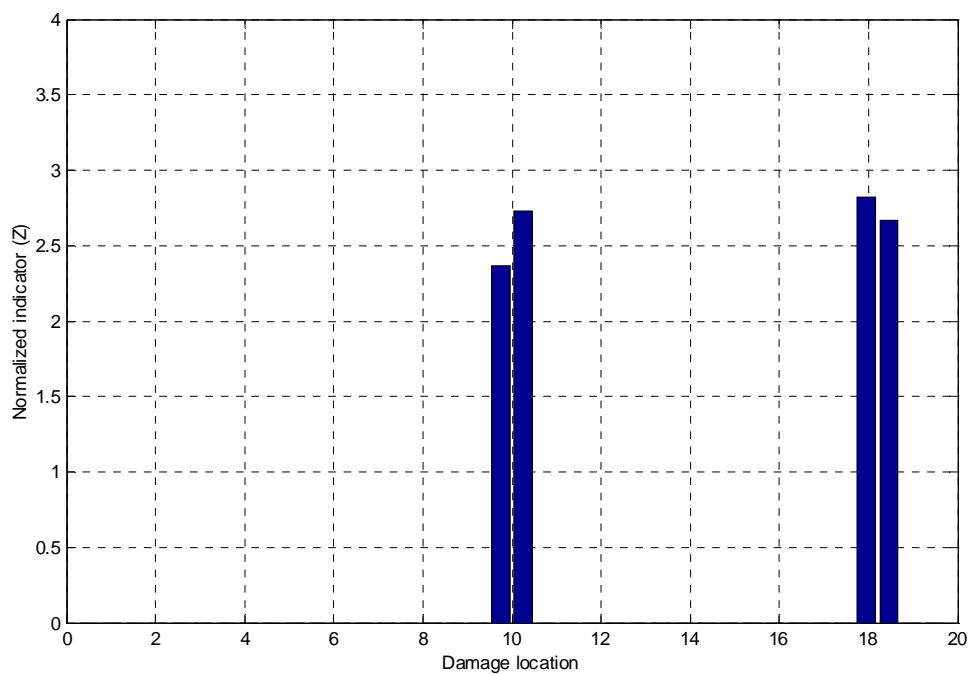
Figure 6.29 Normalized indicator for damage scenario PC6.

6.6 CURVATURE-ENERGY DAMAGE INDEX

As it was discussed in a previous chapter, the presence of damage in a structure increases the magnitude of the curvature at that section of the structure. In this chapter a new damage index based on the *modal* curvature is proposed. It is based on the concept of the flexibility matrix. The proposed modal curvature-based matrix can be defined by

$$[X]_{n \times n} = [\Phi'']_{n \times m} [\Lambda]_{m \times m}^{-1} [\Phi'']_{m \times n}^{T} \tag{6.10}$$

where n is the number of points for mode shape measurements (or measured and interpolated and m is the number of measured modes. $[\Phi'']$ is the modal curvature matrix formed by the curvature mode shapes $\{\phi_i''\}$:

$$[\Phi''] = \left[\{\phi_1''\} \quad \{\phi_2''\} \quad \cdots \quad \{\phi_m''\} \right]$$

$[\Lambda]$: Modal stiffness matrix

For the damaged structure, the proposed curvature- energy matrix can be expressed as

$$[X^*]_{n \times n} = [\Phi_*'']_{n \times m} [\Lambda_*]_{m \times m}^{-1} [\Phi_*'']_{m \times n}^{T} \tag{6.11}$$

For the undamaged structure, the corresponding curvature-energy matrix is given by equation (6.10). In terms of these curvature-energy matrices, the relationship between

damaged and undamaged states, is defined by

$$\{\chi\} = \{\chi_*\} \cdot / \{\chi_u\} \tag{6.12}$$

where the symbol **./** is used to indicate that the division of the vectors is done element by element.

$\{\chi_u\}$: diagonal of the matrix [X].

$\{\chi_*\}$: diagonal of the matrix [X*].

It is proposed to define the damage index for the j*th* location as

$$\kappa_j = \left| \chi_j - 1 \right| \tag{6.13}$$

6.7 NUMERICAL SIMULATIONS

The procedure presented above was used to calculate the curvature-energy matrices of the undamaged and damaged structures considered (simply-supported beam and the plane frame). The same damage scenarios presented in Chapter III are used. The amplitudes of the mode shapes obtained from the free vibration analysis are used to numerically compute the modal curvatures. Next, the proposed damage index is calculated for each one of the damage scenarios.

- Simply-supported beam

The proposed damage index for the damage scenarios SD1 to SC4 is shown in Figures 6.30 to 6.32, calculated using only two curvature mode shapes. As the two previous methods, the new technique is able to detect the single cracks in the beam for the damage scenarios SD1, SD2 and SC1, SC2. When two cracks are induced in the beam (damage scenarios SC3 and SC4), the proposed method is capable of detecting the location of the two defects, as evidenced by the peaks in the index κ_j in Figure 6.32.
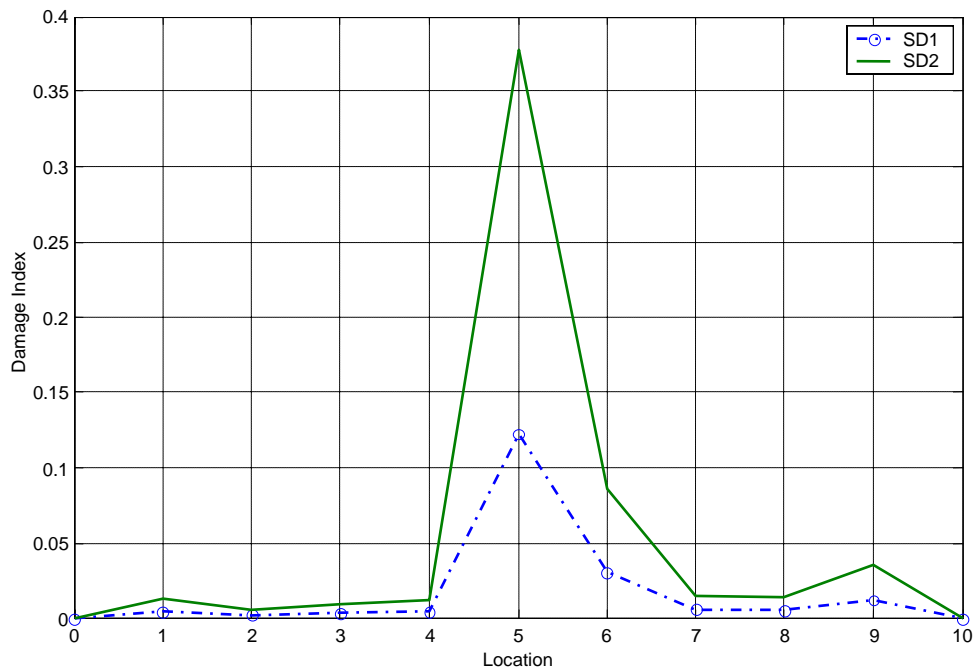
Figure 6.30 Curvature-energy damage index for the beam with damage scenarios SD1 and SD2.
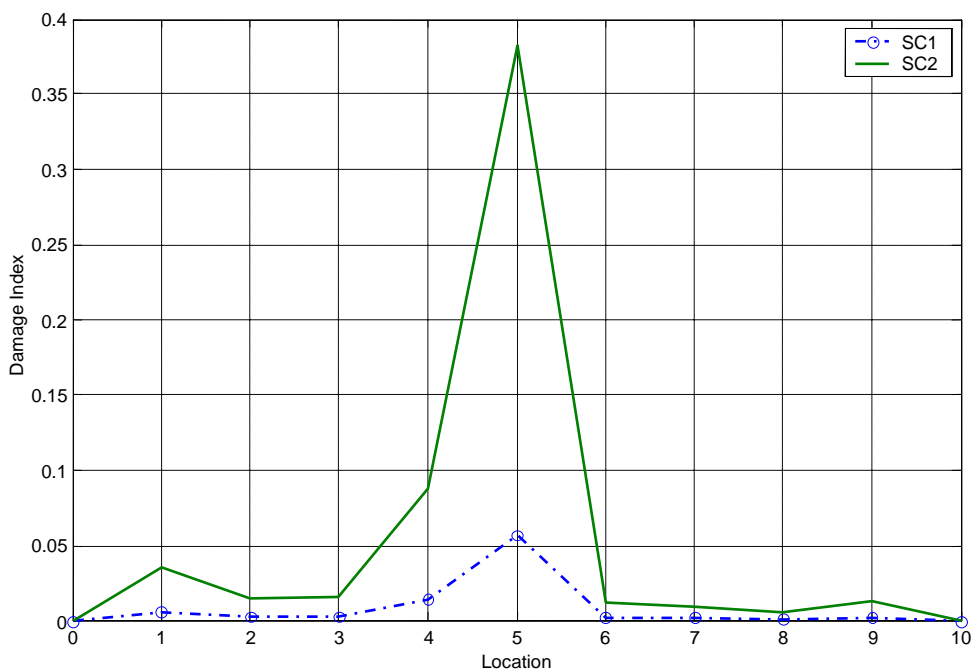
Figure 6.31 Curvature-energy damage index for the beam with damage scenarios SC1 and SC2.
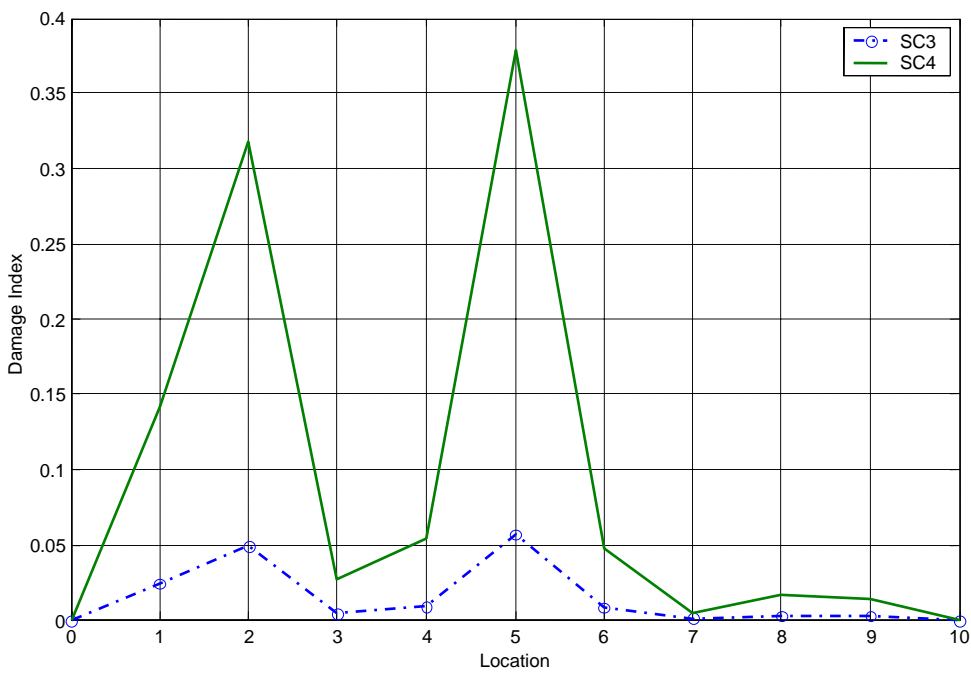
Figure 6.32 Curvature-energy damage index for the beam with damage scenarios SC3 and SC4.

- Plane frame

The proposed damage index is next applied to detect damage in the plane frame. The results for the damage scenarios PC1 to PC6 are shown in Figures 6.33 to 6.35, where only the first two curvature mode shapes were used. Again, the peak value of the index occurred at the damaged region. In a similar way as in the analysis of the beam with multiple damage, the plot of the damage index clearly indicates the location of the two damaged regions of the frame.
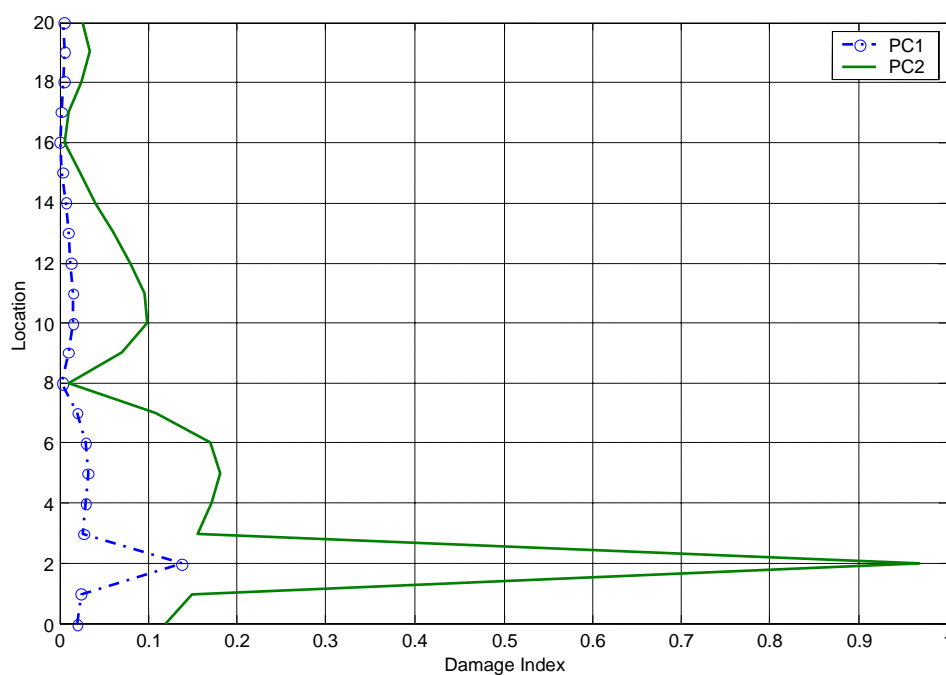
Figure 6.33 Curvature-energy damage index for the frame with damage scenarios PC1 and PC2.
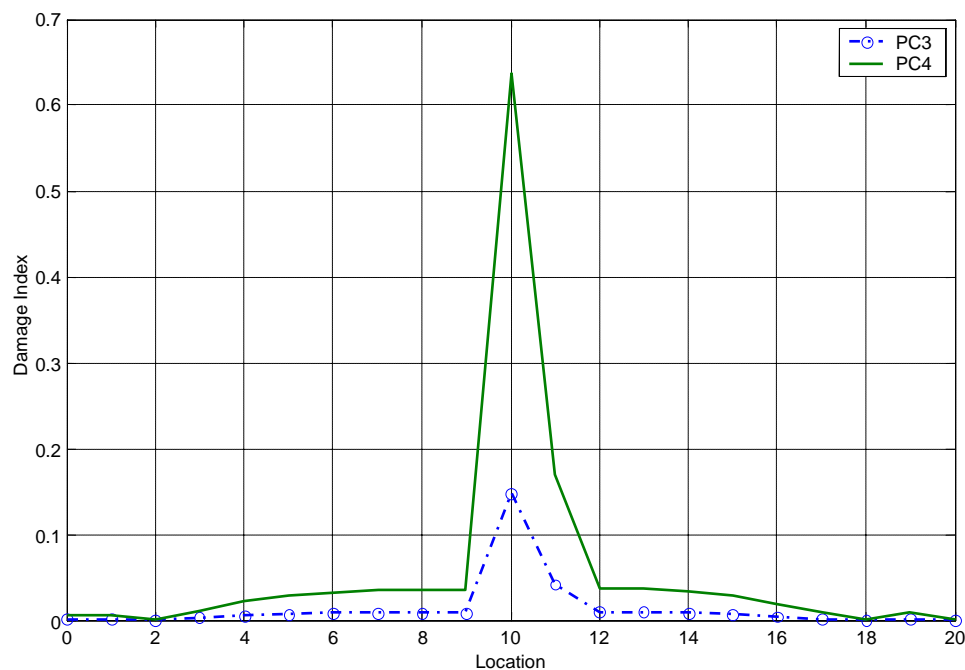
Figure 6.34 Curvature-energy damage index for the frame with damage scenarios PC3 and PC4.
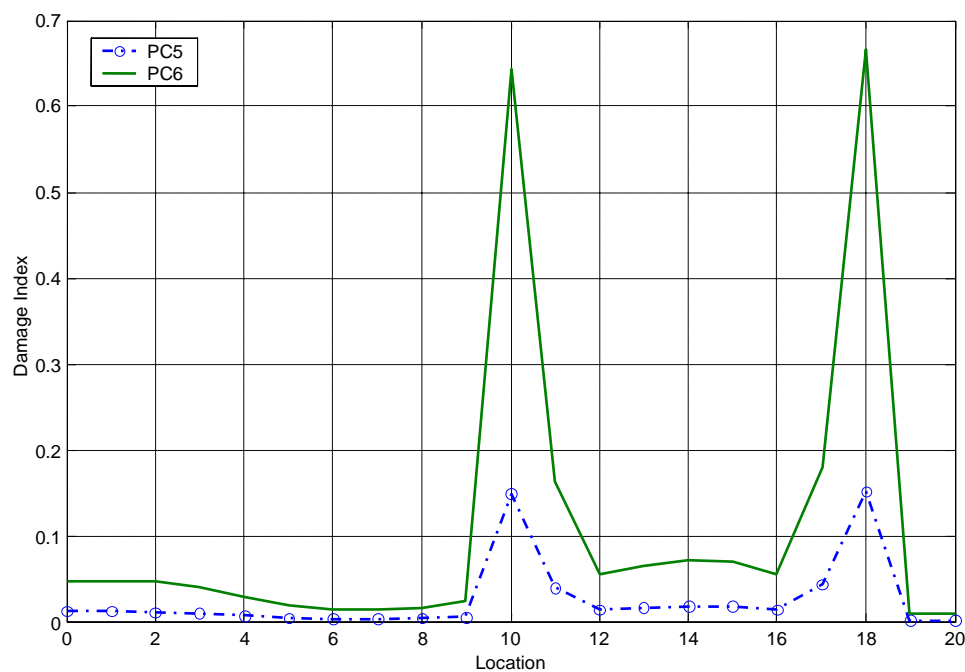
Figure 6.35 Curvature-energy damage index for the frame with damage scenarios PC5 and PC6.

6.8 SUMMARY

A new damage identification method based on the modal curvature is proposed in this chapter. Two existing methodologies are also presented and evaluated. One of these methods is based on the difference between the modal curvatures of the damaged and undamaged structure. The other method is based on the variation of the modal energy in the elements of the structure. Numerical examples are presented to compare the effectiveness of the methods studied to indicate the presence and locate the position of damage in simple structures. Two structures were used to evaluate the three methods. The first structure analyzed was a simply-supported beam. For each of the six scenarios of damage, the values of the damage indices for all the methods were calculated.

The curvature-difference method can indicate correctly the location of the region damaged of the beam, when the first two curvature modes are used in the damage scenarios that simulate one damaged element. In the multiple damage scenarios if the results of the two modes are used is possible to detect the location of damage.

From the evaluation of the second method, it was observed that it was possible to clearly locate the damage in all the damage scenarios studied using only two mode shapes. This method showed a good performance in the case of multiple damage. The results of the analyses indicate that the damage index formulated in this thesis correctly localizes the defects simulated in the beam. An advantage of the method is that to locate the damage it requires only a few modes (the lower two in the examples considered).

Next, a plane frame was analyzed. Six scenarios of damage were studied and the damage indices of each method were calculated. The curvature difference method could indicate correctly the location of the damaged region of the beam when the first two modes were used and a single element was damaged. The damage index β was evaluated next. This method proved to be capable to locate the damaged zones of the beam and plane frame in all of the damage scenarios analyzed and using the first three modes. The new damage index was applied to the same structures. This damage index correctly localized the damaged zones of the beam and frame by using only two mode shapes.

CHAPTER VII

METHODS BASED ON THE FREQUENCY RESPONSE FUNCTION

7.1 INTRODUCTION

The structural damage identification methods studied in the previous chapters are based on measured modal data (frequencies and mode shapes). There are other kinds of methods based on Frequency Response Function (FRF) data. Using measured FRFs for damage detection may have certain advantages over the traditional methods using modal analysis data (He 1999). First, numerical errors inherent in modal analysis results due to inaccurate curve fitting and unavailable residual terms are avoided. Second, no more effort is needed to process measured FRF data in order to obtain modal analysis data. Finally, the most significant advantage lies in the fact that FRF data provide abundant information on the dynamic behavior of a structure. In comparison, modal analysis data, due to the numerical process used to extract them, lose much of the information that FRF data have to offer.

In this chapter, an existing methodology is studied and two damage identification methods based on the FRF-curvature are proposed. A new concept based on the Receptance Energy is formulated. Numerical simulations are performed to compare the

effectiveness of the existing and proposed procedures to locate the damage. First, a brief introduction to the theory of the harmonic vibrations and the FRF is presented.

7.2 FREQUENCY RESPONSE FUNCTION : HARMONIC VIBRATIONS

The general mathematical representation of a single degree of freedom (SDOF) system is expressed by

$$m\ddot{x}(t) + c\dot{x}(t) + kx(t) = F(t) \tag{7.1}$$

Assuming that the forcing function is harmonic of the form $F(t) = F_o e^{i\Omega t}$ and the damping is linear and viscous, the *Frequency Response Function (FRF)* can be defined by

$$H(\Omega) = \frac{1}{1 - \left(\dfrac{\Omega}{\omega_n}\right)^2 + i2\varsigma\left(\dfrac{\Omega}{\omega_n}\right)} \tag{7.2}$$

For multiple degree of freedom (MDOF) systems with classic damping, the *Frequency Response Function (FRF) between the degrees of freedom r and s* is defined as

$$Hrs(\Omega) = \sum_{j=1}^{n} \frac{\phi_{rj}\phi_{sj}}{\omega_j^2 - \Omega^2 + 2\xi_j\omega_j\Omega i} \tag{7.3}$$

$H_{rs}(\Omega)$ is the response of the DOF r due to a single harmonic force excitation of unit amplitude applied at the DOF s. This particular FRF where the response or output is described in terms of the displacement and the input is a force is known as the Receptance function.

The functions $H_{rs}(\Omega)$ can be arranged in matrix form. This leads to a Receptance Matrix defined as

$$[H(\Omega)] = \begin{bmatrix} H_{11} & H_{12} & \cdots & H_{1n} \\ H_{21} & H_{22} & \cdots & H_{2n} \\ \vdots & \vdots & \ddots & \vdots \\ H_{n1} & H_{n2} & \cdots & H_{nn} \end{bmatrix} \tag{7.4}$$

In a more general case the Receptance Matrix for MDOF systems with viscous damping, can be expressed as

$$[H(\Omega)] = \left[[K] - \Omega^2 [M] + i\Omega [C] \right]^{-1} \tag{7.5}$$

The Receptance Matrix is symmetric and therefore

$$H_{rs}(\Omega) = \frac{\overline{X}_r}{F_s} = H_{sr} = \frac{\overline{X}_s}{F_r} \tag{7.6}$$

where $\overline{X}_k$ and F_k are, respectively, the Fourier transform of the displacement and applied force time histories at the kth degree of freedom.

The property in Equation (7.6) is known as the *principle of reciprocity*. The displacement, velocity and acceleration are mathematically interrelated response quantities. Therefore, by knowing the FRF in terms of any one of the response parameters one can derive any of the other FRF forms. For instance, the mobility is defined by

$$Y_{rs}(\Omega) = i\Omega H_{rs}(\Omega) = \sum_{j=1}^{n} \frac{i\Omega\phi_{rj}\phi_{sj}}{\omega_j^2 - \Omega^2 + 2\xi_j\omega_j\Omega i} \tag{7.7}$$

Similarly the Accelerance or Inertance is defined by

$$A_{rs}(\Omega) = -\Omega^2 H_{rs}(\Omega) = \sum_{j=1}^{n} \frac{-\Omega^2\phi_{rj}\phi_{sj}}{\omega_j^2 - \Omega^2 + 2\xi_j\omega_j\Omega i} \tag{7.8}$$

The Accelerance matrix can be expressed by

$$[A(\Omega)] = \begin{bmatrix} A_{11} & A_{12} & \cdots & A_{1n} \\ A_{21} & A_{22} & \cdots & A_{2n} \\ \vdots & \vdots & \ddots & \vdots \\ A_{n1} & A_{n2} & \cdots & A_{nn} \end{bmatrix} \tag{7.9}$$

Table 7.1 displays the different formulations of the FRF. A brief review of the Frequency Response Function in the Frequency Domain (Fourier Analysis) is presented in Appendix B.

Receptance (Admittance)	$\dfrac{Displacement}{Force}$
Accelerance (Inertance)	$\dfrac{Acceleration}{Force}$
Mobility	$\dfrac{Velocity}{Force}$
Dynamic Stiffness	$\dfrac{Force}{Displacement}$
Apparent Mass	$\dfrac{Force}{Acceleration}$
Mechanical Impedance	$\dfrac{Force}{Velocity}$

Table 7.1 Frequency Response Function Formulations.

7.3 THE FREQUENCY RESPONSE FUNCTION (FRF) CURVATURE METHOD

This method was proposed by Sampaio et al. (1999). The method is an extension of the procedure proposed by Pandey et al. (1991) based on mode shape curvature. The approach accounts for all the frequencies in the measurement range, and not only the natural frequencies. It uses FRF (Receptance) data rather than mode shape data. The method uses something similar to an "operational mode shape" defined, for each frequency by the frequency response at various locations on the structure.

The FRF-curvature for any frequency Ω is defined by

$$H''(\Omega)_{i,j} = \frac{H(\Omega)_{i+1,j} - 2H(\Omega)_{i,j} + H(\Omega)_{i-1,j}}{h^2}$$ (7.10)

where

$H(\Omega)_{i,j}$: the receptance FRF measured at location i due to a force input at position j.

h: the distance between two consecutive measurement points: *(i) and (i+1)* or *(i) and (i-1)*

In this work, the receptance FRF is calculated with Equation (7.3). This implies that the structure has classical viscous damping.

For an applied force at point j, the absolute difference between the FRF curvatures of the damaged and undamaged structure at a location i, in a predetermined frequency range, is defined as

$$\Delta H''_{i,j} = \sum_{\Omega} \left| H''_*(\Omega)_{i,j} - H''(\Omega)_{i,j} \right|$$ (7.11)

Finally, the change in the FRF curvatures for several force location are added. This leads to a parameter S_i for the ith measurement point defined as,

$$S_i = \sum_j \Delta H''_{i,j}$$ (7.12)

7.4 NUMERICAL SIMULATIONS

The previously presented methodology was used to calculate the FRF curvature difference between the FRF-curvature of undamaged and damaged structures. As it was done with the previous methods, simply-supported beam and the plane frame with the different damage scenarios presented earlier are considered. It was assumed that the modal damping ratio ξ_j was constant for all the modes and equal to 0.05. The first five mode shapes were used to compute the values of the Receptance function H_{rs} in the frequency range from 10 to 100 rad/s. This range of frequencies was chosen because the method shows a better performance in a range before the first resonant frequency (Sampaio et al. 1999).

- Simply-supported beam.

The FRF curvature differences for damage scenarios SD1 to SC4 are illustrated in Figures 7.1 to 7.3. The quantity plotted in the figures is the parameter *Si* defined in Equation (7.12). The input force was applied at 2 locations: at points 3 and 5. Note from the figures that the peak value occurred at the damaged region. As it can be verified from Figure 7.3, the method is capable of indicating simultaneously the location of the two damaged regions of the beam. Figure 7.4 shows a two-dimensional plot of the FRF-curvature difference defined in Equation (7.11) for the frequency range 10-100 rad/s. Figure 7.5 shows the surface of the FRF-curvature difference for a frequency range extending from 10 to 220 rad/s. This is done to observe the performance of the FRF-curvature near the first natural frequency of the damaged beam. This frequency is equal

to 221.8 rad/sec. As it can be observed in Figure 7.4, the localization of damage in the frequency range 10-100 rad/sec is clearly defined.
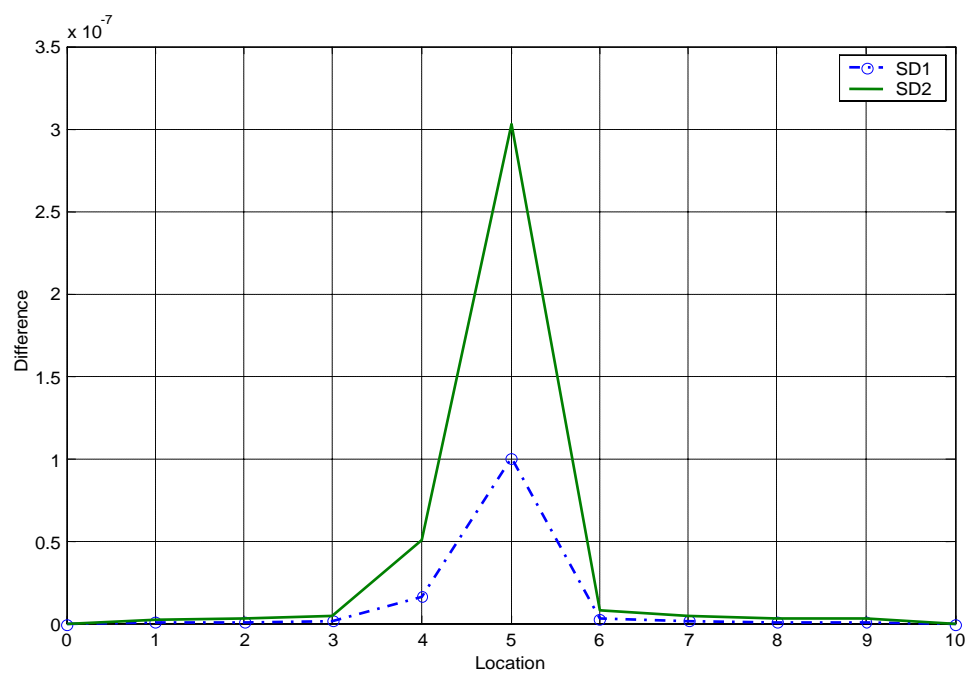
Figure 7.1 FRF curvature differences for the beam with damage scenarios SD1 and SD2.
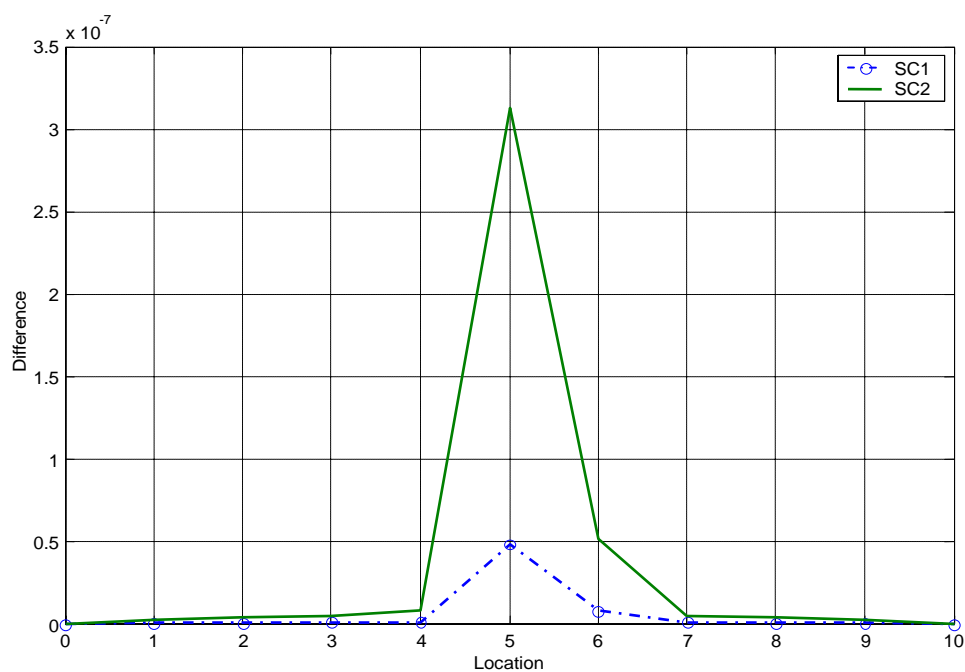
Figure 7.2 FRF curvature differences for the beam with damage scenarios SC1 and SC2.
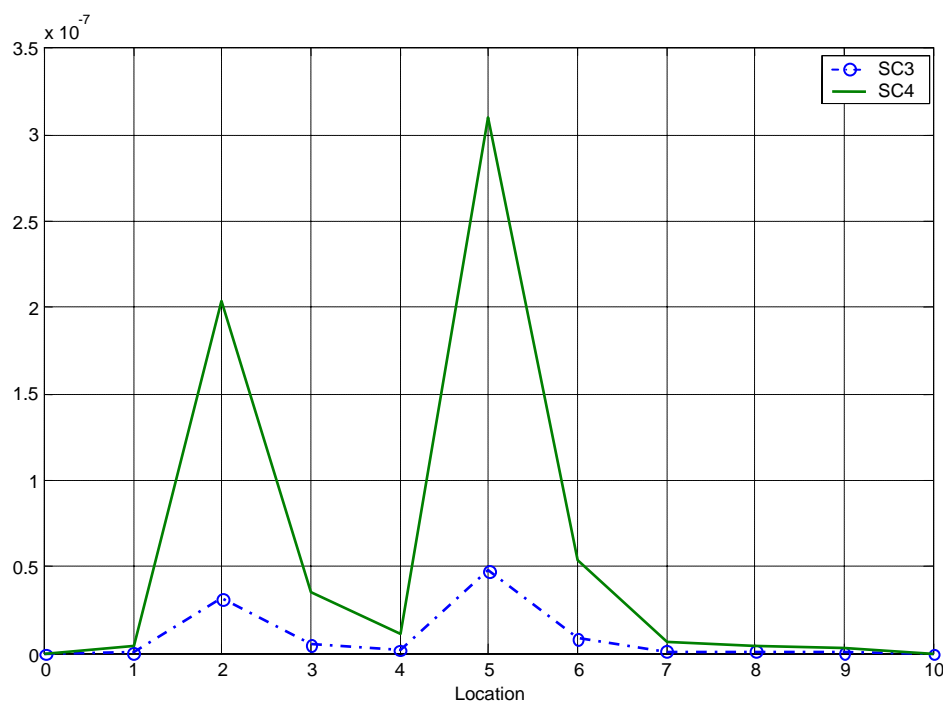
Figure 7.3 FRF curvature differences for the beam with damage scenarios SC3 and SC4.
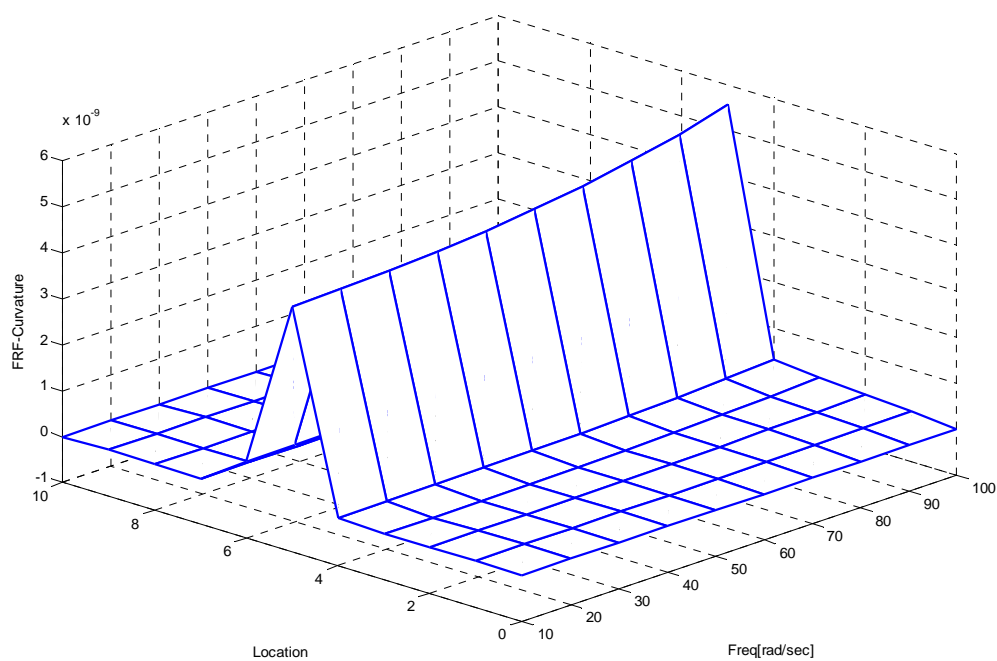
Figure 7.4 Surface of FRF curvature differences in the frequency range 10-100 rad/s for damage scenario SC2.
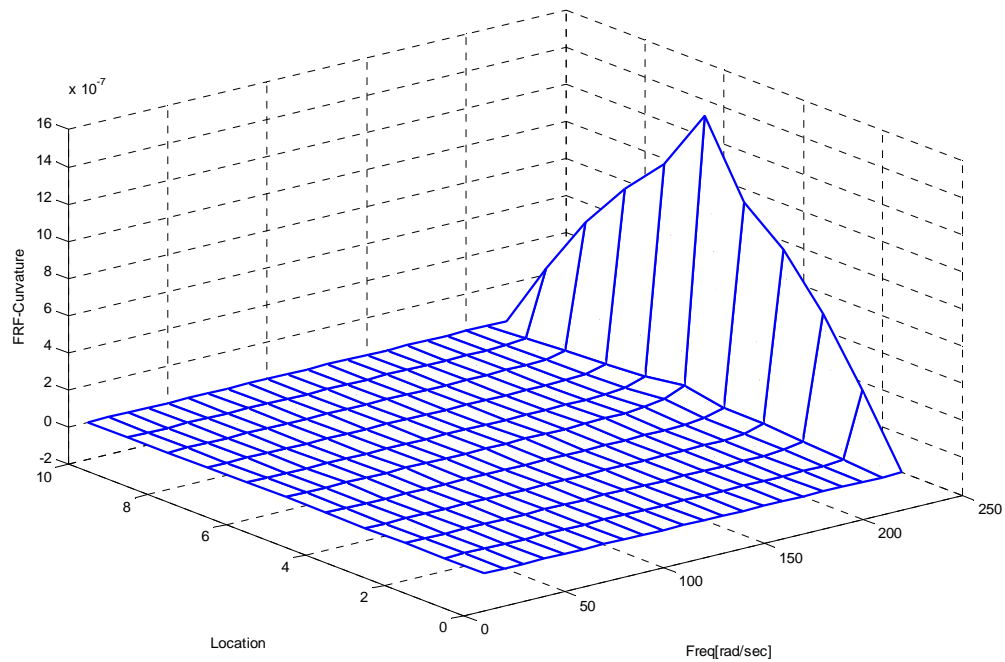
Figure 7.5 Surface of FRF-curvature differences in the frequency range 10-220 rad/s for damage scenario SC2.

- Plane frame

The plane frame in Figure 3.8 is used for the next set of examples. The FRF curvature differences for damage scenarios PC1 to PC6 are shown in Figures 7.6 to 7.8. The frequency range considered to define $\Delta H''_{i,j}$ is 5-50 rad/s. For the damage cases PC1 and PC2, the input force was located at one position (at location 20 on the right column). As in the case of the simply-supported beam, the peak value of *Si* occurs at the damaged zone of the frame. Similarly to the beam with multiple damage, the plot of the FRF curvature difference indicates the location of the damaged zone. Note, however that the FRF-curvature difference has different magnitude at the location of the two cracks, even

though the severity of the damage is the same. This is a disadvantage of the method because we will not be able to estimate the amount of damage with this parameter.
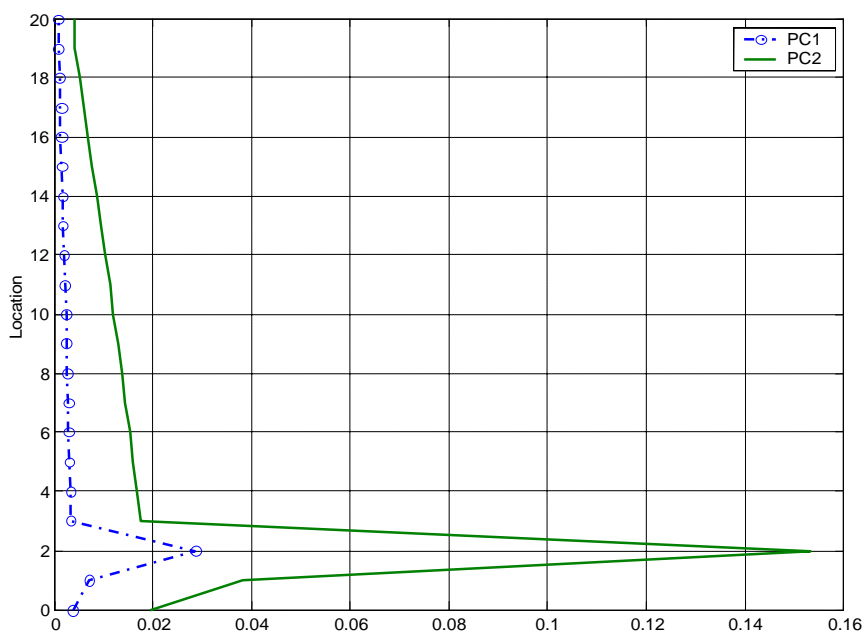
Figure 7.6 FRF curvature differences for the frame for damage scenarios PC1 and PC2.
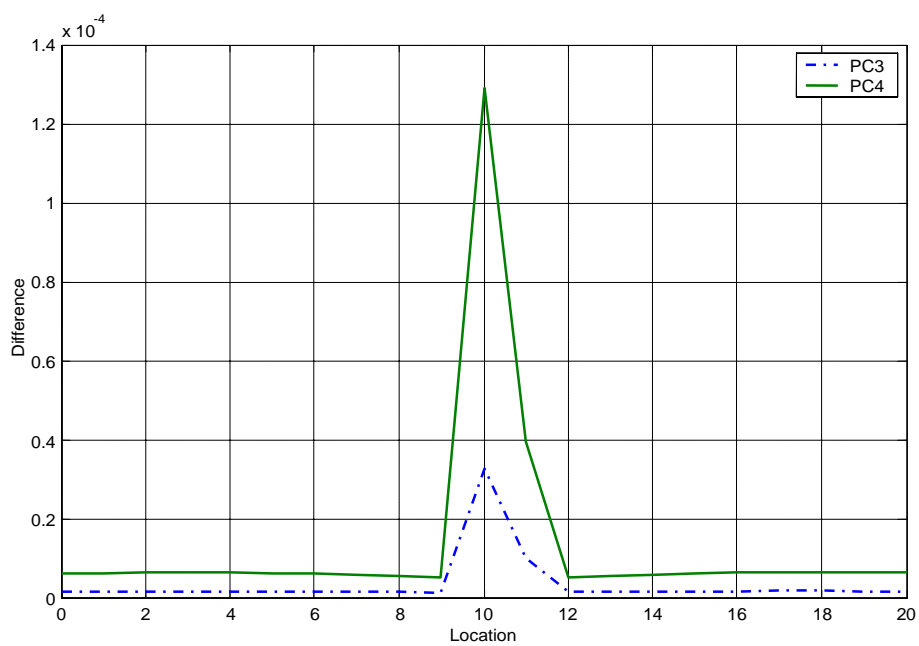
Figure 7.7 FRF curvature differences for the frame for damage scenarios PC3 and PC4.
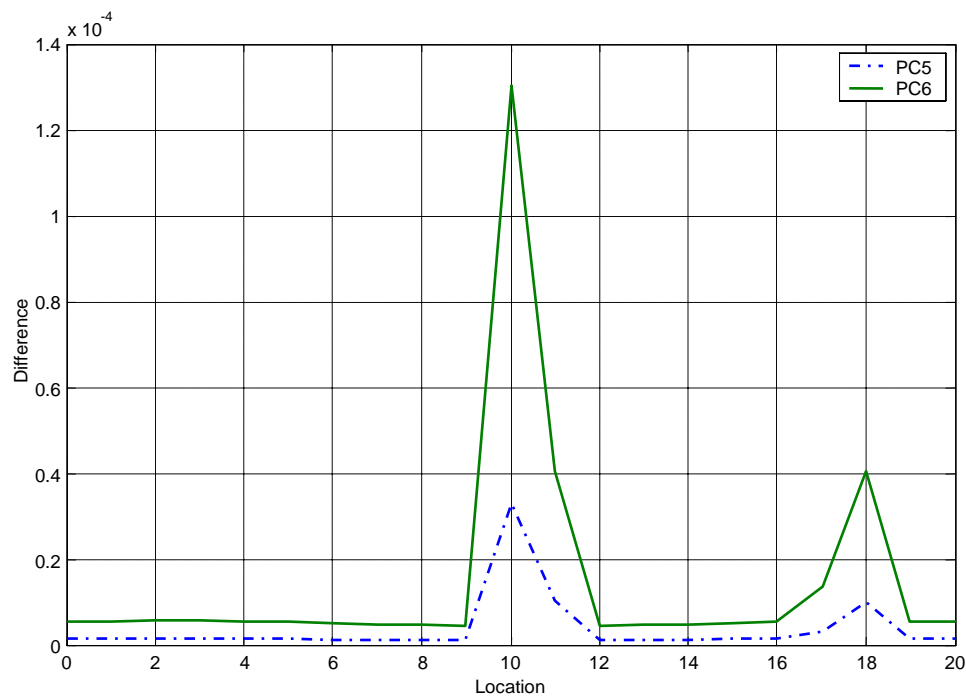
Figure 7.8 FRF curvature differences for the frame with damage scenarios PC5 and PC6.

7.5 THE RECEPTANCE-ENERGY DAMAGE INDEX

In this section a new damage index based on the concept of Receptance-energy, is proposed. The index was conceived to predict the damage location and to estimate the severity of the damage in a structure directly from the measured FRF (Receptance or Accelerance). In the formulation presented here the Receptance function will be used.

The damage indices are based on the variation of the Receptance-energy at the elements of the structure for a given excitation frequency. In a one-span beam, the Receptance-energy can be defined as:

$$\zeta_{(\Omega)} = \int_0^L \left[H''(x;\Omega) \right]^2 dx \tag{7.13}$$

where

L: span of the beam.

$H''(x;\Omega)$: Receptance-curvature for a frequency Ω.

The damage index $\zeta_{(\Omega)}$ is the area under the curve of the curve $H''(x;\Omega)^2$ covering the whole span. Similarly, the integral in Equation (7.13) can be evaluated between two arbitrary limits x_1 and x_2

$$\zeta_{(\Omega)} = \int_{x_1}^{x_2} \left[H''(x;\Omega) \right]^2 dx \tag{7.14}$$

The Receptance-curvature for each frequency can be calculated numerically with Equation (7.10) using the magnitude of the Receptance (it is recalled that the Receptance is a complex function).

The structural system is assumed to be divided into *ne* elements (*j=1,2,…,ne*). For the *j*th element the Receptance-energy can be written as

$$\zeta_j = \int_{x_k}^{x_{k+1}} \left[H''(x;\Omega) \right]^2 dx \tag{7.15}$$

where

x_k , x_{k+1} : coordinates of the nodes of element *j*.

The signature of damage is reflected on the variation of the integrals (7.15). The ratio of the Receptance-energy between the damaged and undamaged jth element of the structure is defined as

$$\eta_j = \frac{\varsigma_j^*}{\varsigma_j} \tag{7.16}$$

where ς_j^* is the Receptance-energy of the structure with damage:

$$\varsigma_j^* = \int_{x_k}^{x_{k+1}} \left[H_*''(x;\Omega) \right]^2 dx \tag{7.17}$$

For a given frequency range, the damage localization index for the jth location and for an external force applied at point p is defined as follows

$$\Psi_{j,p} = \frac{\displaystyle\sum_\Omega \varsigma_j^*}{\displaystyle\sum_\Omega \varsigma_j} \tag{7.18}$$

where the summation covers all the discrete frequencies in the selected range. If several forces are applied at different positions, the damage localization index for the jth location is

$$\Psi_j = \frac{\displaystyle\sum_p \sum_\Omega \varsigma_j^*}{\displaystyle\sum_p \sum_\Omega \varsigma_j} \tag{7.19}$$

For a frequency range, the damage severity index for the jth location, for an applied force at point p, is defined by

$$\Gamma_{j,p} = \frac{\sum_{\Omega} \varsigma_j^* - \sum_{\Omega} \varsigma_j}{\sum_{\Omega} \varsigma_j^*} = 1 - \frac{\sum_{\Omega} \varsigma_j}{\sum_{\Omega} \varsigma_j^*} \qquad (7.20)$$

For several force positions, the damage severity index for the jth location is defined by

$$\Gamma_j = 1 - \frac{\sum_p \left(\sum_{\Omega} \varsigma_j \right)}{\sum_p \left(\sum_{\Omega} \varsigma_j^* \right)} \qquad (7.21)$$

After the damage localization index of element j is computed, the value of the indicator is normalized according to the rule:

$$Z_j = \frac{\left(\Psi_j - \mu_{\Psi j} \right)}{\sigma_{\Psi j}} \qquad (7.22)$$

where

$\mu_{\Gamma j}$: mean value of the damage localization index

$\sigma_{\Gamma j}$: standard deviation of the damage localization index

The damage is assigned to the elements by using the technique proposed by Kim et al. (2003) presented in Chapter VI.

7.6 NUMERICAL SIMULATIONS

Once again, the two structures considered in the previous chapters are analyzed. For the simply-supported beam the Receptance FRF were obtained at 9 locations equally spaced along the longitudinal axis and for the beam and the column of the frame at 19 positions. From the Receptance vector $\{H\}_s$ obtained for a force located at position s, Receptance values at 41 nodal points (corresponding to 40 elements) of the structural model are obtained by using cubic spline interpolation functions. It is recalled that the beam and the right column of the frame were divided into 40 elements. Using the interpolated values of the Receptance FRF, the FRF-curvatures were generated numerically via a central difference approximation. The MATLAB function *quad* was used to evaluate the integrals.

- Simply-supported beam

The damage indices for the damage scenarios SD1 to SC4 are illustrated in Figures 7.9 to 7.17. The indices were calculated in the frequency range 150-190 rad/s. A single input force was applied at location L/2. The method was able to detect damage in all cases. As it is expected, the larger the damage (cases SD2, SC2, SC4), the more pronounced the peaks in the index. Note also that the proposed index succeeded in detecting the damage in the beam with two cracks (Figure 7.11).

Next, the damage severity index Γ_j was calculated for the predicted damaged elements. The damage locations were determined by using the normalized indicator Z_j.

The values of the damage severity along the beam span are shown in Figures 7.12 to 7.17. The damage severities of the elements with the highest values of the damage localization index (Ψ_j), are listed in Table 7.2. The errors in the estimation of damage severity for cases SD1 and SD2 range from 0.2 to 13 % and for cases SC1 to SC4 the errors range from 18 to 22 %. The error represents the difference between simulated and predicted damage severity. The simulated severity for cases SC1 to SC4 is defined in Appendix D. It can be noted that in cases SC3 and SC4, the maximum difference in the estimated severity for the elements with the same crack size was of 2%. As it can be observed for the beam with multiple damage scenarios (cases SC3 and SC4), the proposed method indicates simultaneously the location and severity of the two damaged regions of the beam.
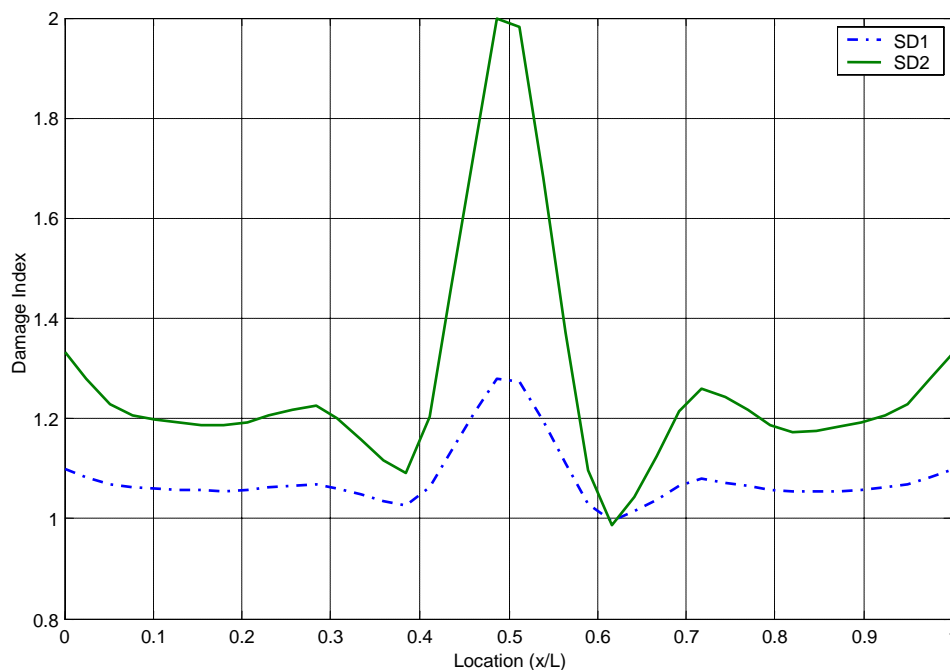
Figure 7.9 Receptance-energy damage index for the beam with damage scenarios SD1 and SD2.
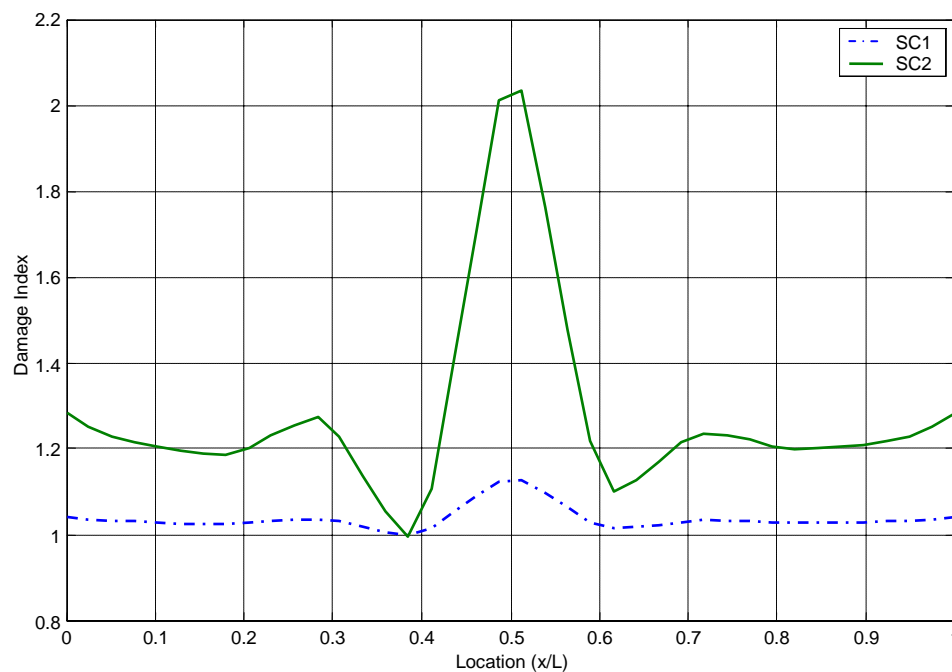
Figure 7.10 Receptance-energy damage index for the beam with damage scenarios SC1 and SC2.
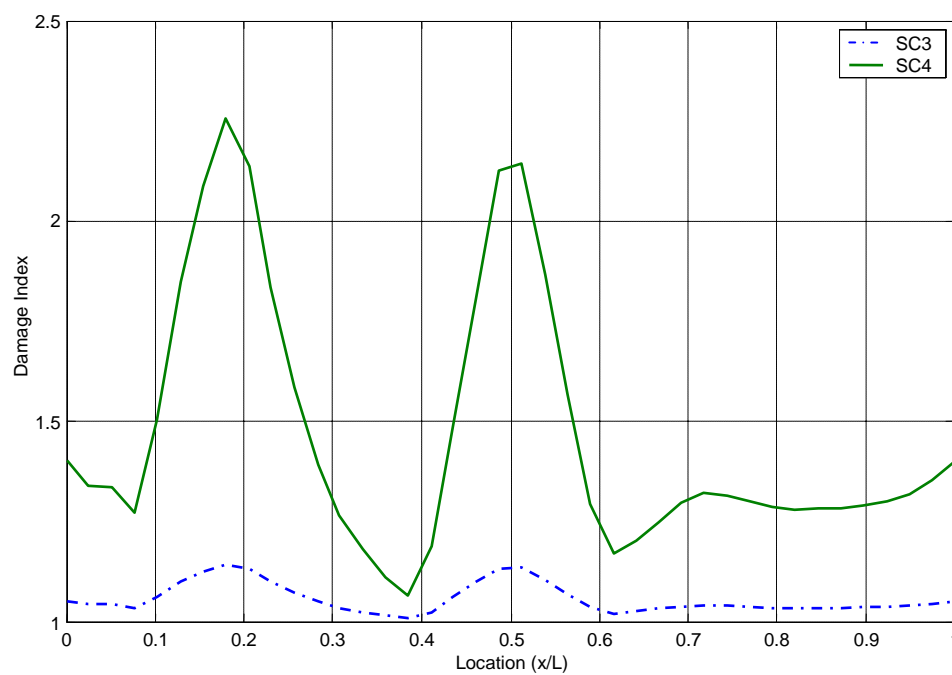
Figure 7.11 Receptance-energy damage index for the beam with damage scenarios SC3 and SC4.
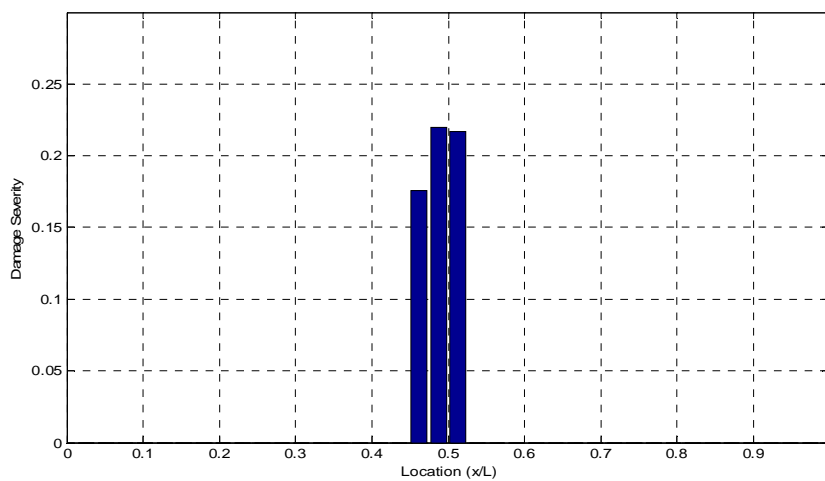
Figure 7.12 Damage severity index for the beam with damage scenario SD1.
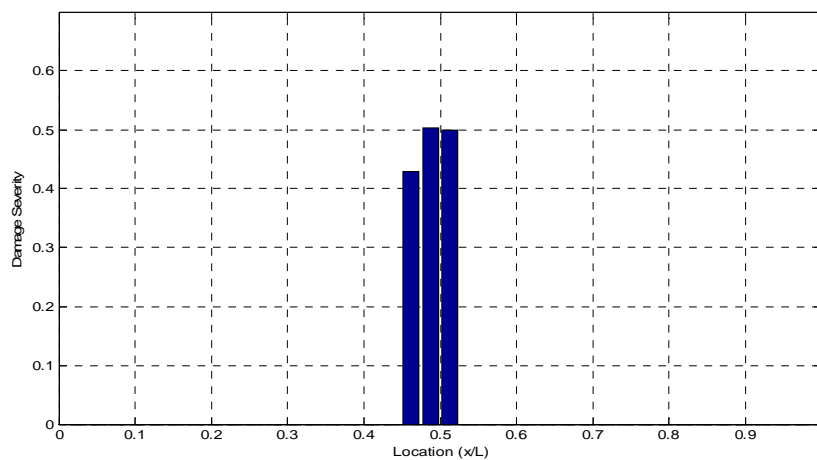
Figure 7.13 Damage severity index for the beam with damage scenario SD2.
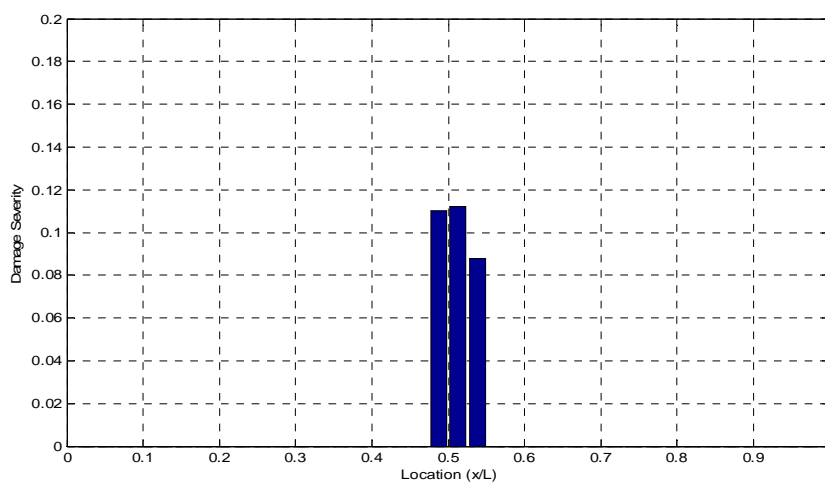
Figure 7.14 Damage severity index for the beam with damage scenario SC1.
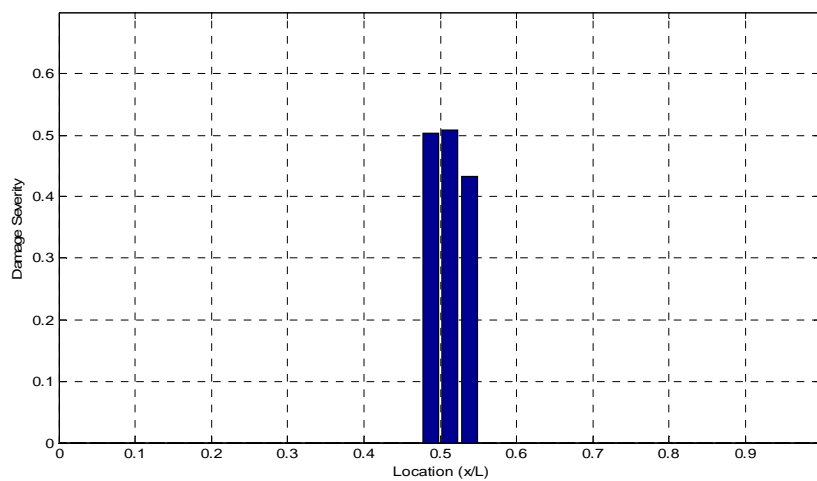
Figure 7.15 Damage severity index for the beam with damage scenario SC2.
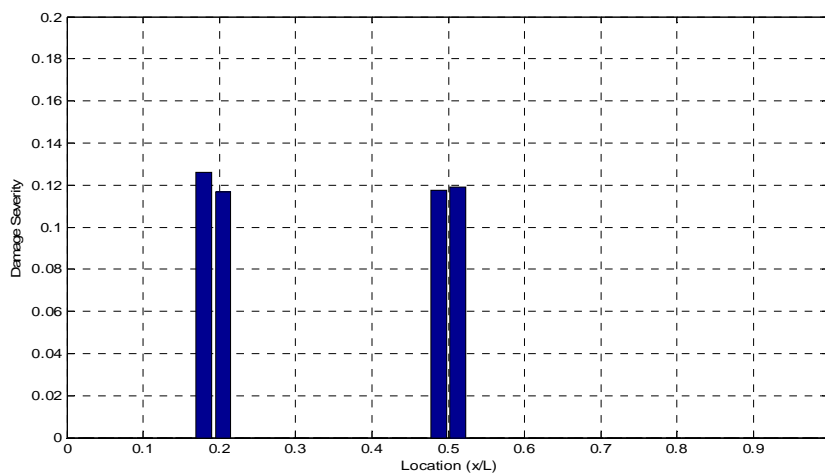
Figure 7.16 Damage severity index for the beam with damage scenario SC3.
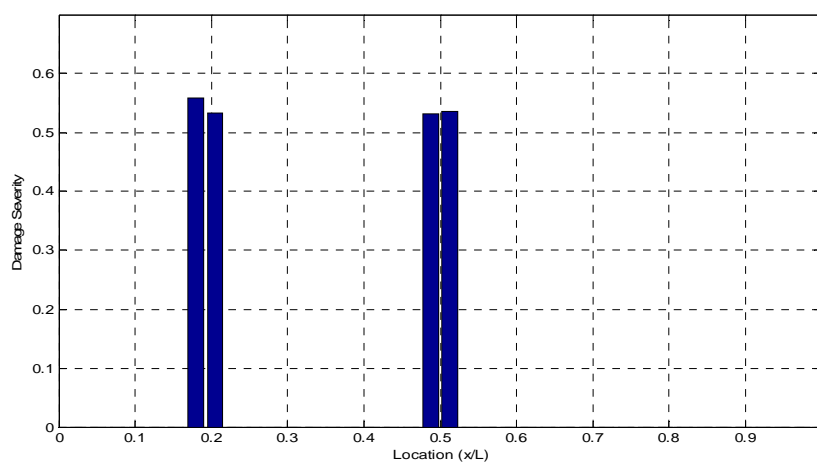
Figure 7.17 Damage severity index for the beam with damage scenario SC4.

Table 7.2. Damage indices: simply-supported beam.

Damage scenario	Element with the Highest Ψ_j	Damage Severity Index Γ_j	Simulated Severity
SD1	20	0.22	0.25
SD2	20	0.50	0.50
SC1	21	0.11	0.11
SC2	21	0.51	0.46
SC3	8 , 21	0.13 , 0.12	0.11
SC4	8 , 21	0.56 , 0.54	0.46

- Plane frame

The first two cases studied for the second structure analyzed, are the damage scenarios PC1 and PC2. The values of the damage localization index Ψ_j are shown in Figure 7.18, and the corresponding damage severity indices are shown in Figures 7.21 and 7.22. The indices were calculated in the frequency range 10 to 50 rad/s. A scheme of multiple input forces (MIF) was used. The forces were applied at 2 locations.

The values of the damage localization index for damage scenarios PC3 to PC6 are shown in Figures 7.19 and 7.20. The indices were calculated in a frequency range of 200-300 rad/s. The damage severity indices Γ_j for the elements with predicted damage are shown in Figures 7.23 to 7.26. The damage locations were determined by using the normalized indicator Z_j. Multiple input forces were also used. The damage severity indices Γ_j for the elements with the highest values of the damage localization index Ψ_j, are listed in Table 7.3. It is observed that the errors in the estimation of damage severity for cases PC1 and PC2 are 8 and 35 % respectively and for cases PC3 to PC6 the errors range from 15 to 23 %. The simulated severity is defined in Appendix D. It can be noted

that in cases PC5 and PC6, the maximum difference in the estimated damage severity index for the elements with the same crack size was 1 %.

As in the case of the simply-supported beam, the peak values occur at the damaged regions. In a similar way to the beam with multiple damage, the damage index correctly indicated the location of the damaged zone. As it can be observed for the multiple damage scenarios (cases PC5 and PC6), the proposed method indicates simultaneously the location and severity of the two damaged regions of the frame.
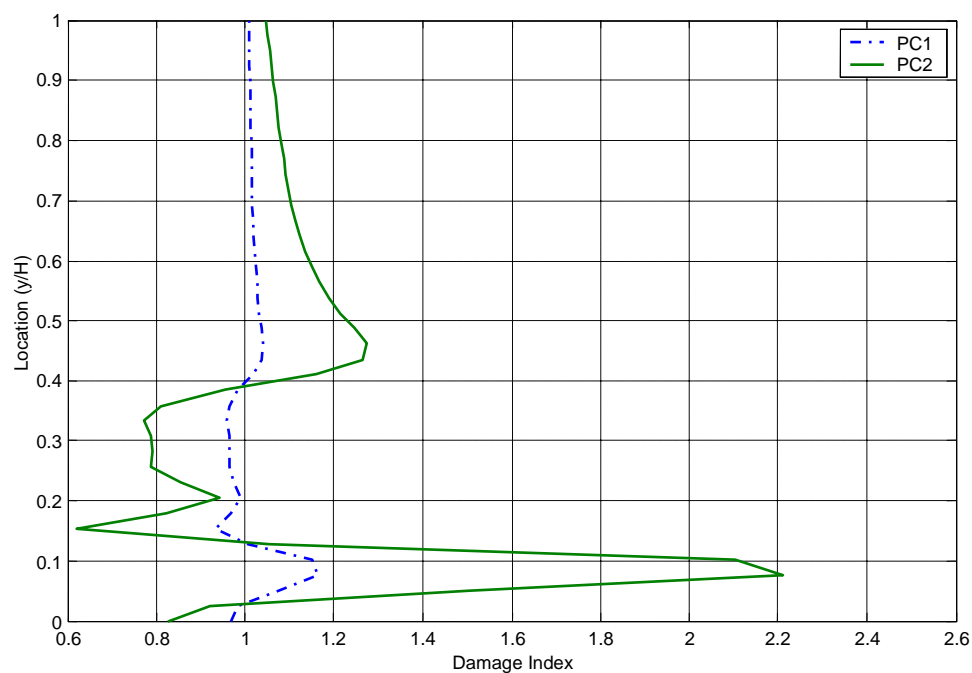
Figure 7.18 Damage localization index for the frame with damage scenarios PC1 and PC2.
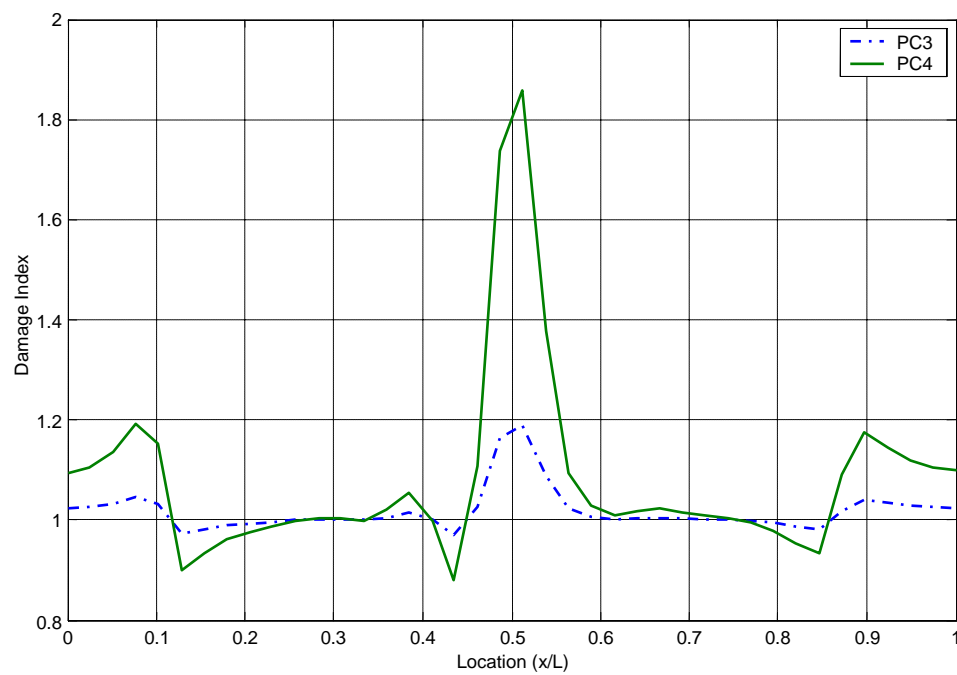
Figure 7.19 Damage localization index for the frame with damage scenarios PC3 and PC4.
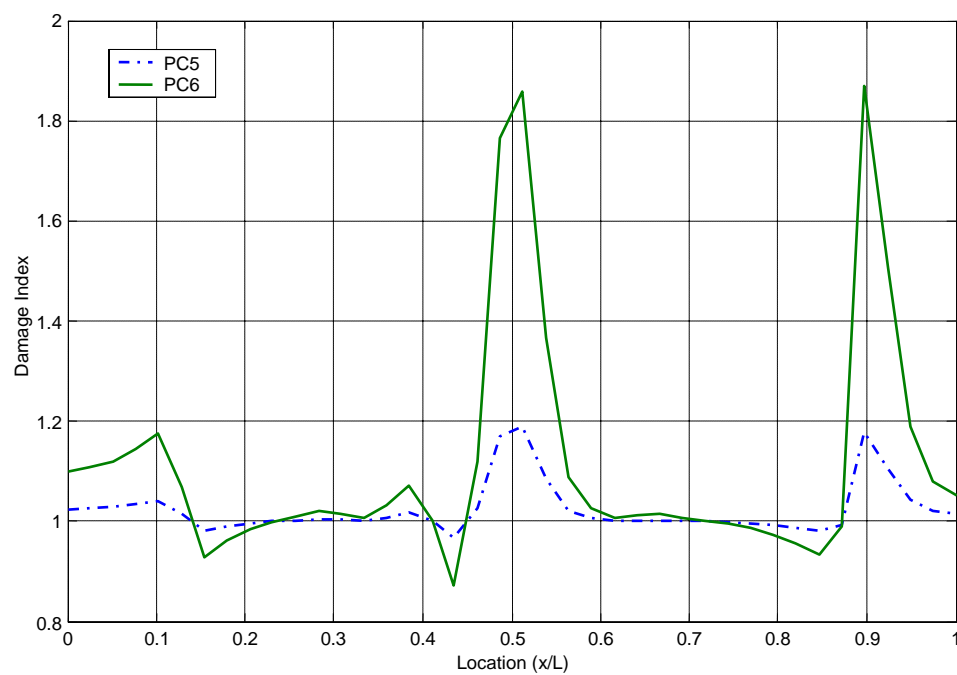
Figure 7.20 Damage localization index for the frame with damage scenarios PC5 and PC6.
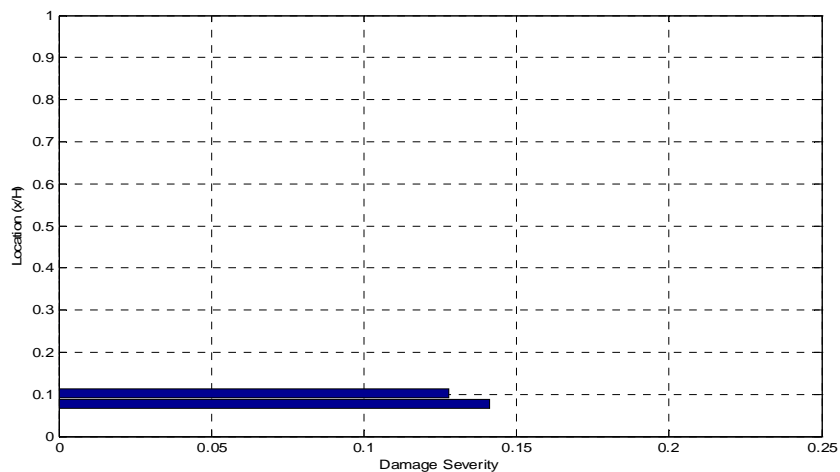
Figure 7.21 Damage severity index for the frame with damage scenario PC1.
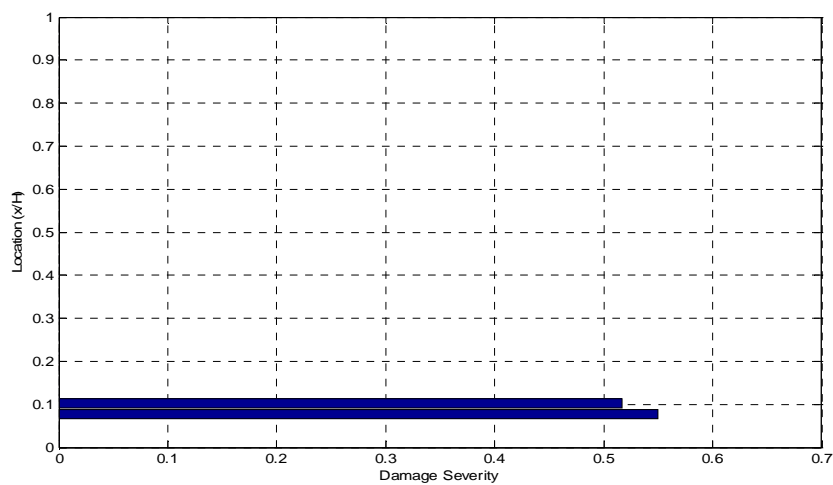
Figure 7.22 Damage severity index for the frame with damage scenario PC2.
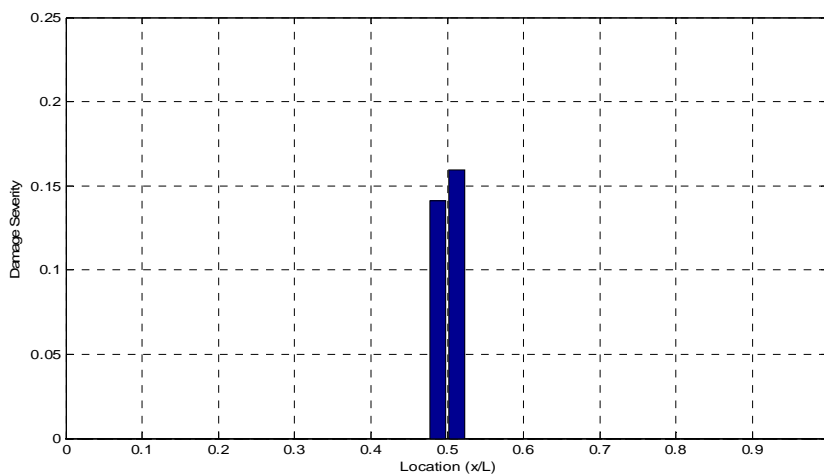
Figure 7.23 Damage severity index for the frame with damage scenario PC3.
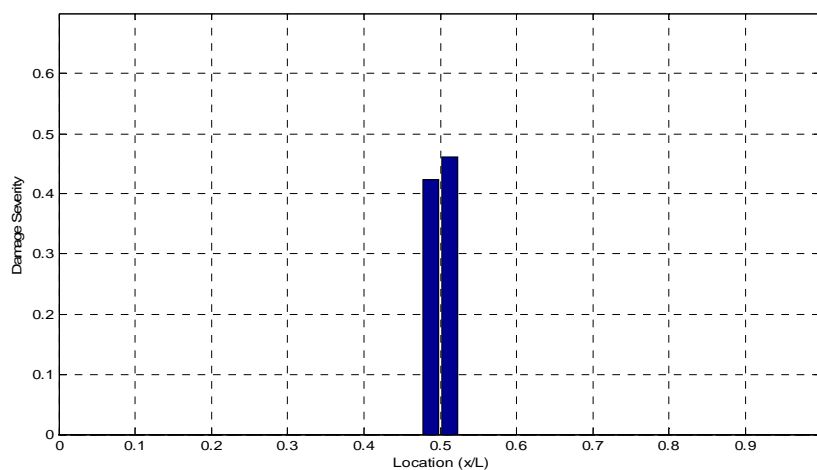
Figure 7.24 Damage severity index for the frame with damage scenario PC4.
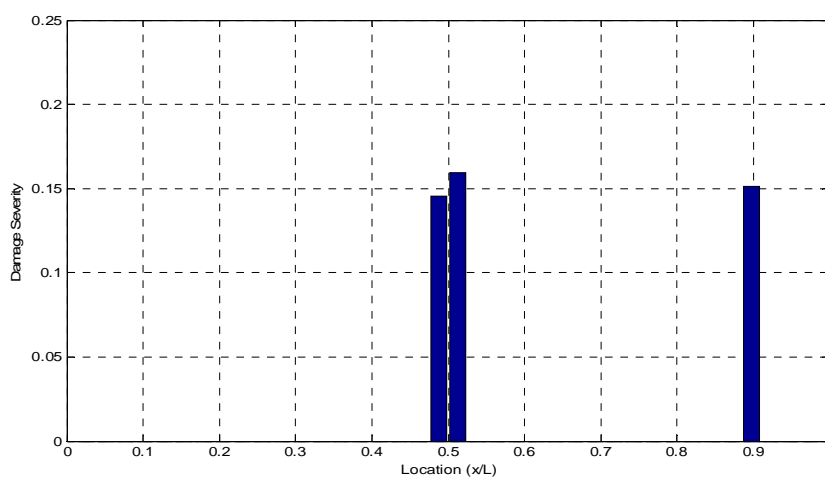
Figure 7.25 Damage severity index for the frame with damage scenario PC5.
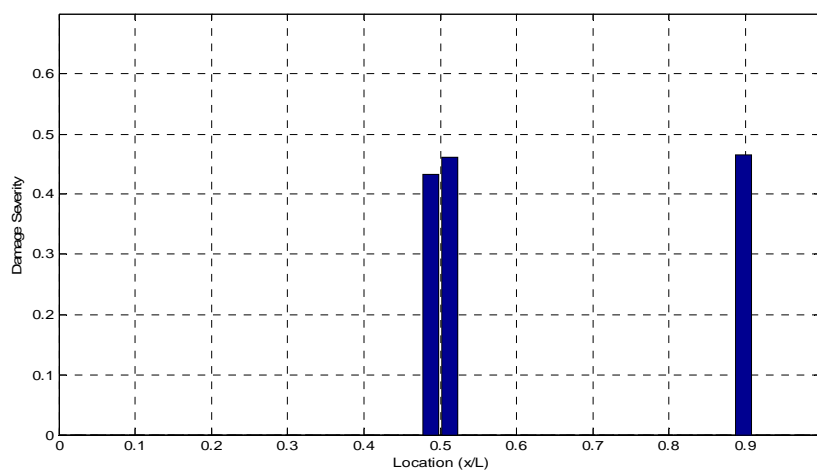
Figure 7.26 Damage severity index for the frame with damage scenario PC6

Table 7.3. Damage indices: plane frame.

Damage scenario	Element with the Highest Ψ_j	Damage Severity Index Γ_j	Simulated Severity
PC1	4	0.14	0.13
PC2	4	0.54	0.40
PC3	21	0.16	0.13
PC4	21	0.46	0.40
PC5	21, 36	0.16 , 0.15	0.13
PC6	21, 36	0.46 , 0.46	0.40

7.7 DAMAGE INDEX η

In this thesis a new damage localization index is proposed as a variation of the Stubbs et al. (1995) method based on modal strain energy. The new index uses FRF-curvature data rather than mode shape data. The FRF-curvature for each frequency is computed using the absolute value of the receptance function H_{rs} (or the Accelerance function A_{rs}). The second derivative is calculated with a central difference approximation.

For a given frequency Ω, the FRF-curvature is defined for FRFs at all the measurement locations 1,2, …, n. The excitation is assumed to be applied at the location or dynamic degree of freedom j:

$$\left\{ H''(\Omega) \right\}_j = \left\{ H_{1j}''(\Omega) \quad H_{2j}''(\Omega) \quad \cdots \quad H_{nj}''(\Omega) \right\}^T \tag{7.23}$$

For a selected frequency range and for a force applied at point j, a partial damage index at location i is first defined as

$$\Delta \eta_{i,j} = \sum_{\Omega} \frac{\left(H''_{*i,j}(\Omega)^2 + \psi_j^*\right) \cdot \psi_j}{\left(H''_{i,j}(\Omega)^2 + \psi_j\right) \cdot \psi_j^*} \tag{7.24}$$

where

$H''_{i,j}(\Omega), H''_{*i,j}(\Omega)$: the FRF-curvature for the undamaged and damaged structure, respectively, calculated at location i for a force input at position j.

$$\psi_j = \sum_i H''_{i,j}(\Omega)^2 ; \psi_j^* = \sum_i H''_{*i,j}(\Omega)^2 \tag{7.25}$$

The proposed damage index is defined by adding up the partial indices for several force locations

$$\eta_i = \sum_j \Delta \eta_{i,j} \tag{7.27}$$

7.8 NUMERICAL SIMULATIONS

The methodology presented before was used to calculate the damage localization index for the undamaged and the damaged structures previously studied (the simply-supported beam and the plane frame). The different damage scenarios presented earlier are considered again. The first five mode shapes were used to compute the values of the Receptance (H_{rs}) for a frequency range between 10 to 100 rad/s. A constant modal damping ratio $\xi = 0.05$ was used. To assess the influence of the input force location on

the results, the damage index was calculated by using a single input and multiple input forces locations.

- Simply-supported beam

In this case eight damage scenarios were analyzed. The proposed damage localization index for the damage scenarios SD1 to SC4 are illustrated in Figures 7.27 to 7.30. Two new damage scenarios were added. They are identified as SD3 and SD4. They differ in the severity of damage: for case SD3 is 25% and for case SD4 is 50% of the stiffness. In both cases the damaged element is located at L/5 from the left support of the beam. The results for the new damage scenarios are displayed in Figure 7.28.

Figures from 7.27 to 7.30 illustrate the case of a single input force (SIF) location, and the Figures 7.31 and 7.32 correspond to the case of multiple input forces (MIF). In the latter case the input forces are applied at locations 3 and 5. In all these figures, the maximum value of the damage localization index occurs at the damaged region. As it can be observed, the proposed damage index can locate damage by using only one input force. The method was capable of indicating the location of the two damaged regions of the beam) in the cases of multiple damage, using a single excitation (Figure 7.30) and using a pair of input forces (Figure 7.32).

- Plane frame

The index based on the FRF curvature for the frame with damage scenarios PC1 to PC6 are shown in Figures 7.33 to 7.35 for a frequency range from 5 to 50 rad/s.

The first natural frequency of the frame is 99.8 rad/sec. In cases PC1 and PC2, the input force was located at position 20 on the column (SIF). In cases PC3 and PC4, the input force was located at location 10 on the beam. As in the case of the simply-supported beam, the peak value of the index occurs at the damaged zone of the frame. It can be observed from Figures 7.33 and 7.34 that is possible to locate the damage by using only one input force location in the cases of damage that simulate a single element damaged. Figure 7.35 corresponds to the case of multiple input forces (MIF). The input forces were applied at 3 positions: locations 5, 10, 15. As it can be seen, the peaks at positions 10 and 18 indicate the location of the damaged elements of the frame.
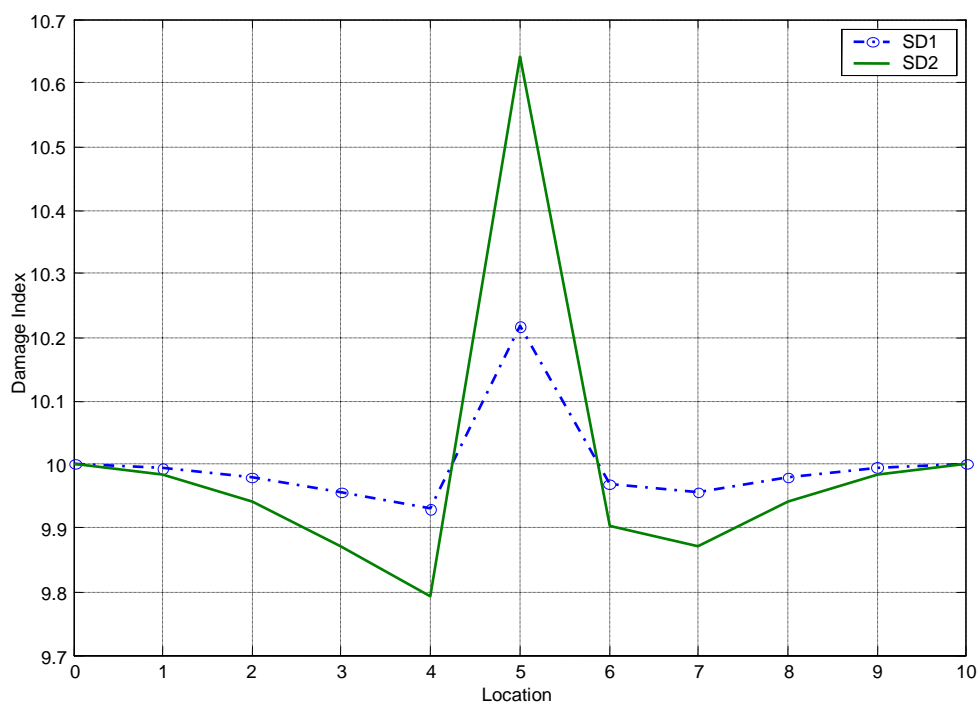
Figure 7.27 Damage Index η for the beam with damage scenarios SD1 and SD2 and SIF.
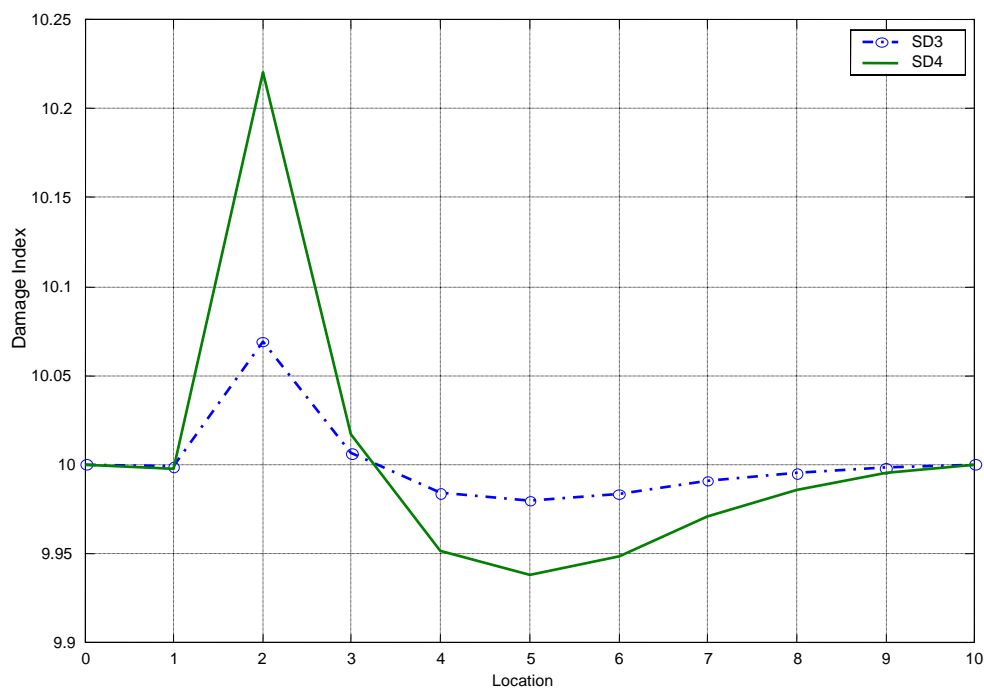
Figure 7.28 Damage Index η for the beam with damage scenarios SD3 and SD4 and SIF.
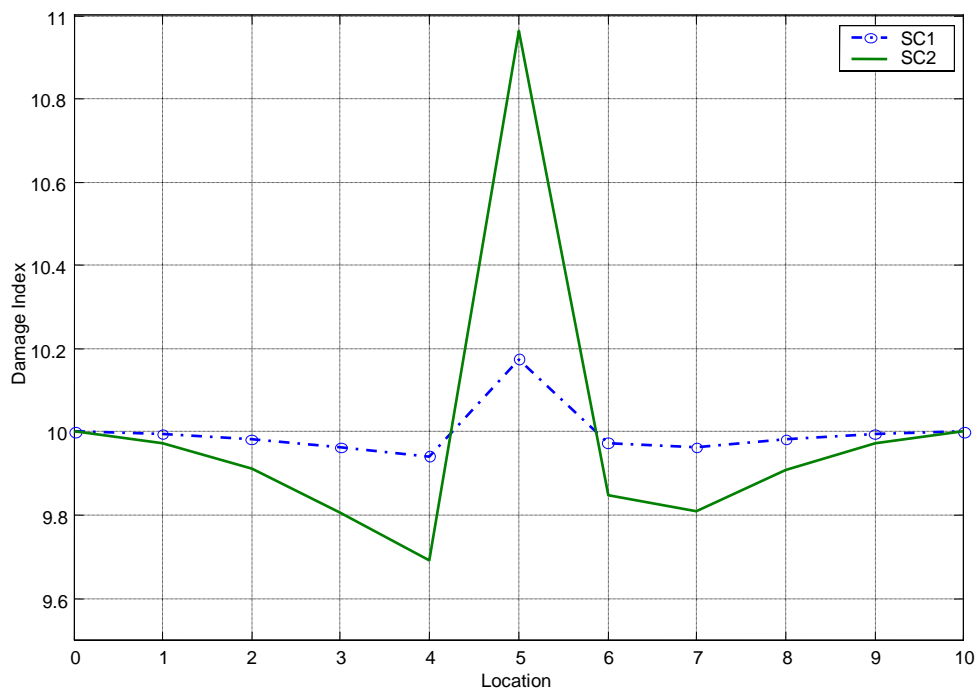
Figure 7.29 Damage Index η for the beam with damage scenarios SC1 and SC2 and SIF.
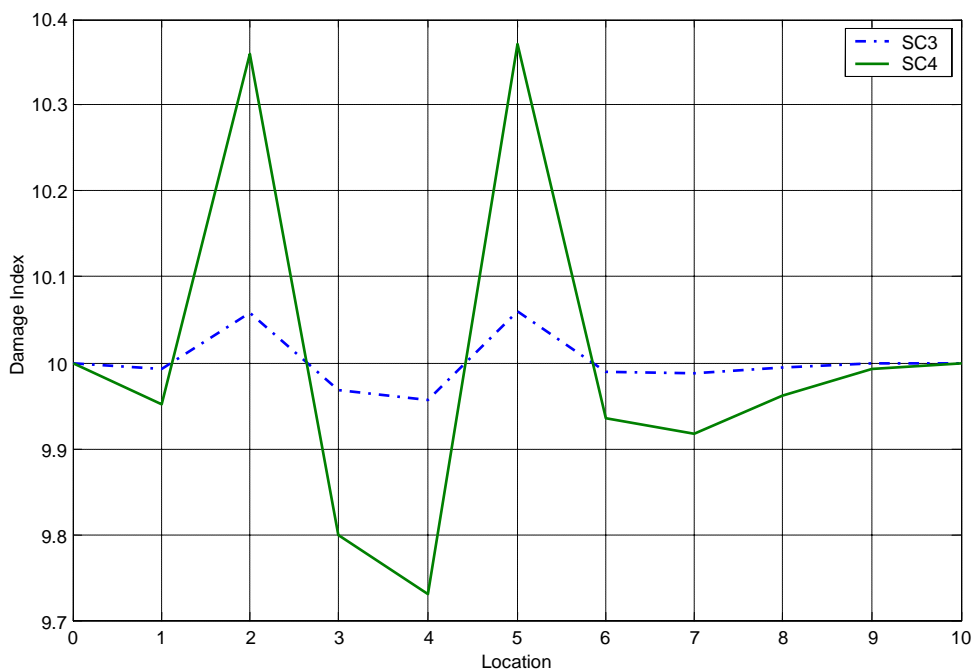
Figure 7.30 Damage Index η for the beam with damage scenarios SC3 and SC4 and SIF.
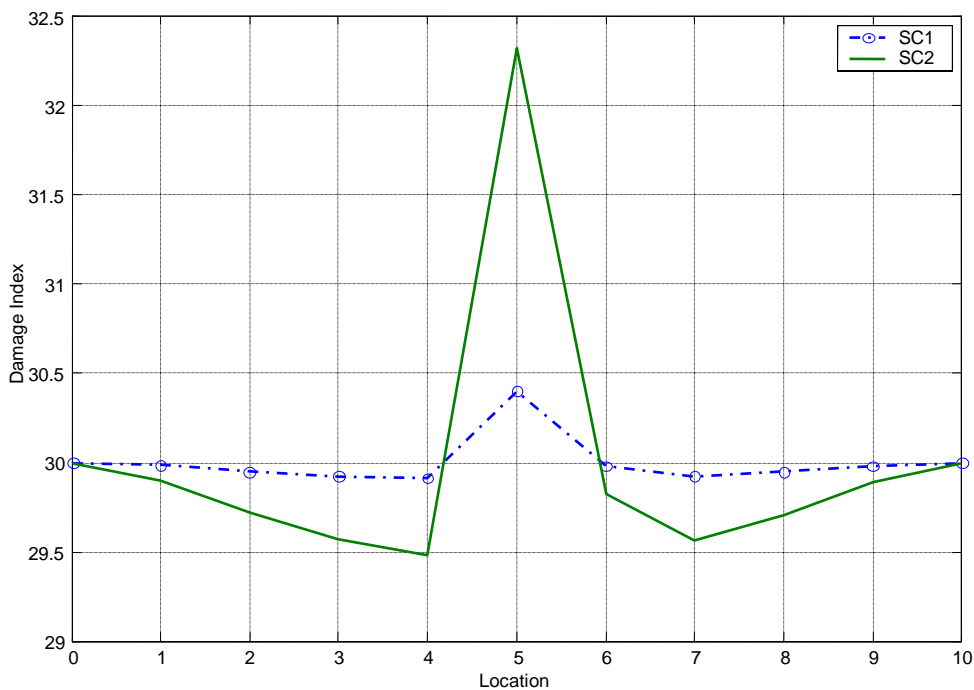
Figure 7.31 Damage Index η for the beam with damage scenarios SC1 and SC2 and MIF.
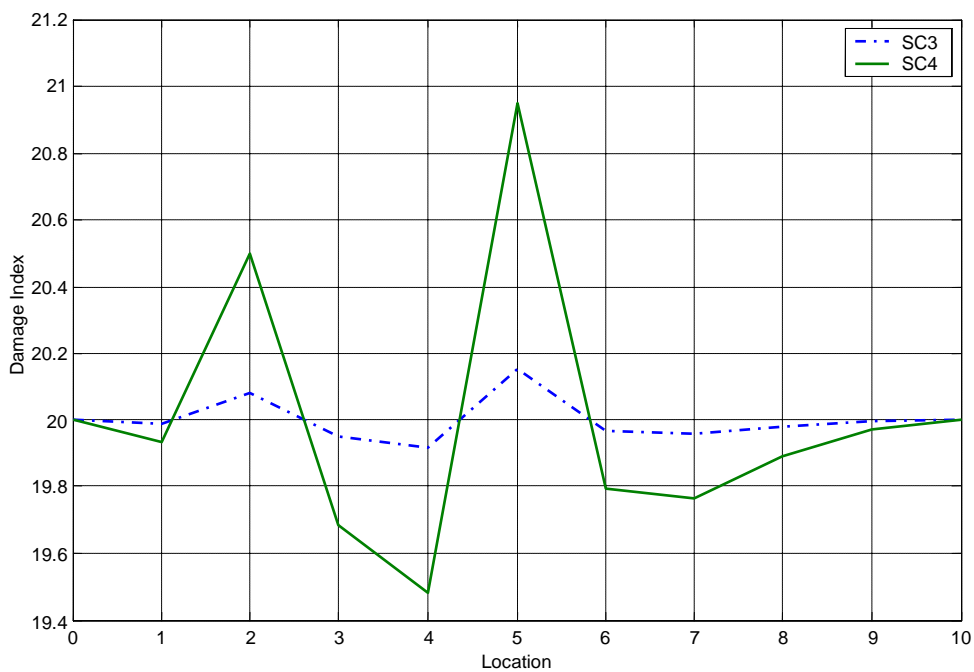
Figure 7.32 Damage Index η for the beam with damage scenarios SC3 and SC4 and MIF.
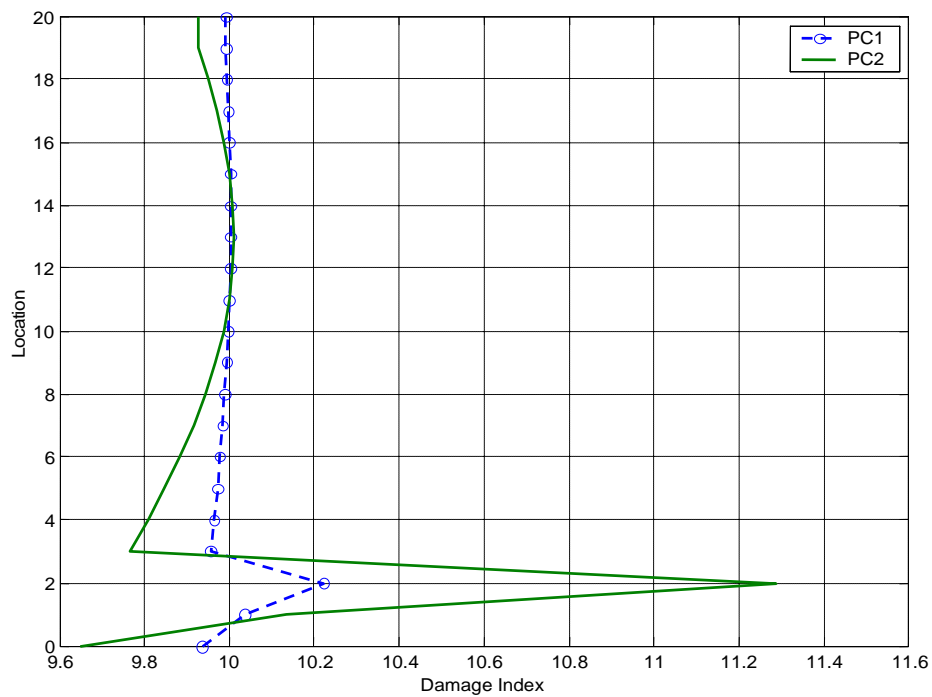
Figure 7.33 Damage Index η for the frame with damage scenarios PC1 and PC2 and SIF.
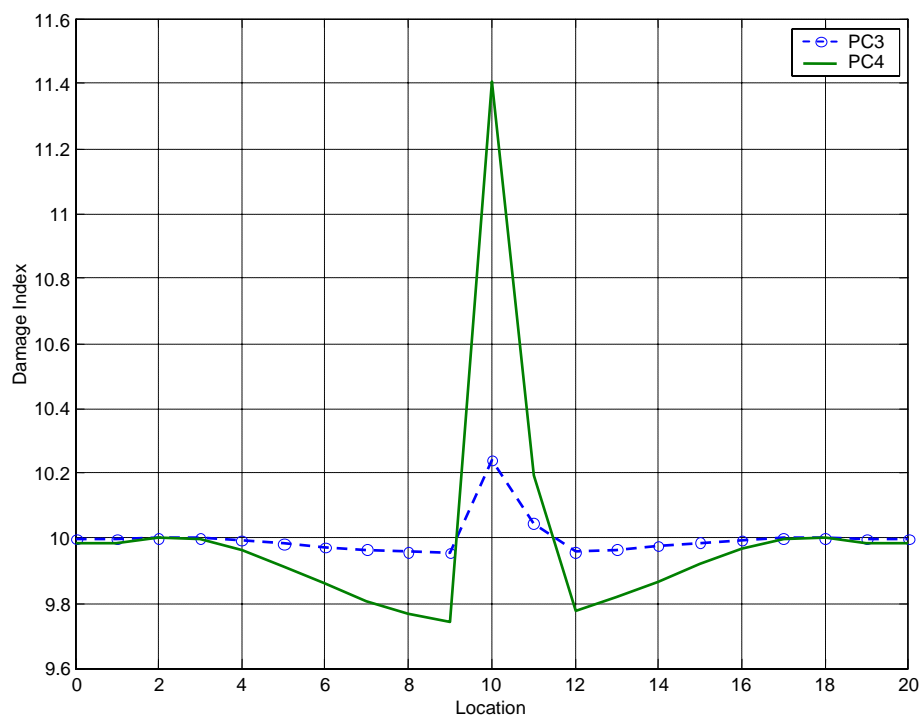
Figure 7.34 Damage Index η for the frame with damage scenarios PC3 and PC4 and SIF.
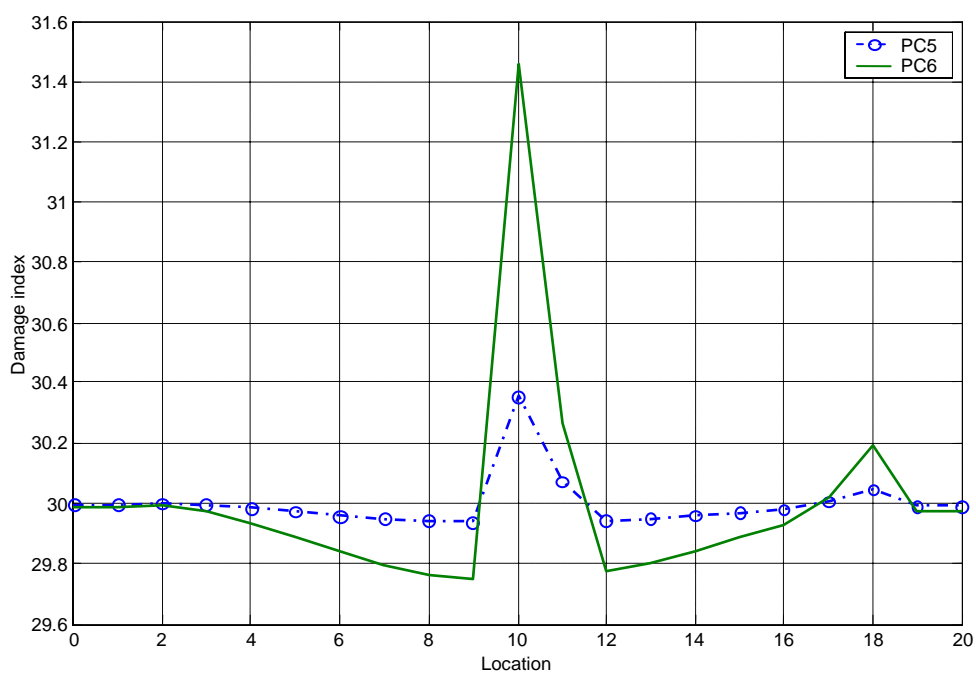
Figure 7.35 Damage Index η for the frame with damage scenarios PC5 and PC6 and MIF.

7.9 SUMMARY

In this chapter, two damage identification methods based on the FRF are proposed, and one existing methodology is presented. A new damage index based on the concept of Receptance-Energy is proposed. This index was designed to predict the damage location and to estimate the severity of the damage in a structure directly from measured FRFs (either Receptance or Accelerance). Numerical examples using simple structures are presented to compare the effectiveness of the methods studied in finding the damage. Two structures were considered for all the three methods

The FRF-curvature difference method can indicate correctly the location of the damaged zones in the beam and plane frame for single and multiple damage scenarios. It was found that for the structures with two cracks the FRF-curvature differences at the damage location are different even though the severity of damage was the same. This is a potential weakness of the method because it makes it difficult to calibrate the index with the magnitude of the damage. A possible advantage of the method is that it can locate the damage by using only one input force.

For the damage indices formulated in this work based on the Receptance-Energy, the results obtained indicate that the proposed method can localize and estimate the damage severity for the single and multiple damage scenarios simulated in the beam and frame. For single-span beams, a significant feature of the proposed method is that it can locate the damaged zones by using a single input force. Although some errors were

obtained in the quantification of the damage severity because the index seems sensitive to the frequency range used, for practical purposes they could be acceptable.

The results of the simulations with the damage index $\boldsymbol{\eta}$ indicate that the proposed index can correctly localize the damage, at least for the damage scenarios studied. The damage index can locate the damage by using one input force in the damage scenarios that simulate one damaged element. For the case of multiple damage scenarios, the method showed a better performance for the simply-supported beam.

CHAPTER VIII

APPLICATION OF THE DISCRETE WAVELET TRANSFORM TO DAMAGE IDENTIFICATION

8.1 INTRODUCTION

Most of the methods that use modal analysis are based on the Fourier transform. In other words, the Fourier transform is used to extract the modal information (natural frequencies and vibration modes), or it is used to calculate the FRF from a transient time signal. The theory of the Fourier transform is very well established, and it is a quick and easy tool to find the frequency components in a signal. The Fourier analysis consists in transforming a signal from the time or space domain to the frequency domain. A disadvantage of the Fourier analysis is that the time or space information is lost in the transformation, and it is not possible to determine when or where a local event occurs. In order to overcome this drawback, wavelet analysis has been considered recently for structural identification and damage detection. Wavelet analysis may be viewed as an extension of the traditional Fourier transform with a window adjustable in location and size. The advantage of wavelet analysis lies in its capacity to examine local information with a ''zoom lens having an adjustable focus'' to provide multiple levels of details and approximations of the original signal. In this Chapter, a wavelet-based methodology for structural damage identification is formulated. Numerical examples are presented to illustrate the effectiveness of the proposed procedure to indicate the location of damage in simple structures.

8.2 THE CONTINUOUS WAVELET TRANSFORM.

The Continuous Fourier Transform (CFT) is defined as

$$F(\omega) = \int_{-\infty}^{\infty} f(t)e^{-i\omega t} dt \tag{8.1}$$

The results of the CFT are the Fourier coefficients $F(\omega)$, which when multiplied by a sinusoid of appropriate frequency ω, yields the constituent sinusoidal components of the original signal.

The Continuous Wavelet Transform (CWT) is defined as the sum over all time of the signal function of time or space multiplied by a scaled, shifted version of a wavelet function ψ. For a space signal,

$$Cw(a,b) = \int_{-\infty}^{\infty} f(x)\psi(a,b,x) dx \tag{8.2}$$

The results of the CWT are wavelet coefficients Cw that are a function of the scale a and position b. Multiplying each coefficient by the appropriately scaled and shifted wavelet yields time signals whose synthesis can recover the original signal.

To perform the CWT, a basic wavelet function must be selected from the existing wavelet families. The basic wavelet function, known as the "mother wavelet" $\psi(x)$, is dilated by a value a and translated by the parameter b. The dilation (expansion or

compression) and the translation yield a set of basis functions defined as

$$\psi(a,b,x) = \frac{1}{\sqrt{a}} \psi\left(\frac{x-b}{a}\right) \tag{8.3}$$

The translation parameter, b, indicates the space (or time) position of the relocated wavelet window in the wavelet transform. Shifting the wavelet window along the space (or time) axis implies examining the signal $f(x)$ in the neighborhood of the current window location. The scale parameter, a, indicates the width of the wavelet window. A smaller value of a implies a higher resolution filter, i.e., the signal is examined through a contracted wavelet window in a smaller scale. The wavelets coefficients defined in equation (8.2) indicate how similar is the function being analyzed $f(x)$ to the wavelet function $\psi(a,b,x)$.

In terms of a selected mother wavelet function $\psi(x)$, the continuous wavelet transform of a signal $f(x)$ is defined as

$$Cw(a,b) = \frac{1}{\sqrt{a}} \int_{-\infty}^{\infty} f(x)\psi\left(\frac{x-b}{a}\right) dx \tag{8.4}$$

The scale parameter a and the translation parameter b are real numbers, and a must be positive.

8.3 THE DISCRETE WAVELET TRANSFORM.

One of the drawback of the CWT is that a very large number of wavelet coefficients $C(a,b)$ are generated during the analysis. In addition, the CWT is said to be *redundant*, in the sense that it contains more than the necessary information to retrieve the original signal. Therefore, instead of using a continuum of dilations and translations, discrete values of the parameters a and b are used. The dilation is defined as $a = 2^j$ and the translation parameter takes the values $b = k2^j$, where $(j,\ k) \in Z$, and Z is the set of integers. This sampling of the coordinates (a,b) is known as *dyadic sampling* because consecutive values of the discrete scales differ by a factor of 2. Using the discrete scales, the discrete wavelet transform (DWT) can be defined as

$$C_{j,k} = 2^{-j/2} \int_{-\infty}^{\infty} f(x)\psi(2^{-j}x - k)dx = \int_{-\infty}^{\infty} f(x)\psi_{j,k}(x)dx \tag{8.5}$$

The signal resolution is defined as the inverse of the scale $1/a = 2^{-j}$, and the integer j is referred to as the level. The signal can be reconstructed from the wavelet coefficients $C_{j,k}$ and the reconstruction algorithm is called the inverse discrete wavelet transform (IDWT):

$$f(x) = \sum_{j=-\infty}^{\infty} \sum_{k=-\infty}^{\infty} C_{j,k} 2^{-j/2} \psi(2^{-j}x - k) \tag{8.6}$$

If the dyadic scale is used for *a and b*, and a level J is considered, the level-J *detail coefficients* are defined by

$$cD_J(k) = \int_{-\infty}^{\infty} f(x)\psi_{j,k}(x)dx \qquad (8.7)$$

In the discrete wavelet analysis, a signal can be represented by its approximations and details. For this we define the detail at level j as

$$D_j(x) = \sum_{k=-\infty}^{\infty} cD_j(k)\psi_{j,k}(x) \qquad (8.8)$$

and the approximation at level J is defined as the sum of the details up to that level, i.e.,

$$A_J(x) = \sum_{j>J} D_j(x) \qquad (8.9)$$

There are two types of details. Those associated with indices $j < J$ correspond to the scales $a = 2^j < 2^J$ and are the fine details. The other ones, which correspond to $j > J$, are the coarser details. The details and approximations are related. The signal $f(x)$ is the summation of the approximations A_J and of the fine details up to that level:

$$f(x) = A_J(x) + \sum_{j<J} D_j(x) \qquad (8.10)$$

From the previous equation, it is obvious that the approximations are related to one another by

$$A_{J-1}(x) = A_J(x) + D_J(x) \qquad\qquad (8.11)$$

Equations (8.10) and (8.11) provide a tree structure of a signal and also a reconstruction procedure for the original signal. The wavelet tree structure with details and approximations at various levels (shown in the following section) gives information of the signal characteristics that may not be clearly appreciated in the original signal.

8.4 ONE-STAGE FILTERING AND MULTIPLE-LEVEL DECOMPOSITION.

To implement the DWT it is convenient to use the concept of digital filter. The approximations and details functions can be regarded as the signals obtained by passing the original signal through two types of filters. For many signals, the low-frequency content is the most important part. This part is what gives the signal its identity. The high-frequency content, on the other hand, imparts flavor. In wavelet analysis the concepts of approximations and details are introduced to separate the low and high frequency components. The approximations are the high-scale, low-frequency components of the signal. The details are the low-scale, high-frequency components. During the filtering process the original signal $f(t)$ passes through two complementary filters and emerges as two signals as shown in Figure 8.1. Unfortunately, by performing this operation one winds up with twice as much data as one started with (Misiti et al. 2001). To correct this problem, the notion of downsampling is introduced. This simply means throwing away every second data point. This process produces the DWT coefficients.

The actual lengths of the detail and approximation coefficient vectors are slightly more than half the length of the original signal. This has to do with the filtering process, which is implemented by convolving the signal with a filter. The convolution "smears" the signal, introducing several extra samples into the result. The decomposition process can be iterated, with successive approximations being decomposed in turn, so that one signal can be broken down into many lower-resolution components. The resulting process is referred to as the wavelet decomposition tree and it is shown on Figure 8.2. Since the analysis process is iterative, in theory it can be continued indefinitely. In practice, the selection of a suitable number of levels is based on the nature of the signal. A down-sampling technique (Strang and Nguyen 1996) can be used to efficiently reduce the data size in the tree and the Mallat algorithm, a fast wavelet transform (FWT) procedure, can be used to greatly reduce the computational efforts involved.
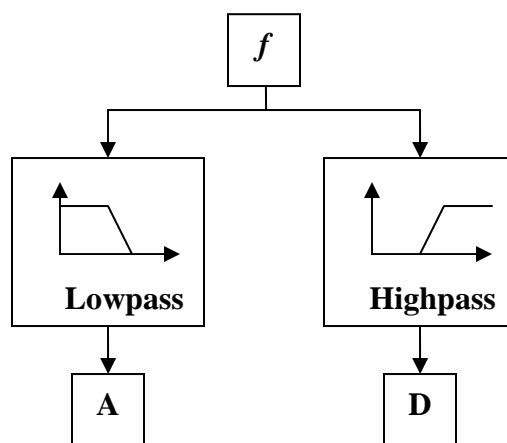
Figure 8.1 One stage filtering.
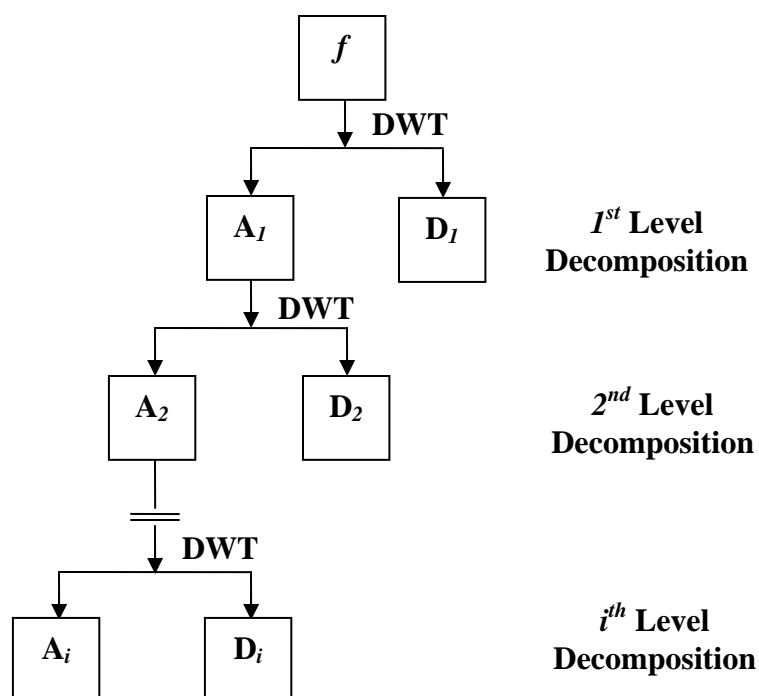
Figure 8.2 Wavelet decomposition tree.

8.5 BOUNDARY DISTORTIONS.

Typically, the DWT is defined for sequences with length of some power of two (the dyadic scale), and different ways of extending samples of other sizes are needed. Methods for extending the signal include: zero-padding, smooth padding, periodic extension, and boundary value replication (symmetrization). The basic algorithm for the DWT is not limited to dyadic lengths and it is based on a simple scheme: convolution and downsampling. As usual, when a convolution is performed on finite-length signals, border distortions arise (Misiti et al. 2001). For damage identification purposes, these distortions can create a problem because the boundary conditions (supports) and joints of structural elements can generate disturbances similar to actual defects.

To deal with border distortions, the border should be treated differently from other parts of the signal. Various methods are available to deal with this problem, referred to as "wavelets on the interval". Often it is preferable to use simple schemes based on signal extension on the boundaries. This involves the computation of a few extra coefficients at each stage of the decomposition process to get a perfect reconstruction. It should be noted that extension is needed at each stage of the decomposition process. The available signal extension modes in the Wavelet Toolbox of MATLAB are: zero-padding, symmetrization, smooth padding and periodic-padding. The details of these extension modes are presented in Appendix C.

8.6 DWT METHODOLOGY FOR DAMAGE IDENTIFICATION.

8.6.1. Criteria for wavelet selection.

To apply the discrete wavelet transform it is very important to select the most appropriate wavelet for the analysis. The selection is usually done by trial and error, but by examining the properties it is possible to discard many candidates and expedite the process. To analyze the response signals in this work the optimal wavelet is chosen according to the following criteria described by Ovanesova and Suárez (2004):

1. From the available wavelets, eliminate those that do not allow carrying out a FWT. They are the Gaussian, Mexican Hat, Morlet, Shannon and Meyer wavelets.

2. The orthogonal and biorthogonal wavelets remain after the first elimination. Both permit to apply the FWT using filter banks.

3. The requirement to satisfy symmetry and exact reconstruction of the analyzed signal limit the choice to the Haar wavelet and biorthogonal wavelets.

4. The two candidate wavelets have a significant difference in regularity. Thus, regularity is the last property that singles out the wavelet to perform the analyses. The irregularity of the Haar wavelet leaves the biorthogonal wavelets as the choice for the analyses.

5. The regularity of the different biorthogonal wavelets increase with the wavelet order N.

8.6.2 Wavelet methodology for damage identification.

The main idea behind the use of wavelet transform for structural damage identification purposes is the fact that damage introduces small discontinuities in the structural response at the damaged zones (Ovanesova and Suárez 2004, Liew and Wang 1998). The proposed structural damage identification method based on the DWT, uses the measured Receptance FRF as the input signal. The Receptance function at a selected fixed frequency measured at various locations along the structure is the signal to be decomposed with the DWT. The procedure is described next in a step-by-step way:

1. For the structure analyzed, obtain the Receptance FRF at n locations.

2. Perform a Multilevel Wavelet Decomposition of the signal using a selected wavelet. The wavelets coefficients $cD_j(k)$ are calculated from the equation (8.7).

3. For a level j extract the Detail function D_j. The values of the D_j are obtained from Eq. (8.8).

4. For a level j plot and examine the Detail function D_j over the longitudinal axis of the structure analyzed. An abrupt change in the distribution of the detail indicates the presence of damage, except when this perturbation is caused by a geometric discontinuity.

8.7 NUMERICAL SIMULATIONS.

The proposed procedure presented above was used to estimate the damage localization. The FRF and the FRF-first derivative of the damaged structures with simulated damage were generated numerically. The FRF-first derivative was obtained numerically by using a central finite-divided difference based on the Taylor series. In the numerical examples the magnitude of the FRF is used. The beam and plane frame used throughout this thesis were once again chosen to present numerical examples.

To select the appropriate type of wavelets to perform the wavelet decomposition, several wavelets were studied, following the methodology mentioned earlier. The signal for the case SW1 described next was analyzed by the DWT using three different wavelets: db1, db5, and bior5.5. These wavelets are known, respectively, as the Daubechies-1, Daubechies-5 and the biorthogonal wavelets-5.5. The signal analyzed by these wavelets is one of the FRF curves shown in Figure 8.3 (the one for damage scenario SW1) for $\Omega = 100$ rad/s. The FRF corresponds to the simply-supported beam described in Chapter III.

The decompositions performed for the first two levels of the wavelet tree are shown in Figures 8.3 to 8.5. The abrupt changes in the level-1 details due to the damage occur in the db5 and bior5.5. As it can be seen in Figures 8.6 and 8.7, the level-1 details of the decompositions performed with the bior5.5 wavelet exhibit a better performance to indicate the localization of damage. Therefore, the latter wavelet is selected for the wavelet analysis. To avoid the boundary distortions, the signal extension mode '*spd*', included in the Wavelet Toolbox of MATLAB (Misiti et al. 2001) is used.

8.7.1 Simply-supported beam

- Case 1.

The simply-supported beam described in Chapter III is used for the first set of numerical examples. The beam was divided into 50 finite elements and damage was inflicted at element 26 (~L/2) by reducing the flexural stiffness *EI* by 50 %. The values of the FRF-Receptance for an excitation frequency of 100 rad/sec are shown in Figure 8.3. The first natural frequency of the beam is 221.3 rad/sec. After the DWT is applied to the response signal and both the presence of damage and its location are detected from the damaged beam response by the bior5.5 wavelet. The values of the level-1 details are shown in Figure 8.8.

- Case 2.

The damage scenario SW2 consists of a single crack inflicted near the mid-span (element 26). The crack depth is $h_c = 0.25$ H, where H is the section depth. The

magnitude of the Receptance FRF for an excitation frequency of 100 rad/s is shown in Figure 8.3. The level-1 details of the decompositions performed by the bior5.5 wavelet are shown in Figure 8.9. The abrupt changes in the level-1 details due to the crack indicate the localization of damage.

- Case 3.

The damage case SW3 corresponds to a multiple damage scenario. Cracked elements are introduced at two different locations. The cracks depth is $h_c = 0.25\ H$. The absolute value of the Receptance FRF for an excitation frequency of 100 rad/s is shown in Figure 8.4. The level-1 details of the decompositions performed with the bior5.5 wavelet are shown in Figure 8.10. The spikes in the level-1 details are centered around the cracks positions and thus they indicate the localization of the damage.
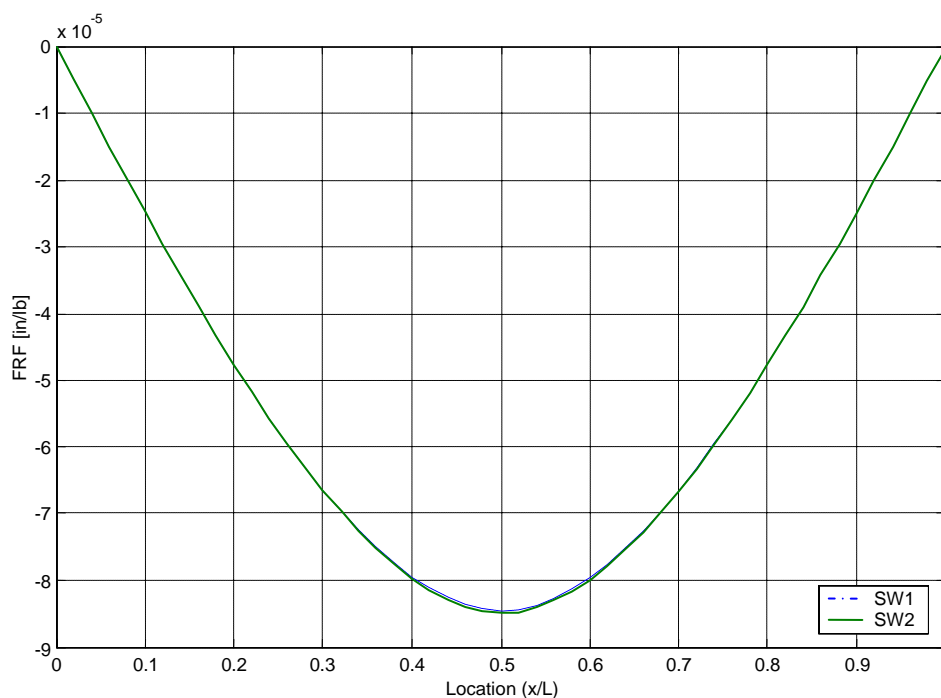
Figure 8.3 Receptance FRF for the beam with damage scenarios SW1 and SW2.
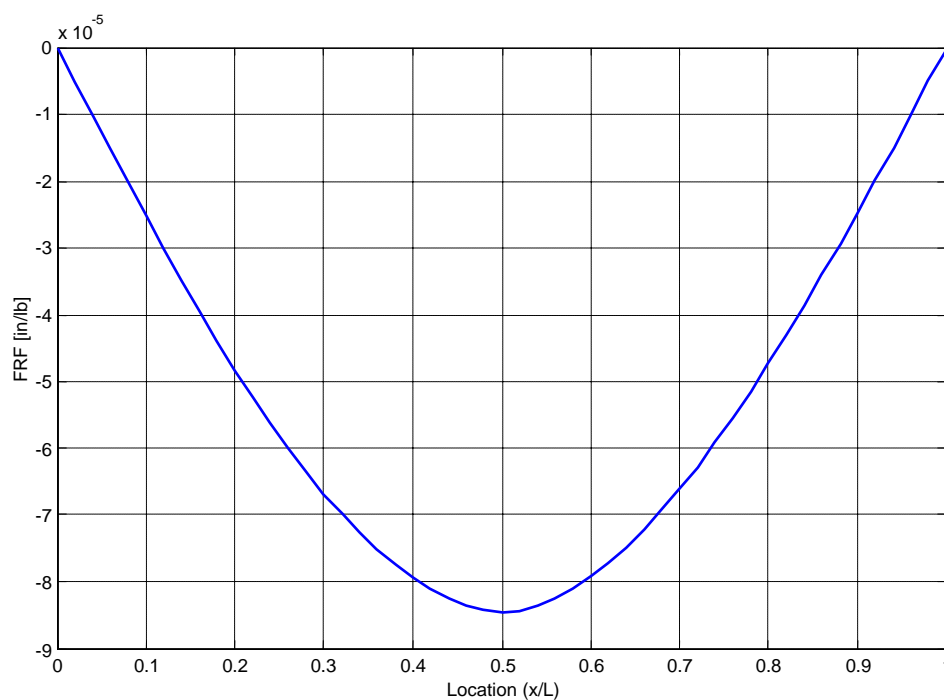
Figure 8.4 Receptance FRF for the beam with damage scenario SW3.
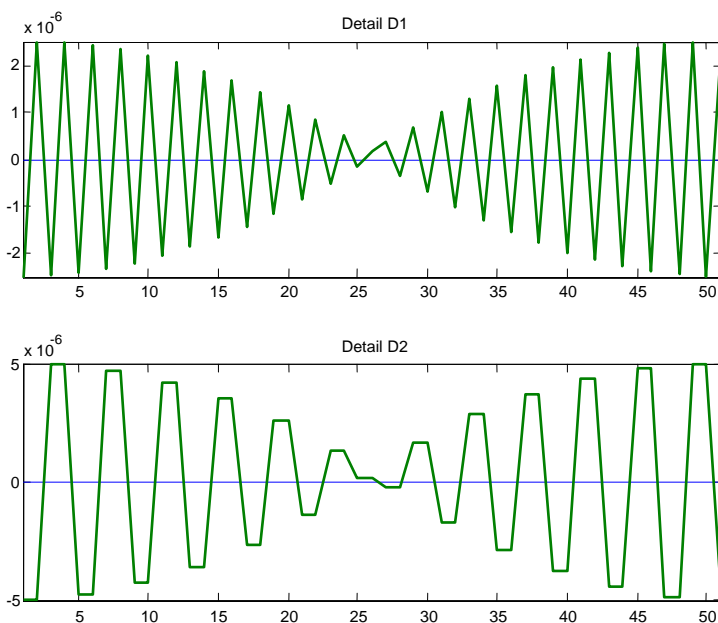
Figure 8.5 DW decomposition with wavelet 'db1' for the beam with damage scenario SW1.
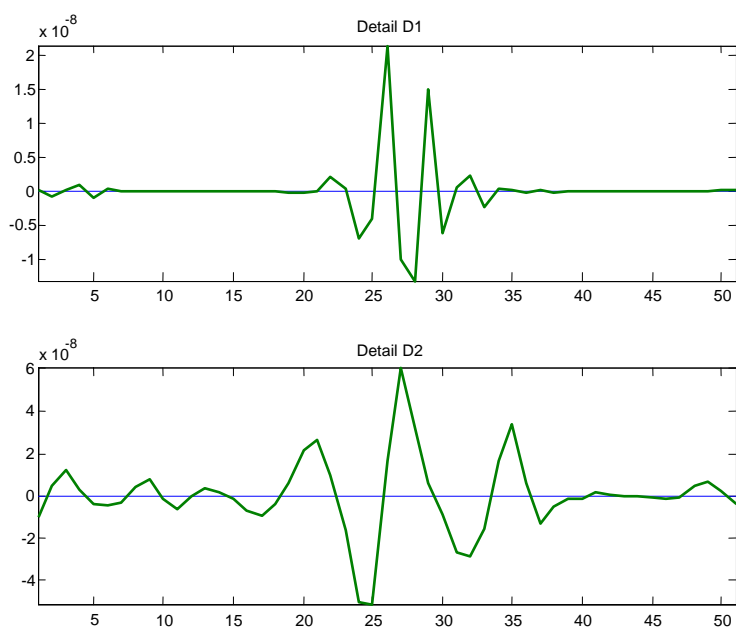
Figure 8.6 DW decomposition with wavelet 'db5' for the beam with damage scenario SW1.
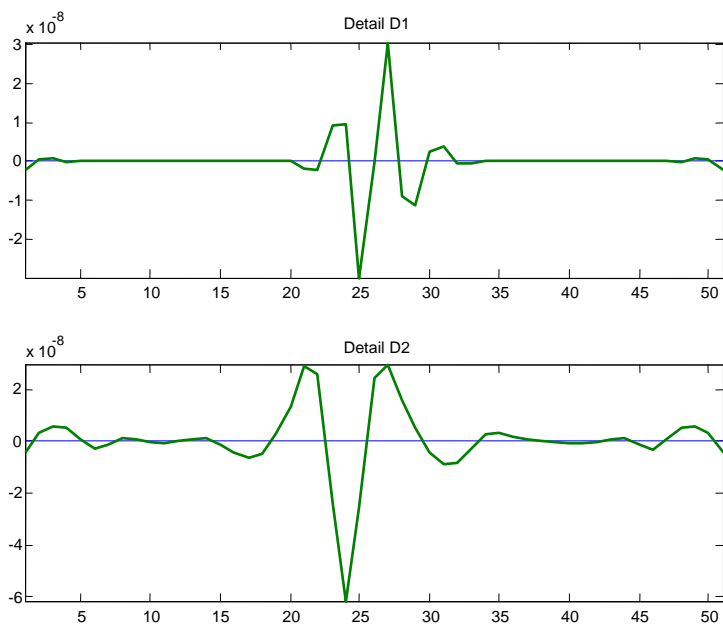
Figure 8.7 DW decomposition with wavelet 'bior5.5' for the beam with damage scenario SW1.
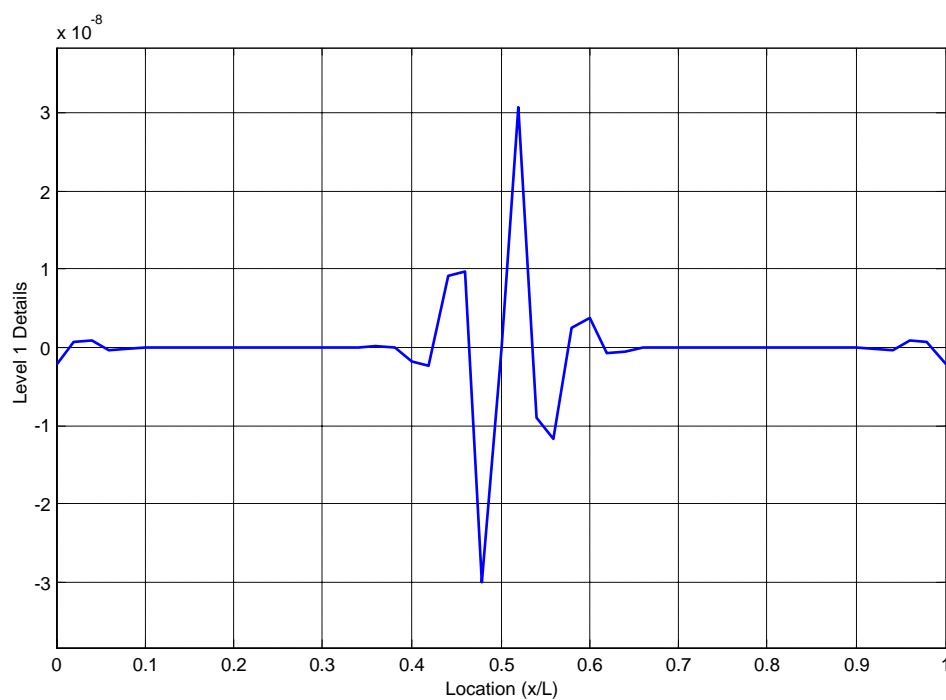
Figure 8.8. DW decomposition of the FRF for the beam with damage scenario SW1.
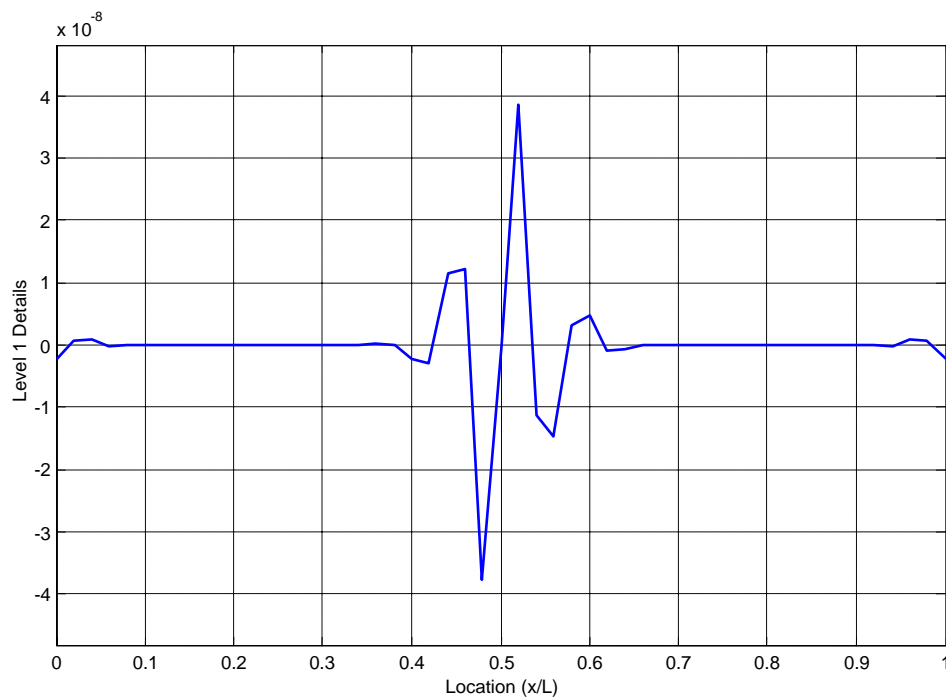
Figure 8.9 DW decomposition of the FRF for the beam with damage scenario SW2.
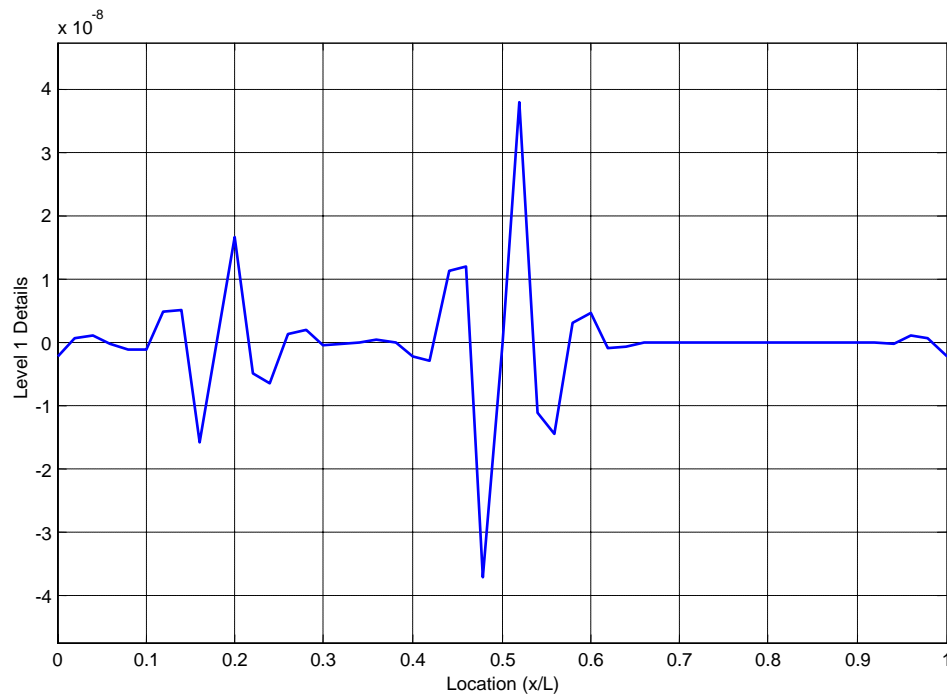
Figure 8.10 DW decomposition of the FRF for the beam with damage scenario SW3.

8.7.2 Plane frame

- Case 1.

The plane frame described in Chapter III is used in the second set of numerical examples. The beam of the frame was divided into 100 finite elements. The damage scenario PW1 is simulated by a crack inflicted near to the beam mid-span (element 51). The crack depth is $h_c = 0.1H$. The values of the Receptance FRF for the excitation force at L/2 are shown in Figure 8.11. When the DWT is applied to the signal in Figure 8.11, the values of the level-1 detail are those shown in Figure 8.13. As it can be observed the bior5.5 wavelet was capable of detecting the damage location from the response of the

damaged frame. The two spikes at the beginning and at the end in the detail-1 graph are produced by the geometric discontinuities at the beam-column joints and should therefore be ignored.

- Case 2.

The damage scenario PW2 consists of a single crack near the mid-span (element 51). The crack depth is now $h_c = 0.25H$. The magnitude of the Receptance FRF is shown in Figure 8.11. After the DWT with the bior5.5 wavelet was applied to the FRF curve of the damaged frame, the location of the damage was detected. The values of the level-1 detail as a function of relative position along the beam are shown in Figure 8.14.

Next, the DWT is applied to the FRF-first derivative of the frame with the same damage. The level-1 detail is shown in Figure 8.15. The abrupt and rapid changes in the level-1 detail at the crack position indicate the localization of damage.

- Case 3.

The damage case PW3 is a multiple damage scenario. It corresponds to two cracked elements at different locations 0.25L and 0.5L. The depth of cracks is $h_c=0.25H$. The values of the Receptance FRF are shown in Figure 8.12. The level-1 detail of the decompositions performed with the bior5.5 wavelet is shown in Figure 8.16. The abrupt changes in the level-1 detail due to the cracks indicate the localization of the multiple damage.

Next, the DWT is applied to the FRF-first derivative of the frame with the same damage case PW3. The level-1 detail is shown in Figure 8.17. The spikes at the level-1 details within the span indicate the localization of the two cracks. As it can be noted, the values of the detail function at the two cracks are different, even though the two cracks have the same size. This is a drawback because it will be difficult to calibrate the details with the amount of damage.

- Case 4

The damage scenario PW4 is simulated by introducing two cracked elements at the locations 0.5L and 0.95L, where L is beam span. The crack depth is h_c=0.25H. The signal analyzed is the FRF-first derivative. Figure 8.18 shows the level-1 detail obtained with the bior5.5 wavelet. Small disturbances are observed in this figure at the beginning and at the end in the detail graph. This impedes the detection of the crack located at $x/L = 0.95$. However, the detection of this crack can be facilitated by performing a level-2 decomposition. Figure 8.19 shows the level-2 detail where the spikes at the right end are magnified whereas those at the left end due to the corner are low.
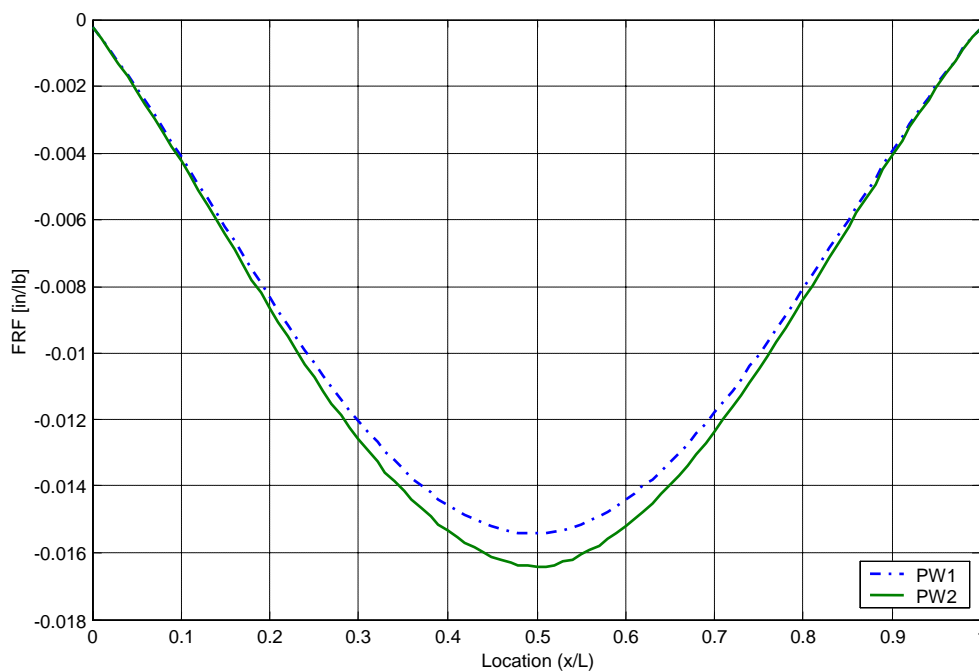
Figure 8.11 Receptance FRF for the frame with damage scenarios PW1 and PW2.
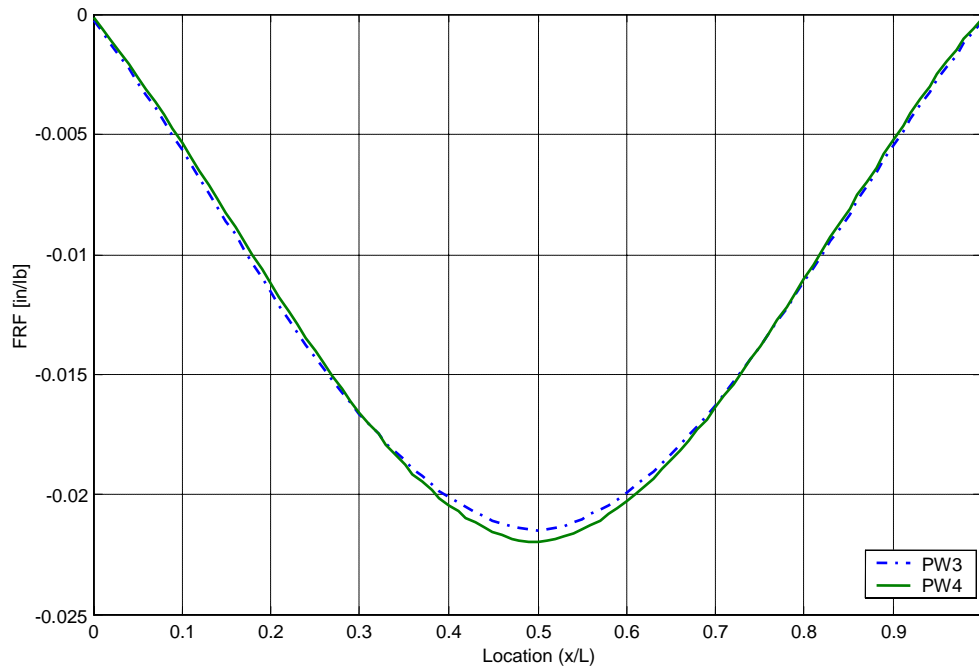
Figure 8.12 Receptance FRF for the frame with damage scenarios PW3 and PW4.
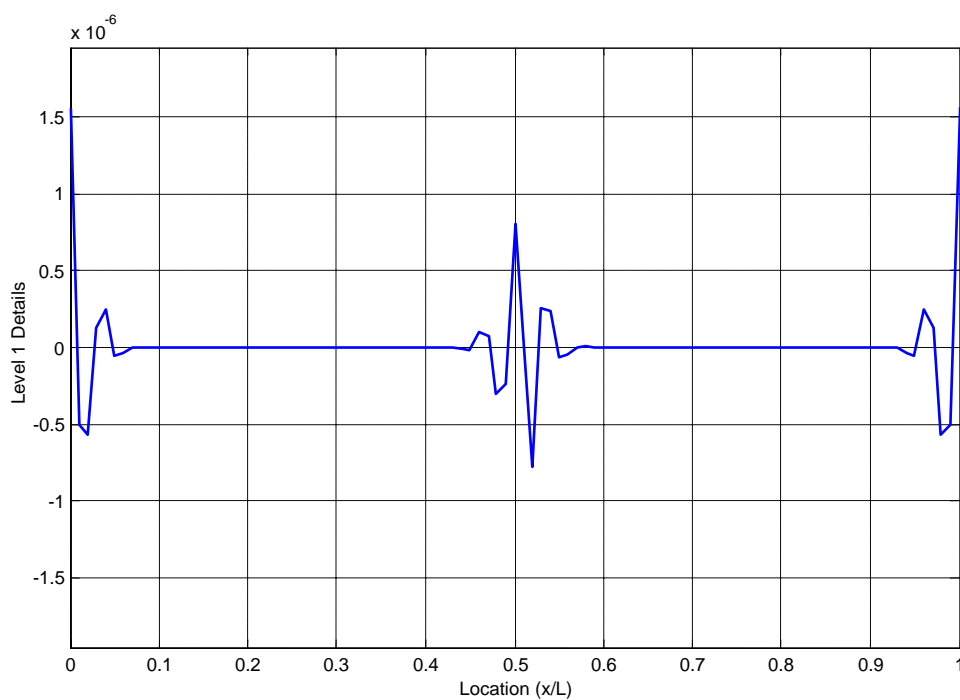
Figure 8.13 DWT decomposition of the FRF for the frame with damage scenario PW1.
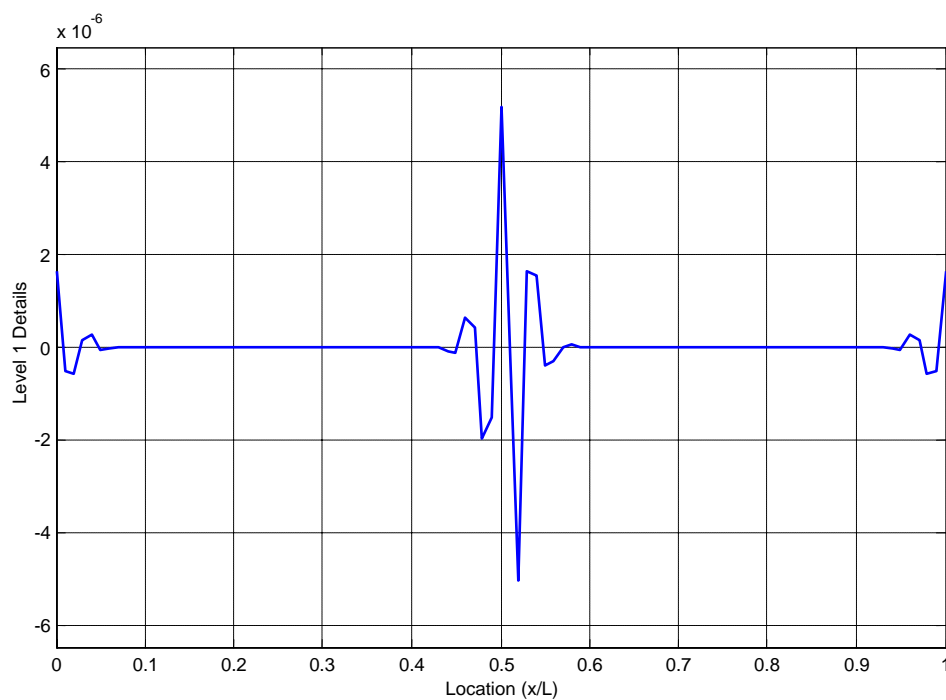
Figure 8.14 DWT decomposition of the FRF for the frame with damage scenario PW2.
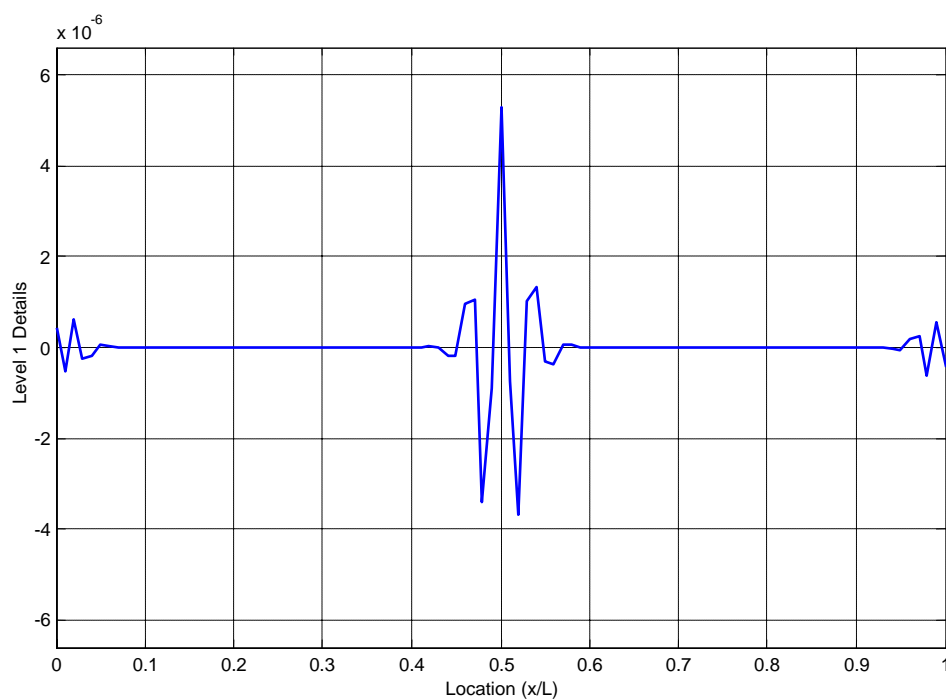
Figure 8.15 DWT decomposition of the FRF-1st Derivative for the frame with damage scenario PW2.
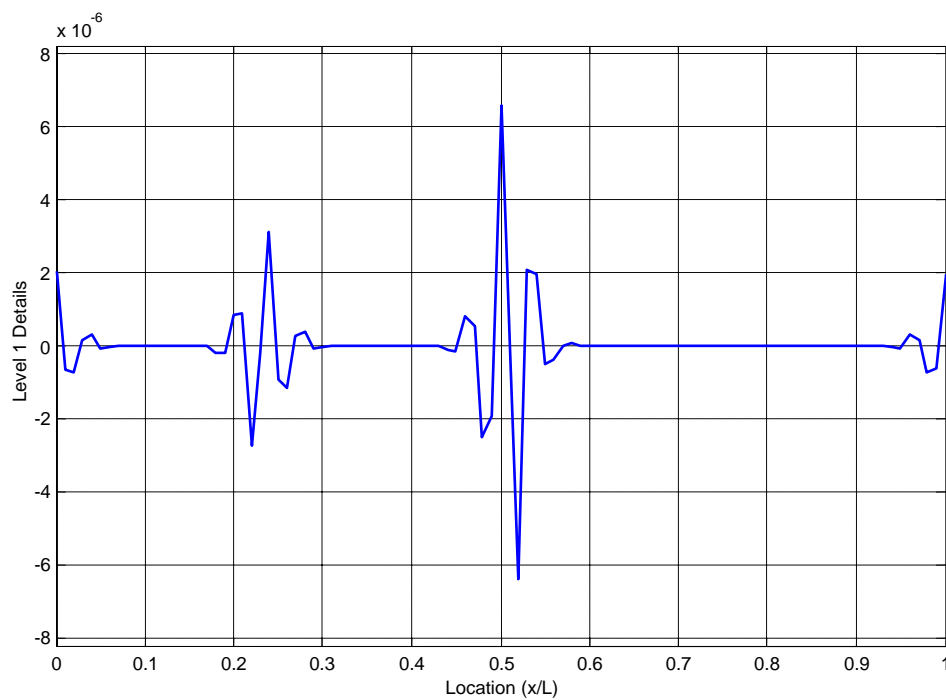
Figure 8.16 DWT decomposition of the FRF for the frame with damage scenario PW3.
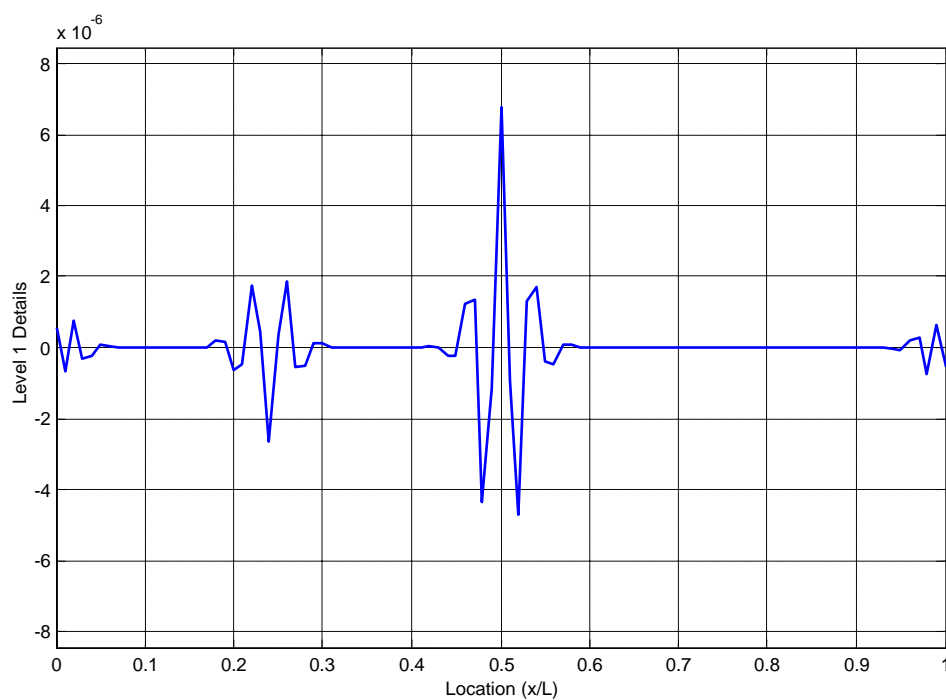
Figure 8.17 DWT decomposition of the FRF-1ˢᵗ Derivative for the frame with damage scenario PW3.
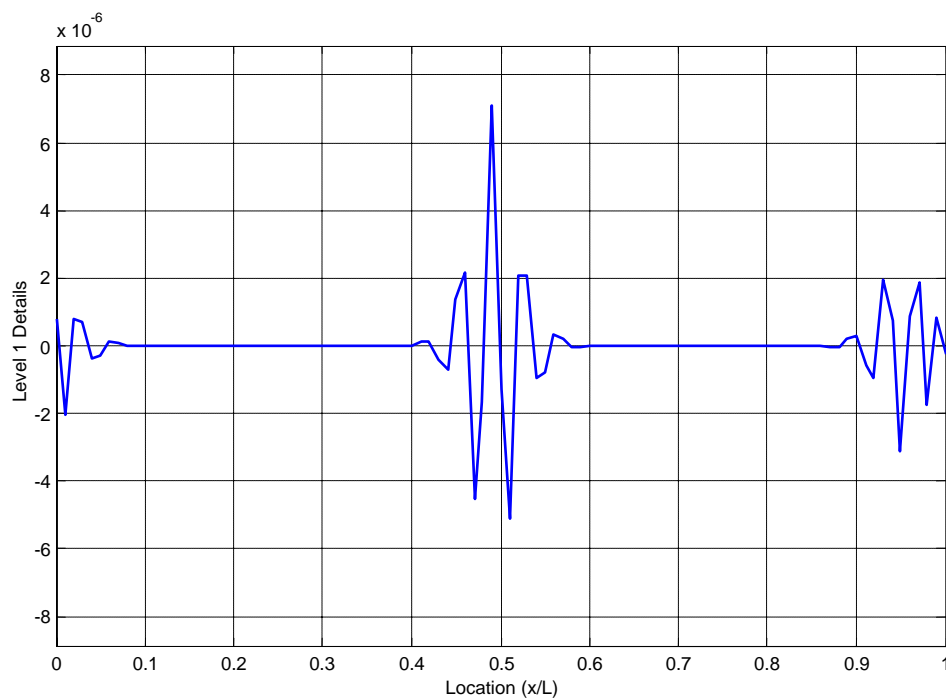
Figure 8.18 DWT decomposition of the FRF-1ˢᵗ Derivative for the frame with damage scenario PW4.
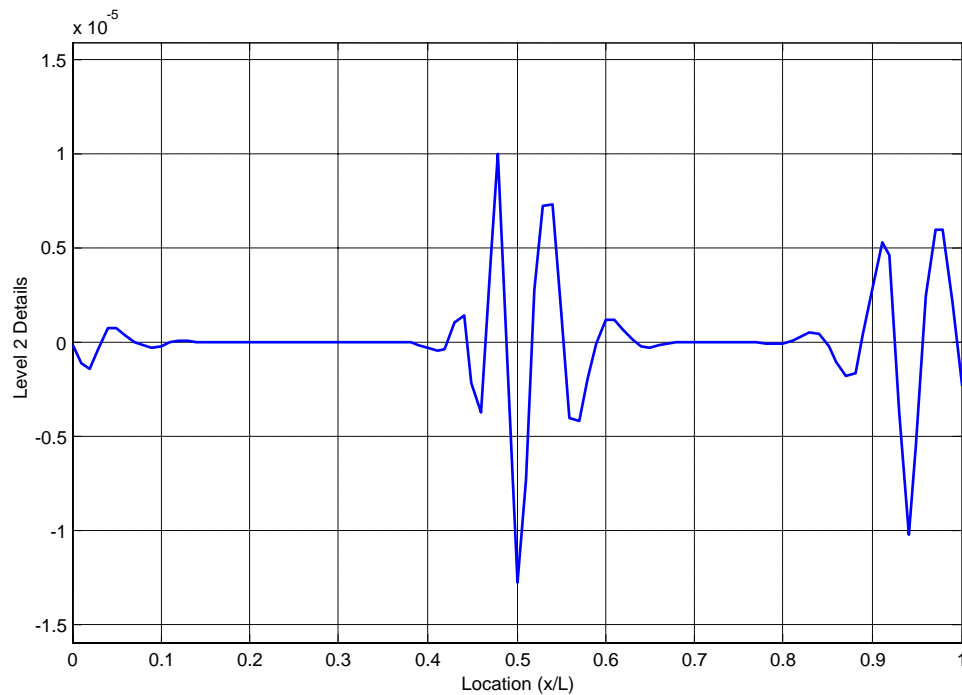
Figure 8.19 Level-2 DWT decomposition of the FRF-1st Derivative for the frame with damage scenario PW4.

8.8 SUMMARY

In this chapter, a brief review of the wavelet theory is presented. Next, a methodology based on the DWT for damage identification is formulated. Numerical examples are presented to compare the effectiveness of the proposed method in two simple structures. The Receptance FRF and the FRF-first derivative were used as the input signal. Several wavelets were studied to choose the most appropriate one to perform the decompositions. The wavelet selected was the biorthogonal wavelet bior5.5.

In the case of the simply-supported beam, the abrupt changes in the level-1 details due to the crack indicate the localization of the damage in both single and multiple

damage scenarios. It was found that the signal extension mode used practically eliminated the effect of the boundary conditions.

For the case of the plane frame, the drastic changes (spikes) in the level-1 details accurately indicate the location of the structural damage if the cracked element is located at a sufficient distance from the discontinuity in the geometry of the structure. When the crack was placed at the right end of the beam, it was only possible to detect the damage by using the level-2 details. It was observed that in this case, the wavelet-based methodology gives better results when the FRF-first derivative is used as the response signal. It was found that the value of the details for the same severity of damage were different. Therefore, if it is desired to quantify the damage, this issue has to be studied further. However, the numerical simulations showed that the DWT analysis was capable of detecting the discontinuities in the FRF signal that is associated with damage in all the cases considered. It must be pointed out that the FRFs for the two structures were obtained with a large number of "sensors" (displacement degrees of freedom in the simulations). The minimum number of sensors to pick up the damage is a topic that needs to be resolved in future studies.

CHAPTER IX

CONCLUSIONS

9.1 SUMMARY AND CONCLUSIONS

This thesis examined the several existing structural damage identification methods that are based on changes in the dynamic characteristics of the structure and proposes new methods. These methods are based on the premise that modal parameters are a function of the physical properties of the structure and provide a global way to evaluate the structural condition. In this thesis, several structural damage identification methodologies were developed and tested via numerical simulations. The proposed methodologies are based on the modal curvature matrix, the FRF-curvature and on the application of the Discrete Wavelet Transform that discloses the location of damage by detecting the discontinuities in the FRF signal.

The most significant conclusions obtained from the research carried out in the thesis are summarized in the following paragraphs:

a) The direct comparison of the natural frequencies and mode shapes did not reveal any significant change in all the damaged structures studied. Therefore, changes in natural frequencies or in the mode shapes alone are not precise enough to locate damage.

In a real life situation when the modal properties are measured, the method will perform even worse because of the unavoidable errors in the measurement.

b) The structural damage identification technique referred to as the eigenparameter method, which is based on changes in the displacement mode shapes, was able to indicate the location of the region damaged for the simply-supported beam with only one crack. For the case of multiple damage scenarios the eigenparameter was not competent to clearly locate the damaged zones. For the relative difference method, the results obtained indicate that the parameter RD introduced factors of uncertainty about the correct locations of damage.

c) The results of the present study showed that the method based on the changes in the pseudo-flexibility matrix is sensitive enough to detect the presence and indicate the location of damage in simply-supported beams and plane frames with single crack scenarios. The methodology is based on the premise that there is an increase in the local flexibility of the structure due to the presence of damage. In the structures with multiple damage scenarios, the method based on the flexibility matrix could not locate the damaged zones clearly. Therefore, this method seems suitable to locate damage in structures where the damage is located at the zones where the maximum bending moments occur, such as at the mid-span of the simply supported beams.

d) In general, the methodologies based on the modal curvatures and on the modal strain energy exhibited a superior performance in detecting and locating damage that those mentioned in the previous paragraphs. The results of the analyses indicate that the

new curvature-energy damage index formulated in this study correctly localizes the damaged zones in the two structures considered. An advantage of the proposed method is that it requires only a few modes to indicate the position of damage.

e) The results of the numerical simulations verified the capability of the Damage Index η proposed in this thesis to correctly localize the damage. It was shown that the proposed damage index can locate the damage by using only one input force to obtain the Frequency Response Function in the damage scenarios that simulate one damaged element. For the case of the multiple damage scenario, the technique displayed a better performance for the simply-supported beam.

f) For the new damage method based on the Receptance-Energy formulated in this work, the results of the numerical examples indicate that the proposed indices performed well in detecting, locating and quantifying damage. This is true for both the single and multiple damage scenarios simulated in the structures. In the case of simple-span beams, a significant feature of the proposed method is that it can locate the damaged zones of the structure by using a single input force to determine the Receptance Function. Although some errors were obtained in the quantification of the damage severity because the index is sensitive to the frequency range used, it is deemed that these errors are within acceptable margins. However, it is realized that this issue still needs further study. The main advantage of this procedure is that it does not require performing a modal analysis for the identification of mode shapes, as it is the case of the other methods. In other words, it directly uses the measured FRFs without further processing.

g) The wavelet transform, a powerful and relatively new mathematical tool to detect subtle changes, trends and discontinuities in signal, was used in this thesis as a methodology for structural damage identification. The method is based on the application of the Discrete Wavelet Transform. The Receptance FRF and the FRF-first derivative were used as the input signals. The numerical examples verified that the proposed method can locate the cracks based on the simulated response signal. It is shown that DWT analysis is capable of detecting the discontinuities in the FRF signal in single and multiple damage scenarios. Because the formulated method does not require to know the response of the undamaged structure, the DWT-based technique can provide an alternative to the damage identification methods based on modal analysis. The method can be used for various levels of damage assessment, including identifying damage occurrence and location.

9.2 RECOMMENDATIONS FOR FUTURE WORK

In this investigation the study of the existing and proposed damage identification methodologies has been limited to the analytical and numerical aspects only. The performance of these methodologies must be studied experimentally to test whether they can be used in real existing structures.

It is well known that the cost and labor associated with experimental testing can be quite high. Therefore, the numerical simulation of existing and new methods is important to screen out these procedures that do not perform satisfactorily. In this way the set of methods that require experimental verification will be reduced. Nevertheless,

experimental work using these methods is a requisite to confirm whether they can be successfully implemented for damage assessment in complex structures. Real signals obtained by measuring the structural response should be used in order to demonstrate the reliability and capability of the proposed procedures in the presence of noise and the uncertainties associated with experimental methods.

The proposed methodologies could be applied to detect defects on beam-column connections, plate and shells structures, and trusses. Damage in form of cracks with different orientations should also be studied. Other areas of possible future investigation include the simulation of damage on post-tensioned and pre-tensioned structures.

For the wavelet-based methodology, a procedure to reduce the number of measurement points is required. A method based on wave propagation could be developed, in which only one or two sensors are required to provide the response signal. The wavelet-based methodology proposed in this thesis was shown to be capable of pointing out the location of the damage. The issue of damage quantification has to be further developed and experimentally validated. A wavelet-based method to detect and locate damage in bridge structures using vibration induced by vehicular traffic data is also worth studying.

REFERENCES

1. Cawley, P. and Adams, R.D. (1979). "The locations of defects in structures from measurements of natural frequencies." *Journal of Strain Analysis*, 14 (2): 49–57.

2. Doebling, S.W., Farrar, C. R., Prime, M. B. and Shevitz, D.W. (1996). "Damage identification and health monitoring of structural and mechanical systems from changes in their vibration characteristics: A literarure review." *Research Rep. No. LA-13070-MS*, ESA-EA, Los Alamos National Laboratory, Los Alamos, N.M.

3. Dong C., Zhang, P., Feng, W. and Huang,T. (1994). "The sensitivity study of the modal parameters of a cracked beam." *Proc. of the 12th International Modal Analysis Conference*, Honolulu, Hawaii 98-104.

4. Fox, C. H. J. (1992). "The location of defects in structures: a comparison of the use of natural frequency and mode shape data." *Proc. of the 10th International Modal Analysis Conference*, 522–528.

5. Gounaris, G. and Dimarogonas, A. (1988). "A finite element of a cracked prismatic beam for structural analysis." *Computers & Structures,* 28(3): 309-313.

6. Gysin, H.P., (1986). "Critical application of an error matrix method for location of finite element modeling inaccuracies", *Proc. of the 4th International Modal Analysis Conference*, Los Angeles, California, 1339-1351.

7. Haisty, B. S. and Springer, W. T. (1988). "A general beam element for use in damage assessment of complex structures." *ASME Journal of Vibration, Acoustics, Stress and Reliability in Design,* 110(3): 389-394.

8. He, J. (1999). "Damage detection and evaluation". In: "Modal analysis and testing." Eds. Silva, J. and Maia, N. Kluwer, Dordrecht. p. 325-344.

9. Hou, Z., Noori, M. and St. Amand, R. (2000). "Wavelet –based approach for structural damage detection." *ASCE Journal of Engineering Mechanics*, 124(10): 1059-1066.

10. Kim, J., Ryu, Y., Cho, H. and Stubbs, N. (2003). "Damage identification in beam-type structures: frequency-based method vs. mode-shape-based method." *Engineering Structures*, 25(1): 57-67.

11. Ko, J.M., Wong, C.W. and Lam, H.F. (1994). "Damage detection in steel framed structures by vibration measurement approach." *Proc. of the 12th International Modal Analysis Conference*, Honolulu, Hawaii, 280-286.

12. Lawson, C. L. and Hanson, R. J. (1974). *Solving Least Squares Problems*. Prentice-Hall, Englewood Clifs, N J.

13. Lee, U. and Shin, J. (2002). "A frequency response function-based structural damage identification method." *Computers & Structures.* 80: 117-132.

14. Liew, K.M. and Wang, Q. (1998). "Application of wavelet theory for crack identification in structures." *ASCE Journal of Engineering Mechanics,* 124 (2): 152–157.

15. Mannan, M.A. and Richardson, M.H. (1992). "Detection and location of structural cracks using FRF measurements." *Proc. of the 10th International Modal Analysis Conference*, San Diego, California, 652-657.

16. Misiti, M., Misiti, Y., Oppenheim, G. and Poggi, J. (2001). *Wavelet toolbox — user's guide*, The Math Works Inc, Natick, MA.

17. Ovanesova, A. and Suárez, L. E. (2004). "Applications of wavelet transforms to damage detection in frame structures." *Engineering Structures,* 26(1): 39-49.

18. Pandey, A.K., Biswas, M. and Samman, M.M. (1991). "Damage detection from changes in curvature mode shapes." *Journal of Sound and Vibration*, 145(2): 321-332.

19. Pandey, A.K. and Biswas, M., (1994). "Damage detection in structures using changes in flexibility." *Journal of Sound and Vibration*, 169(1): 3-17.

20. Park, Y.S., Park, H.S. and Lee, S.S. (1988). "Weighted-Error-Matrix application to detect stiffness damage-characteristic measurement." *Modal Analysis*: *The International Journal of Analytical and Experimental Modal Analysis*, 3(3):101-107.

21. Qian,G.L., Gu, S.N. and Jiang, J.S. (1990). "The dynamic behaviour and crack detection of a beam with a crack." *Journal of Sound and Vibration*, 138(2): 233-243.

22. Raghavendrachar, M. and Aktan, A.E. (1992). "Flexibility by multireference impact testing for bridge diagnostics." *ASCE Journal of Structural Engineering,* 118(8): 2186-2203.

23. Ren, W.X. and De Roeck, G. (2002). "Structural damage identification using modal data. I: Simulation verification." *ASCE Journal of Structural Engineering*, 128(1): 87-95.

24. Rytter, A., "Vibration based inspection of civil engineering structures," Ph. D. Dissertation, Department of Building Technology and Structural Engineering, Aalborg University, Denmark, (1993).

25. Salawu, O.S. and Williams, C. (1994). "Damage location using vibration mode shapes." *Proc. of the 12th International Modal Analysis Conference*, Honolulu, Hawaii, 933-939.

26. Salawu, O.S. and Williams, C. (1993). "Structural damage detection using experimental modal analysis." *Proc. of the 11th International Modal Analysis Conference*, Kissimmee, Florida, 254-260.

27. Sampaio, R. P., Maia, N. M. and Silva, J. M. (1999). "Damage detection using the frequency-response-function curvature method*." Journal of Sound and Vibration*, 226(5): 1029-1042.

28. Strang, G. and Nguyen, T. (1996). *Wavelet and filter banks*, Wellesley-Cambridge Press, Wellesley, MA.

29. Stubbs, N., Kim, J. and Charles, R.F. (1995). "Field verification of a nondestructive damage localization and severity estimation algorithm." *Proc. of the 13th International Modal Analysis Conference,* Nashville, Tennessee, 210-218.

30. Stubbs, N. and Osegueda, R. (1990a). "Global non-destructive damage evaluation in solids" *Modal Analysis*: *The International Journal of Analytical and Experimental Modal Analysis*, 5(2): 67-79.

31. Stubbs, N. and Osegueda, R. (1990b), "Global damage detection in solids-experimental verification," *Modal Analysis*: *The International Journal of Analytical and Experimental Modal Analysis*, 5(2): 81-92.

32. Wang, Q. and Deng, X. (1999). "Damage detection with spatial wavelets." *International Journal of Solids and Structures*, 36: 3443-3468.

33. Yuen, M.,(1985)."A numerical study of the eigenparameters of a damaged cantilever." *Journal of Sound and Vibration*, 103(3): 301-310.

APPENDIX A

METHODS BASED ON: STIFFNESS MATRIX CHANGES

A variation on the use of the dynamically measured flexibility matrix is the use of the dynamically measured stiffness matrix, defined as the pseudoinverse of the dynamically measured flexibility matrix. However, this methods exhibit defined limitations. When modal data are used, it is usually unrealistic to expect many vibration modes to be available from the experiments. This may result in significantly inaccurate stiffness matrices, as higher frequency modes, which are more important for constructing the stiffness matrix, are usually not as available as lower vibration modes.

A.1 DIRECT ERROR MATRIX METHOD-(EMM)

The EMM was originally formulated to correct/update theoretical models using measured data. The model updating methods using experimental modal analysis are used to validate predictions from theoretical models. Most updating procedures locate zones of errors in the finite element model before the updating. If it is assumed that the (analytical) system matrices to be updated were obtained from a prior vibration measurement, then the error localization step can be used to detect and locate damage in a structure from any two measurements of the vibration response.

For two matrices [K] and [K*] the error matrix between them is defined as

$$[\Delta K] = [K^*] - [K_u]$$

(A.1)

In model updating procedures [K*] represents the experimentally derived stiffness matrix while [K$_u$] is the analytical matrix. Both matrices are numerically obtained derived using pseudo-inverse of the mode shape matrix and the orthogonality properties.

The system matrix [K] is defined by

$$[K] = [\Phi^T]^+ [\Lambda] [\Phi]^+$$

(A.2)

where

$[\Phi]^+$: pseudo-inverse of the mode shape matrix

$[\Lambda]$: diagonal modal stiffness matriz.

A.2 MODIFIED MATRIX STIFFNESS ERROR METHOD -(MEMM)

Many modified versions of the direct error matrix have been suggested. For two matrices [K] and [K*] the modified error matrix between them is defined as

$$\left[\Delta K\right]=\left[K_{u}\right]\left\{\left[F_{u}\right]-\left[F_{*}\right]\right\}\left[K_{u}\right]. \tag{A.3}$$

In the latter equation, $[K_u]$ is obtained from equation (A.2) while the pseudo-flexibility matrices $[F_u]$ and $[F_*]$ are obtained from the frequencies and mode shapes of the undamaged and damaged structures respectively.

APPENDIX B

FREQUENCY DOMAIN: FREQUENCY RESPONSE FUNCTION

The general mathematical representation of a single degree of freedom system is expressed in Equation (B.1):

$$m\ddot{x}(t) + c\dot{x}(t) + k\dot{x}(t) = f(t) \tag{B.1}$$

An equivalent equation of motion for Equation (B.1) is determined for the Fourier or frequency (ω) domain. This representation has the advantage of converting a differential equation to an algebraic equation. This is accomplished by taking the Fourier transform of Equation (B.1).

Thus, Equation (B.1) becomes:

$$\left[-m\omega^2 + ic\omega + k \right] X(\omega) = F(\omega) \tag{B.2}$$

Restating the above equation:

$$B(\omega)X(\omega) = F(\omega) \tag{B.3}$$

where,

$$B(\omega) = \left[-m\omega^2 + ic\omega + k \right] \tag{B.4}$$

Equation (B.3) states that the system response $X(\omega)$ is directly related to the system forcing function $F(\omega)$ through the quantity $B(\omega)$, the impedance function. If the system forcing function $F(\omega)$ and its response $X(\omega)$ are known, $B(\omega)$ can be calculated. That is:

$$B(\omega) = \frac{F(\omega)}{X(\omega)} \tag{B.5}$$

More frequently, the system response, $X(\omega)$, due to a known input $F(\omega)$, is of interest.

$$X(\omega) = \frac{F(\omega)}{B(\omega)} \tag{B.6}$$

Equation (B.6) becomes:

$$X(\omega) = H(\omega)F(\omega) \tag{B.7}$$

where

$$H(\omega) = \frac{1}{\left[-m\omega^2 + ic\omega + k\right]}$$ (B.8)

The quantity $H(\omega)$ is known as the Frequency Response Function of the system. The Frequency Response Function relates the Fourier transform of the system input to the Fourier transform of the system response.

Under certain conditions, an arbitrary function f(t) can be described by an integral $F(\omega)$ given by

$$F(\omega) = \int_{-\infty}^{+\infty} f(t)e^{-i\omega t} dt$$ (B.9)

Similarly the Fourier transform of the system response can be described by the integral

$$X(\omega) = \int_{-\infty}^{+\infty} x(t)e^{-i\omega t} dt$$ (B.10)

The ratio of the functions (B.9) and (B.10) can be computed in order to obtain an expression for the corresponding Frequency Response Function:

$$H(\omega) = \frac{X(\omega)}{F(\omega)} \tag{B.11}$$

It is possible to derive an expression for the response x(t), from the inverse Fourier transform of $X(\omega)$:

$$x(t) = \int_{-\infty}^{+\infty} [H(\omega)F(\omega)] e^{i\omega t} d\omega \tag{B.12}$$

The frequency spectrum is now a continuous function of ω, in contrast to the frequency spectrum obtained for periodic time functions which consists of discrete components only. As a consequence, the F(ω) values represent an amplitude which is continuously distributed along the frequency and therefore represent units of amplitude per unit frequency, i.e., what is known as a spectral density.

To obtain x(t) it is then necessary to evaluate the integral in (B.12) which often leads to difficulties from a mathematical point of view. On the other hand, there are a number of situations where the Fourier transform analysis is inadequate, yielding completely meaningless solutions of the integral. Attempting to solve these situations, through adequate mathematical manipulations, results in the use of a 'modified' Fourier transform, known as the Laplace transform, which can be easily found in the appropriate litterature.

In practice, the forcing function may be quite irregular, even if it is periodic, and may be determined only experimentally. Such cases correspond to having a graphical representation of the signal and no analytical expression to describe it. These situations can still be handled by means of adequate discretization and numerical procedures applied to the signal.

APPENDIX C

SIGNAL EXTENSION MODES: WAVELET TOOLBOX OF MATLAB

Zero-padding (**'zpd'**): This method assumes that the signal is zero outside the original support. The disadvantage of zero-padding is that discontinuities are artificially created at the border.

Symmetrization (**'sym'**): This method assumes that signals or images can be recovered outside their original support by symmetric boundary value replication. It is the default mode of the wavelet transform in the toolbox. Symmetrization has the disadvantage of artificially creating discontinuities of the first derivative at the border.

Smooth padding of order 1 (**'spd' or 'sp1'**): This method assumes that signals or images can be recovered outside their original support by a simple first-order derivative extrapolation: padding using a linear extension fit to the first two and last two values. Smooth padding works well in general for smooth signals.

Smooth padding of order 0 (**'sp0'**): This method assumes that signals or images can be recovered outside their original support by a simple constant extrapolation. For a signal extension is the repetition of the first value on the left and last value on the right.

Periodic-padding (1): (**'ppd'**): This method assumes that signals or images can be recovered outside their original support by periodic extension. The disadvantage of periodic padding is that discontinuities are artificially created at the border.

Periodic-padding (2): (**'per'**): If the signal length is odd, the signal is first extended by adding an extra-sample equal to the last value on the right. Then a minimal periodic extension is performed on each side. The same kind of rule exists for images. This last mode produces the smallest length wavelet decomposition. But the extension mode used for IDWT must be the same to ensure a perfect reconstruction.

APPENDIX D

STIFFNESS MATRIX OF THE CRACKED ELEMENT

The relation between displacements and forces in the base system (see Figure 2.1) can be obtained as

$$\{\delta^*\} = [C^*]\{F^*\} \tag{D.1}$$

where

$$\{\delta^*\} = \{u_{i+1} \quad \theta_{i+1}\}^T \tag{D.2}$$

$$\{F^*\} = \{P_{i+1} \quad M_{i+1}\}^T$$

The element stiffness matrix in the base system (Figure 2.1) is obtained by inversion of the flexibility matrix $[C^*]$:

$$[k^*] = [C^*]^{-1} \tag{D.3}$$

Thus the relation between forces and displacements is

$$\{F^*\} = [k^*]\{\delta^*\} \tag{D.4}$$

The forces and displacements $\{F\}$, $\{\delta\}$ in the local system (Figure 2.2) are obtained from forces in the base system with the relation

$$\{F\} = [T]\{F^*\} \tag{D.5}$$

$$\{\delta^*\} = [T]^T \{\delta\} \tag{D.6}$$

where

$$\{F\} = \{P_i \quad M_i \quad P_{i+1} \quad M_{i+1}\}^T$$

$$\{\delta\} = \{u_i \quad \theta_i \quad u_{i+1} \quad \theta_{i+1}\}^T$$

$$[T] = \begin{bmatrix} -1 & 0 \\ -L & -1 \\ 1 & 0 \\ 0 & 1 \end{bmatrix}$$

The matrix [T] is obtained from the equilibrium conditions. From equations (D.3), (D.4) and (D.5) is obtained the following expression:

$$\{F\} = [T]\{F^*\} = [T][k^*]\{\delta^*\} \tag{D.7}$$

Replacing (D.6) in the latter equation yields

$$\{F\} = [T][k^*][T]^T \{\delta\} = [T][C^*]^{-1}[T]^T \{\delta\} \tag{D.8}$$

Finally, from this equation the matrix [K] in the local system can be expressed as

$$[K] = [T][C^*]^{-1}[T]^T \tag{D.9}$$

EQUIVALENT FLEXURAL STIFFNESS

For the undamaged element the displacement u_i caused by a unit value of the force P is

$$u_i = C_{1,1}^{(0)} = \frac{L^3}{3EI} \tag{D.10}$$

From equations (2.9) and (2.10) for the cracked element the displacement u_i^* is

$$u_i^* = C_{1,1}^{(0)} + C_{1,1}^{(1)} \tag{D.11}$$

The equivalent moment of inertia (Ie) of an uncracked element that produces the displacement u_i^*, can be calculate as

$$I_e = \frac{L^3}{3E\left(u_i^*\right)} \tag{D.12}$$

The damage severity in terms of the reduction in the flexural stiffness can be expressed as

$$D = 1 - \frac{EI_e}{EI} \tag{D.13}$$

> `restart:with(linalg):`

Warning, the protected names norm and trace have been redefined and unprotected

`# beta1:=FI(s)/(b*h^2);beta2:=FII(s)/(b*h);`

> `k2:=P^2*(beta2^2)*(Pi*x);`

$$k2 := P^2\,\beta2^2\,\pi\,x$$

>

> `k1:=(6*M*(Pi*x)^(1/2)*beta1+3*P*L*(Pi*x)^(1/2)*beta1)^2;`

$$k1 := (\,6\,M\,\sqrt{\pi\,x}\,\beta1 + 3\,P\,L\,\sqrt{\pi\,x}\,\beta1\,)^2$$

> `k1:=simplify(k1):`
> `IN1:=Int(k1,x=0..a);`

$$IN1 := \int_0^a 9\,\pi\,x\,\beta1^2\,(\,2\,M + P\,L\,)^2\,dx$$

> `IN1:=int(k1,x=0..a);`

$$IN1 := \frac{9}{2}\,\pi\,\beta1^2\,(\,2\,M + P\,L\,)^2\,a^2$$

> `IN2:=Int(k2,x=0..a);`

$$IN2 := \int_0^a P^2\,\beta2^2\,\pi\,x\,dx$$

> `IN2:=int(k2,x=0..a);`

$$IN2 := \frac{1}{2}\,P^2\,\beta2^2\,\pi\,a^2$$

> `W1:=(b/Ep)*IN1+(b/Ep)*IN2;`

$$FW := \frac{9}{2}\,\frac{b\,\pi\,\beta1^2\,(\,2\,M + P\,L\,)^2\,a^2}{Ep} + \frac{\dfrac{1}{2}\,b\,P^2\,\beta2^2\,\pi\,a^2}{Ep}$$

> `C11:=diff(W1,P,P):`

$$C11 := \frac{b\,\pi\,a^2\,(\,9\,\beta1^2\,L^2 + \beta2^2\,)}{Ep}$$

> `C12:=diff(W1,P,M);`

$$C12 := 18\,\frac{b\,\pi\,\beta1^2\,a^2\,L}{Ep}$$

>

> `C22:=diff(W1,M,M);`

$$C22 := 36\,\frac{b\,\pi\,\beta1^2\,a^2}{Ep}$$

> `C21:=diff(W1,M,P);`

$$C21 := 18\,\frac{b\,\pi\,\beta1^2\,a^2\,L}{Ep}$$

Flexibility coefficients due to the crack:

> `Cc:=linalg[matrix](2,2,[C11,C12,C21,C22]);`

$$Cc := \begin{bmatrix} \dfrac{b\,\pi\,a^2\,(9\,\beta1^2\,L^2 + \beta2^2)}{Ep} & 18\,\dfrac{b\,\pi\,\beta1^2\,a^2\,L}{Ep} \\ 18\,\dfrac{b\,\pi\,\beta1^2\,a^2\,L}{Ep} & 36\,\dfrac{b\,\pi\,\beta1^2\,a^2}{Ep} \end{bmatrix}$$

> `T:=matrix(2,4,[-1, -L,1,0,0,-1,0,1]);`

$$T := \begin{bmatrix} -1 & -L & 1 & 0 \\ 0 & -1 & 0 & 1 \end{bmatrix}$$

> `kk1:=(L^3)/(3*EI):kk2:=(L^2)/(2*EI):kk3:=L/(EI):`

The flexibility matrix of the uncracked element [Co] :

> `Co:=linalg[matrix](2,2,[kk1,kk2,kk2,kk3]);`

$$Co := \begin{bmatrix} \dfrac{1}{3}\dfrac{L^3}{EI} & \dfrac{1}{2}\dfrac{L^2}{EI} \\ \dfrac{1}{2}\dfrac{L^2}{EI} & \dfrac{L}{EI} \end{bmatrix}$$

> `CC:=evalm(Co+Cc):`
>
> `KK1:=multiply(transpose(T),inverse(CC)):`
>

Stiffness matrix of the cracked element [KC]:

> `KC:=simplify((multiply(KK1,T)));`

$$KC(1,1)= 12\,\frac{EI\,Ep}{L^3\,Ep + 12\,b\,\pi\,a^2\,EI\,\beta2^2}$$

$$KC(1,2)= 6\,\frac{Ep\,EI\,L}{L^3\,Ep + 12\,b\,\pi\,a^2\,EI\,\beta2^2}$$

$$KC(1,3)= -12\,\frac{EI\,Ep}{L^3\,Ep + 12\,b\,\pi\,a^2\,EI\,\beta2^2}$$

$$KC(1,4)= 6\,\frac{Ep\,EI\,L}{L^3\,Ep + 12\,b\,\pi\,a^2\,EI\,\beta2^2}$$

$$KC(2,1)= KC(1,2)$$

$$KC(2,2)= 4\,\frac{(L^3\,Ep + 27\,b\,\pi\,a^2\,EI\,\beta1^2\,L^2 + 3\,b\,\pi\,a^2\,EI\,\beta2^2)\,EI\,Ep}{(L\,Ep + 36\,b\,\pi\,\beta1^2\,a^2\,EI)\,(L^3\,Ep + 12\,b\,\pi\,a^2\,EI\,\beta2^2)}$$

$$KC(2,3) = -6\,\frac{Ep\,EI\,L}{L^3\,Ep + 12\,b\,\pi\,a^2\,EI\,\beta2^2}$$

$$KC(2,4) = 2\,\frac{Ep\,EI\,(L^3\,Ep + 54\,b\,\pi\,a^2\,EI\,\beta1^2\,L^2 - 6\,b\,\pi\,a^2\,EI\,\beta2^2)}{(L\,Ep + 36\,b\,\pi\,\beta1^2\,a^2\,EI)\,(L^3\,Ep + 12\,b\,\pi\,a^2\,EI\,\beta2^2)}$$

$$KC(3,1)= KC(1,3)$$

$$KC(3,2)= KC(2,3)$$

$$KC(3,3)= 12\,\frac{EI\,Ep}{L^3\,Ep + 12\,b\,\pi\,a^2\,EI\,\beta2^2}$$

$$KC(3,4)= -6\,\frac{Ep\,EI\,L}{L^3\,Ep + 12\,b\,\pi\,a^2\,EI\,\beta2^2}$$

$$KC(4,1)= KC(1,4)$$

$$KC(4,2)= KC(2,4)$$

$$KC(4,3)= KC(3,4)$$

$$KC(4,4) = 4\,\frac{(L^3\,Ep + 27\,b\,\pi\,a^2\,EI\,\beta1^2\,L^2 + 3\,b\,\pi\,a^2\,EI\,\beta2^2)\,EI\,Ep}{(L\,Ep + 36\,b\,\pi\,\beta1^2\,a^2\,EI)\,(L^3\,Ep + 12\,b\,\pi\,a^2\,EI\,\beta2^2)}$$